FRACTURE TOUGHNESS OF PIPE LINE STEELS

by

RANEN MAITI
B.E. (Met), R E College, Durgapur (1967)
D.I.I.T. (Foundry Engg.), I.I.T. Kharagpur (1969)
M. Tech (Phy. Met), I.I.T. Kharagpur (1971)

A THESIS SUBMITTED IN PARTIAL FULFILLMENT OF

THE REQUIREMENTS FOR THE DEGREE OF

MASTER OF APPLIED SCIENCE

in

THE FACULTY OF GRADUATE STUDIES

Department of METALLURGICAL ENGINEERING

We accept this thesis as conforming

to the required standard

The University of British Columbia,

December, 1978

In presenting this thesis in partial fulfilment of the requirements for an advanced degree at the University of British Columbia, I agree that the Library shall make it freely available for reference and study. I further agree that permission for extensive copying of this thesis for scholarly purposes may be granted by the Head of my Department or by his representatives. It is understood that copying or publication of this thesis for financial gain shall not be allowed without my written permission.

Department of Metallurgical Engineering

The University of British Columbia
2075 Wesbrook Place
Vancouver, Canada
V6T 1W5

Date January 18th, 1979

ABSTRACT

The fracture toughness of two acicular ferrite, HSLA pipeline steels was investigated utilising the linear elastic fracture mechanics analysis (K_{Ic} testing according to ASTM Standard E399-74) as well as the elastic-plastic fracture mechanics analysis (J-Integral and crack opening displacement COD methods).

The tests were conducted at a static strain rate of 10^{-5} /sec, $\dot{K}$ = 10 ksi$\sqrt{in}$/sec with ½ inch thick compact tension specimens. A resistance curve test technique developed by Landes and Begley was employed to obtain the J_{Ic} fracture toughness; whereas the British Standard for COD testing was followed for measuring the δ_c fracture toughness.

The anisotropy in fracture toughness and the tensile properties of the two x-70 steels were measured and explained in terms of sulphur content and rare earth additions.

An attempt was made to correlate the linear elastic fracture toughness K_{Ic} or K_Q values with the

elastic-plastic fracture toughness, J_{Ic}, and COD data for both steels for tests in each of three notch orientations i.e. parallel to the rolling direction (T-L); parallel to the pipe axis; transverse to the rolling direction (L-T). Tests were performed at temperatures throughout the transition range i.e. from RT down to - 196 °C.

Finally the static fracture toughness data as generated in this study, was compared with the dynamic fracture toughness as obtained from IIT test for both steels.

TABLE OF CONTENTS

LIST OF FIGURES

LIST OF TABLES

LIST OF SYMBOLS

$\dot{\varepsilon}$	Strain Rate
ε_{ys}	Yield Strain
K	Stress Intensity Factor
$\dot{K}$	Stress Intensity Rate
K_c	Plane Stress Fracture Toughness
K_{Ic}	Plane Strain Fracture Toughness under Static Loading
K_{Id}	Plane Strain Fracture Toughness under Dynamic Loading
K_Q	Calculated Fracture Toughness
J_{Ic}	Critical J-Integral Plane Strain Fracture Toughness
J_Q	Calculated J-value
G_{Ic}	Crack Extension Force under Plane Strain Condition
G	Crack Extension Force
IIT	Instrumented Impact Testing
COD	Crack Opening Displacement
δ	Crack Opening Displacement
δ_c	Critical COD
δ_m	Critical COD corresponding to Maximum Load
δ_Q	Critical COD corresponding to P_Q Load corresponding to 5% Offset

P_{max}	Maximum Load
P	Load
Δ	Displacement
γ	Austenite
D	Inside Diameter of Pipe
t	Pipe Wall Thickness
σ_H	Hoop Stress
σ	Tensile Stress
σ_{ys}	Yield Stress
σ_f	Flow Stress
E	Young's Modulus
ν	Poisson's Ratio
a	Crack Length
B	Specimen Thickness
w	Depth of Specimen
A_c	Area of Charpy Specimen Ligament
r_y	Plastic Zone Radius
Δa	Crack Extension
Vg	Clip Gauge Displacement
r	Rotational Factor
z	Knife Edge Thickness
V_c	Critical Clip Gauge Displacement
V_m	Clip Gauge Displacement at P_{max}
V_Q	Clip Gauge Displacement at P_Q

ACKNOWLEDGEMENTS

I wish to thank my fellow graduate students and the members of the faculty, in particular Dr. S.R. Bala and Asst. Prof. R.G. Butters for their assistance and helpful discussions during the research work. I very much appreciate the assistance of the technical staff, in particular, J. Walker and H. Tump throughout the experimental programme and R. Bennett, P. Musil and M. Bennett during the preparation of the thesis.

Financial assistance in the form of a 'Commonwealth Scholarship' provided by Canadian Commonwealth Scholarship and Fellowship Committee, Ottawa, is gratefully acknowledged.

I am indebted to my supervisors Prof. E.B. Hawbolt and Prof. J.S. Nadeau for their continuous advice, stimulating discussions, helpful suggestions and immense encouragement throughout the project.

Thanks are also extended to Prof. E. Teghtsoonian, Head, Dept. of MET. ENGG, for providing necessary facilities to carry out the project.

Finally, I thank my wife Biva and daughter Munmun for their patience.

1. INTRODUCTION

In this thesis, Linear Elastic Fracture Mechanics (LEFM) and Elastic Plastic Fracture Mechanics (EPFM) are used to analyse the fracture toughness of two x-70 acicular ferrite, HSLA pipeline steels; the x-70 steels are to be used for the natural gas Alaska Highway pipeline to be built in 1980. It is well established that fracture toughness is a material property analogus to the yield strength and is equally important for pipeline design considerations.

At present, the Drop Weight Tear Test and the standard Charpy v-notch impact test are used as quality control tests to assess the toughness of the steel. Full scale burst tests have established minimum C_V and BDWTT values to protect against catastrophic brittle and ductile failure of the pipelines. Unfortunately, these tests do not provide any measure of the energy required for fracture initiation i.e. the fracture toughness of the material.

The Instrumented Impact Testing (IIT) method possesses the potential to solve this problem. It has

established its superiority over the conventional Charpy test for the following reasons:

i) It distinguishes between the fracture initiation energy and the crack propagation energy.

ii) It provides a measure of the dynamic fracture initiation event when a precracked Charpy specimen is employed.

Therefore, the fracture toughness determined by this method will be more conservative and may be more useful for fracture design.

However, to obtain greater insight into the fracture processes occurring during failure, it is also essential to investigate the static fracture toughness by using conventional low strain rate testing. This approach also has an advantage in that it utilizes a full wall thickness for the test specimens.

The objectives of the present study were:

1) To further characterise the low strain rate fracture toughness of the x-70 steels using LEFM and EPFM.

2) To compare the low strain rate fracture toughness with dynamic fracture toughness data to

determine the value of the rapid inexpensive IIT test for assessing fracture toughness.

The theoretical background of the elastic plastic fracture mechanics and the limitations of the linear elastic fracture mechanics are outlined in this study with a view to examining the applicability of the various fracture toughness testing techniques to the study of HSLA structural steels.

2. PIPE LINE MATERIALS

2.1 Introduction:

Pipelines are economical, reliable systems for transporting energy resources from distant fields, particularly those located in the most severe arctic and submarine environments, such as Siberia, in frigid northern parts of Canada or Alaska, and the North Sea, to the populated markets[1].

To meet the challenge set by the whims of nature, it is necessary for the production of a new class of steels with an unprecedented combination of qualities.

1. Strength - for walls that are thinner, yet more rugged in performance.
2. Toughness - for resistance to fracture at sub-zero temperatures.
3. Field weldability - with resistance to cracking with little or no preheat.
4. All at the lowest possible cost per unit of strength.

The answer to these problems is the evolution of a high strength, low alloy (HSLA), Acicular Ferrite (AF) steel having a yield strength of from 70 to 80 ksi (480 - 550 MPa), a Charpy upper shelf energy of well over 115ft-lb (155 Joule) and a FATT of -60^{o} C.[2]

2.2 Metallurgy of Acicular Ferrite Steels

Acicular ferrite is defined as a highly substructured, non-equiaxed phase that forms on continuous cooling by a mixed diffusion and shear mode. The transformation begins at a temperature slightly higher than the upper bainite transformation range. Acicular ferrite is different from bainitic ferrite; the prior γ - grain boundary network is retained in bainitic structures, but not in acicular ferrite structures. This factor contributes towards higher impact toughness since there are no straight, high angle boundaries to become embrittled by precipitates or segregated impurities [3].

The high strength of the material can be attributed to three strengthening mechanisms.

1. Grain Refinement
2. Dislocation Substructure
3. Precipitation strengthening by Nb(C,N) Niobium Carbonitride.

2.2.1 Effect of Alloy Additions:

Carbon: New steel making practises have been adopted to limit the carbon content to approximately 0.05%; in order to achieve improved weldability and formability. Increasing

the carbon, though it increases the yield strength, impairs the toughness by increasing the transition temperature and lowering the upper shelf energies. This is due to the formation of an increasing amount of cementite. Since about 0.01 to 0.02 % C is adequate to facilitate precipitation strengthening, a higher carbon level is undesirable in acicular ferrite steels.

Molybdenum and Manganese: The combination of molybdenum (0.25 - 0.50 wt %), manganese (1.50 - 2.25 wt %) and to a lesser extent niobium (0.05 wt %) suppresses the transformation temperature of $\gamma \rightarrow \alpha$ to below 700 ^{o}C. The fine grain α structure is ensured by having a fine γ grain as well. The result is a fine grained (ASTM No. 13 to 14) acicular ferrite microstructure. This exceptionally fine grain size, provides the basic building block for both the high strength and the excellent thoughness[4].

Further, molybdenum decreases the rate of Nb(C,N) precipitation in austenite and thereby allows a greater amount of Nb(C,N) in ferrite. This precipitation process results in a higher strength product. Manganese plays a role similar to that of molybdenum.

Niobium: Niobium is a potent micro alloy that improves the steel through three mechanisms.

i) It refines the austenite and ultimately the ferrite grain structure during rolling by inhibiting re-crystallization and grain growth.

ii) It suppresses the nucleation of polygonal ferrite

iii) Finally, it increases strength by precipitation of ultrafine particles of niobium carbonitrides or Nb-C-N clusters during cooling from the finish rolling temperature.

Sulphur: A very low sulphur, of the order of less than 0.005 wt %, is desirable in acicular ferrite steels. Higher sulphur contents impair the impact strength, particularly in the rolling direction (T-L) through the formation of MnS stringers. The detrimental effect of sulphide inclusions can be minimized through the additions of rare earth elements which change the morphology of the sulphides from elongated ribbons to globular equiaxed spheroids[5]. The presence of equiaxed sulphides ensures adequate toughness and reduces the anisotropy in toughness of the processed steel. These steels are often killed with Al and a reduced amount of Si (0.05 to 0.17 wt %) as silicon greater than 0.17 wt % reduces the impact resistance[6].

2.2.2 Mill Production Parameters:

The process control applied during hot-rolling is

extremely important to achieve a favourable balance between the strength and the toughness. The rolling parameters found to be most influential are the slab reheat temperature and the total reduction below 900 °C and to some extent, the finish rolling temperature.

The slab reheat temperature is important for two reasons:

1. It determines the degree of solutionising of Nb(C,N) in γ.
2. It also determines the γ - grain size at the beginning of rolling.

A low slab-preheat temperature of approximately 1150 °C gives rise to a smaller γ - grain size and some undissolved Nb(C,N) particles. During hot rolling γ recrystallizes, but the subsequent grain growth is inhibited by the undissolved Nb(C,N) particles which restrict grain growth. As a result, after several cycles of recrystallization, the γ - grain structure becomes extremely fine. A decrease of the Fracture Appearance Transition Temperature (FATT) from 5 °C to - 90 °C has been reported as the reheat temperature is lowered from 1140 °C to 1030 °C.

As the niobium containing steels do not recrystallize below about 980 °C during hot rolling there is an ever increasing

accumulation of strain in the γ as the rolling is continued in the lower temperature range. This in turn results in heavy deformation of fine grained γ introducing a heavily dislocated structure. This structure provides more sites for the subsequent nucleation and growth of a fine grained ferrite. The heavy deformation of the γ - phase also suppresses the γ - α transformation temperature. The minimum rolling temperature is controlled to ensure that no deformation of the ferrite phase occurs as this would impair the toughness of the final product.

In general, decreasing the slab reheat temperature to limit grain growth, decreasing the finish rolling temperature to limit γ recrystallization and increasing the percentage of reduction in the late rolling stages (to enhance substructure strengthening) results in a more refined ferrite grain structure, thereby improving the strength and toughness of the steel.

2.3 Pipe Fabrication and Strength of Skelp

In testing the strength and toughness of the pipe, the test conditions are important. The usual method is to cut a piece from the curved pipe wall. This piece is flattened prior to specimen fabrication and testing. The flattening introduces a Baüchinger effect that causes the measured yield strength to

be lower than the true yield strength of the pipe. The difference between the measured yield strength of the plate and the fabricated pipe is equal to the strength increase due to the work hardening resulting from the spiral forming of the pipe minus the Baüchinger effect [3].

One of the most important advantages of the acicular ferrite Mn-Mo-Nb steels over the conventional ferrite - pearlite pipe steels is that the yield strength of the acicular ferrite increases continuously with additional pipe processing particularly during cold expansion of the pipe. This means that rapid work hardening takes place during the fabrication of the plate into the pipe. As the amount of work hardening is very large in the acicular ferrite steels and very small or nil in the conventional ferrite - pearlite steels, the net effect of converting skelp into pipe is an increase in the strength of the acicular ferrite steels and a decrease in the strength of the ferrite - pearlite steels.

3. THE BASIS OF DESIGN FOR PIPELINES

3.1 Strength Considerations:

Economy in extracting energy resources requires the use of larger diameter pipelines which can operate at higher pressures. This will maximise the output and reduce the operating costs over the life of the line-pipes[7]. The higher operating pressures and the larger diameters necessitate the use of thicker pipe walls or higher strength material; this is evident from the following Hoop Stress, relationship[8].

$$\sigma_H = \frac{PD}{2t} \qquad \ldots\ldots (3.1)$$

Where P = Operating pressure

D = Inside diameter of the pipe

t = Pipe wall thickness

There are limitations to the pipe wall thickness due to:

1) Restrictions imposed by mill facilities.

2) The toughness requirement of a pipeline .

3) Difficulties in retaining high strength and toughness in very thick plate.

4) Additional problems in welding and field inspection.

The modern trend in line-pipe projects is to use higher strength steel pipes. The idea behind this is essentially economic, and is related to the materials savings realised by using a reduced pipe wall thickness and the increased capacity obtained through using larger diameters and higher pressures.

The current natural gas pipeline projects are committed to x-70 pipe because it is available as a proven product. The future generation of frontier projects aim towards using higher strength steel than x-70 to increase the output and reduce the cost of the line-pipe [9].

However, the improved pipe yield strength and or higher wall thickness only ensure that the line can operate at a particular pressure. The yield strength does not guarantee the integrity of the line with respect to arresting a propagating fracture [7].

3.2 Fracture Control Design:

The modern trend in line-pipe specifications is concerned with increasing the fracture resistance. Extensive fracture research has been conducted by many segments of the industry to prevent the catastrophic brittle failure of gas transmission pipelines [10] or ductile tearing of oil pipelines [9]. Such failures cause a loss of production and at the same time a significant amount of money is required for damage repair. The social and economic implications of these failures have motivated an increased awareness for the development of fracture toughness parameters for pipelines.

The basic fracture control philosophy considers the following three factors [2, 7, 9 - 12]:

1. To prevent brittle fracture propagation by assuring that the pipelines operate above the ductile-to-brittle transition temperature of the material.

2. To prevent ductile fracture initiation by specifying a minimum toughness for a pipe operating at a specific stress level.

3. To control ductile crack propagation by specifying some average toughness that will assure self-arrest.

These criteria should be fulfilled for the minimum design temperature.

Continuing research in this area is being conducted at the Battelle Columbus laboratories under the sponsorship of the American Gas Association. Workers at the Battelle laboratories have evolved fracture control guidelines for pipe which have been adopted by virtually all of the pipeline industries in the world.

3.2.1 Design Criteria for Preventing Brittle Fracture:

Twenty years ago, no consideration was given to the fracture resistance or notch toughness of pipe with the result that pipe commonly operated below its nil-ductility temperature (NDT). The occurrence of very long brittle fractures (one of up to 13 Km [11]) led to the realization that brittle

fracture travelled faster than the decompression velocity of the gas in the gas transmitting line.

The Battelle Drop Weight Tear Test (BDWTT) is used to establish the resistance of the pipe steel to brittle fracture [2, 13]. The test specifies that at the lowest design operating temperature, the pipeline should exhibit 85% shear to ensure that ductile fracture mechanisms are operative. However, for any individual test 60% shear is acceptable.

3.2.2. Design Criteria for Ductile Fracture Initiation Control:

Various fracture mechanics concepts and tests have been developed for assessing ductile fracture initiation. The general objective is to determine the critical stress intensity factor (K_c), which is a measure of the material toughness and which can be related to the critical defect size that causes ductile fracture initiation.

The Battelle Static loading full scale burst studies generated an empirical formulae which relates

a critical crack size with the Charpy upper shelf energies (11 - 14) as given below:

$$\frac{K_c^2 \pi}{8a \sigma_{f2}} = \ln \text{Sec} \left(\frac{\pi M_H \sigma_H}{2 \sigma_f} \right)$$

Where $K_c^2 = \frac{12 E C_v}{A_c}$

K_c = Fracture Toughness parameter

C_v = Impact test absorbed energy (ft-lb), J)

A_c = Specimen fracture area (inch^2, mm^2)

$2a$ = Critical through wall defect length (inch, mm)

σf = Flow stress = Y.S. + 10,000 psi (68.95 MPa)

M_H = Folias Correction factor, a function of $\frac{2\sqrt{2a}}{\sqrt{Dt}}$

d = Pipe diameter, (inch, mm)

t = Wall thickness, (inch, mm)

σ_H = Failure Hoop Stress = $\frac{PD}{2t}$ (psi, MPa)

E = Elastic Modulus (psi, MPa)

This equation is widely used in the pipeline industry to predict the allowable defect size for arresting ductile crack initiation. However, it should be noted that this equation is applicable only over the temperature range of the Charpy upper shelf. Furthermore

it is formulated for static loading conditions and is based upon crack initiation along the pipe axis. In practice, initiation may occur under dynamic loading conditions arising from impacts due to mechanical damage.

For design purposes, pipeline companies calculate the critical crack size that would be detected as a leak during hydraulic proof testing or from NDT technique and then determine from equation (3.2) the minimum Charpy upper shelf energy necessary to prevent the initiation of such a crack.

3.2.3 Design Criteria for Ductile Fracture Propagation and Arrest:

It was originally believed that unstable propagation of a shear fracture would not occur as most shear fractures were arrested over short distances (9, 12). This may be true because the speed of fracture propagation reduces as the gas in the pipeline escapes thereby lowering the stress at the tip of the fracture. However, recent pipeline failures indicate the occurrence of at least eight shear fractures of 100 m or

more in length in the U.S.A. and Canada.

Therefore, to prevent such a failure it was necessary to determine the toughness level sufficient to arrest a propagating ductile fracture.

The Battelle research group suggested that the Charpy v-notch energy was adequate for specifying a material's resistance to ductile failure [2, 11, 13]. From full scale crack propagation studies, a relationship was established to show the minimum Charpy energy required to provide fracture arrest in large diameter pipelines.

$$C_v = 0.0873\ \sigma_H^2\ (Rt)^{1/3}\ A_c \quad \text{(ft - lb, J)} \qquad \ldots\ldots\ (3.3)$$

Where σ_H = Operating stress level = 0.8 σ_{ys} specimen minimum yield stress SMYS (psi, MPa)

R = Pipe Radius (inch, m)

t = Pipe wall thickness (inch, m)

A_c = Area of Charpy specimen ligament ($inch^2$, m^2)

An energy level of 80 ft - lb (108 J) is often used in pipeline steel specifications as an all heat

average toughness value to prevent ductile fracture. Unfortunately, the above relationship has not always correlated well with results from larger diameter (over 42 inch, 107 cm) higher strength (over - 65 grade) and heavier wall pipe [11 - 13]. For AF steels, it is impossible to accurately specify the toughness requirements for ductile failure arrest [13].

3.3 Review of the Design for Fracture Control:

To meet the toughness requirements the pipeline manufacturers carry out the BDWTT and the standard Charpy v-notch tests with specimens having their crack orientations parallel to the pipe axis; this is done because the peak stress is the Hoop stress and this stress opens up the crack along this direction. But pipe steels which are not properly desulphurised or rare earth treated may exhibit anisotropy in mechanical properties especially toughness [15]. Hence for spiral welded pipe minimum toughness properties that are less than the specified minimum, may be obtained for directions other than that parallel to the pipe axis. The lowest toughness would be expected to lie along a direction parallel

to the rolling direction i.e. (T - L) orientation. Hence the measurement of fracture toughness is required in various orientations to establish the weakest crack initiation condition; that combination of toughness and stress that results in a minimum initiation energy should be used to decide the necessary specification condition.

Materials specification is based on maintaining BDWTT of 85% shear and a minimum C_v of 50 ft - lbs (67.8 J) at the lowest operating temperature. The shear specification ensures ductile fracture initiation and the 50 ft - lbs (67.8J) C_v toughness ensures ductile fracture propagation. However, the standard Charpy v-notch test does not provide crack initiation information. The standard Charpy v-notch sample also uses a blunt notch which in no way represents a sharp crack condition as could be realized in service.

3.4 Instrumented Impact Test Approach:

Paul McConnell [15], in his M.A.Sc thesis, made an extensive study of the impact strength and fracture toughness of two acicular ferrite, HSLA

steels. His data will be used for comparison with the results of the present investigation. In evaluation of the fracture toughness of the material, the IIT technique has proven to be rapid and inexpensive. It remains to assess its validity with respect to other fracture toughness test procedures. Fracture toughness data is obtained from an IIT using a Charpy specimen which has been fatigue pre-cracked prior to fracture. The IIT test techniques provides a measure of the crack initiation energy and the crack propagation energy under impact loading. Since the ligament size is small, the measured propagation energy may not be a valid measure of extensive propagation; the combined initiation and propagation energy is equal to the C_v energy for a fatigue precracked specimen. Since this method determines the dynamic properties of the material, the fracture toughness data will be more conservative in the case of strain rate sensitive materials.

McConnell also points out that the present pipeline toughness specifications which require a minimum toughness in the longitudinal axis may be inadequate for fracture control if very low initiation

energies or toughness values less than the specified minimum, are present for a crack parallel to the rolling direction. For this reason he suggests that pipeline toughness specifications are necessary in all directions in the pipe especially in the weakest direction. The material toughness acceptance criteria should be based on the magnitude of the initiation energy from a precracked Charpy specimen as this simulates a sharp crack and therefore a peak stress intensity at the tip of the crack.

Although the fracture toughness calculations in the IIT method are based upon the initiation energy, the theoretical analysis of the process does not define clearly the initiation event. Fracture initiation is assumed to occur at the point of maximum load; this may or may not be a valid assumption. The IIT method gives only the dynamic fracture toughness values K_{Id}. Since the IIT method uses a 10mm x 10 mm square standard Charpy specimen, the stress intensity factor at the specimen crack tip may be different from that experienced at the tip of a defect in the thicker walled pipe. This is true in that no valid plane strain fracture toughness data can be produced at the

minimum operating temperature of the pipe; that is at $-18\ ^{o}C$, due to the pipe wall thickness limitations.

3.5 Project Summary:

A summary of the project proposal is given below:

1. The study is to measure the fracture toughness values of two acicular ferrite, HSLA pipe steels under static loading conditions; No fracture toughness values for these steels have been reported in the literature. This may be due to the fact that the reduced pipe wall thickness 0.54 inch (13.7 mm) makes it impossible to obtain valid plane strain fracture toughness, K_{IC} data for the range of operating temperatures. The fracture toughness data is to be obtained for the fracture path a) parallel to rolling direction i.e. the T-L orientation, b) transverse to the rolling direction i.e. the L-T orientation, and c) parallel to the pipe axis.

2. Both the linear elastic fracture mechanics (LEFM) K_{IC} and the elastic-plastic fracture mechanics (EPFM), J-Integral and COD approach will be utilised to determine the fracture

toughness values throughout the complete temperature range extending from lower shelf through the transition to the upper shelf energies.

3. The comparative study of the fracture toughness transition behaviour of both steels in each of the three test directions by the three test methods will provide complete information on the anisotropy of the toughness and transition behaviour.

4. The fracture toughness data obtained will be compared with reported IIT data for these steels to compare the static and the dynamic fracture toughness.

It is hoped that the analysis of the K_{Ic}, J_{Ic} and COD experimental data may contribute to a more fundamental basis for fracture control of the pipeline steels.

4. THEORY AND TEST PROCEDURES

4.1 Linear Elastic Fracture Mechanics

The fundamental principle of fracture mechanics is that the stress field at the tip of a crack in a structural component can be characterised by a single parameter, K, The Stress Intensity Factor. K is related to the magnitude of the applied nominal stress, 'σ' and the square root of the crack length 'a'. In general, the stress intensity factor is given by [16].

$$K = f(g)\, \sigma \sqrt{a} \quad \ldots\ldots\ldots (4.1)$$

Where $f(g)$ = a parameter that depends upon the specimen and the crack geometry. For example, $f(g) = \sqrt{\pi}$ for an infinite plate containing a through thickness crack of length 2a and subjected to a uniform tensile stress σ [17]. In this case the stress intensity factor reduces to

$$K = \sigma\sqrt{\pi a} \quad \ldots\ldots\ldots\ldots (4.2)$$

For mode I deformation, the crack surfaces are displaced perpendicular to each other in opposite direction. The corresponding stress intensity factor is represented by K_I.

In a thin sheet of metal under tensile loading, the stress at the crack tip in the thickness direction ($\sigma_{33} = 0$) tends to zero [18, 19]. A schematic distribution of the principle stresses at the crack tip is shown in Fig. 4.1. A biaxial state of stress exists which is commonly referred to as the Plane Stress Condition.

As the thickness of the sheet is increased the crack tip is subjected to a triaxial state of stress [18, 19] which severely restricts straining or plastic deformation through the thickness. Such a state of stress is known as Plane Strain.

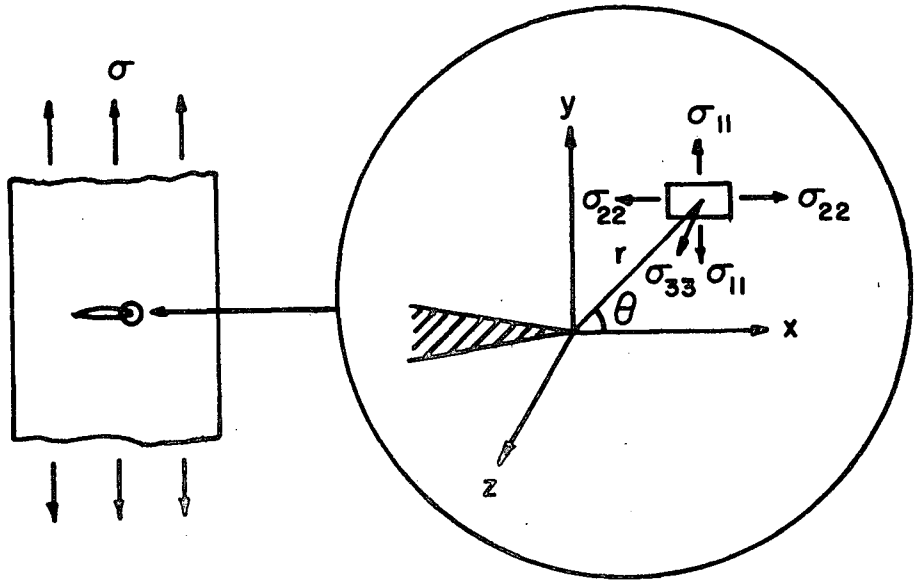

Figure 4.1. Distribution of principal stresses at the crack-tip.

When the stress-intensity factor at the crack tip reaches a critical value, K_c, unstable crack propagation, that is, fracture, occurs. The critical stress intensity factor for static loading under plane stress conditions is designated as K_c whereas K_{Ic} is the critical stress intensity factor for static loading conditions under mode I deformation and a plane strain. K_{Id} represents the critical stress intensity factor for dynamic (impact) loading and plane strain.

These critical values are described as the Fracture Toughness and represent a basic property of the material. From a knowledge of the K_I value for a structural component at service conditions (temperature and strain rate), a design engineer can estimate the flaw size that can be tolerated under a particular stress level (as equation 4.1).

4.1.1 Plane Strain Fracture Toughness:

The linear elastic fracture mechanics (LEFM) analysis can be used for determining K_{Ic} only for the cases where the crack-tip plastic zone is small in

relation to the specimen dimensions. For steels this occurs under the following conditions.

i) Relatively brittle material

ii) Testing at a low temperature, normally below the service temperature

iii) High rates of loading

iv) Thick structural component.

To determine a valid K_{Ic}, the specimen should fail under completely elastic plane strain conditions.

With thinner sections, the critical combinations of load and crack length at instability gives K_c. This K_c value decreases with an increase in thickness; a constant minimum value, K_{Ic}, is reached when plane strain conditions are attained. Therefore, K_{Ic} values are reproducible and are the minimum stress intensity factors. Hence it is termed the Plane-Strain Fracture Toughness property of a material and considered to be a material property analogus to the yield strength. The K_{Ic} value refers to quasi-static test conditions, that is it is determined at strain rates of approximately 10^{-5} / sec ; this corresponds to a stress intensity

rate, $\dot{K}$, of approximately 10 ksi $\sqrt{in}$ per second where

$$\dot{K} = \frac{K_{Ic}}{\text{Time to fracture}}$$

For strain rate sensitive materials increasing the loading rate to that corresponding to an impact test, that is approximately 10/sec ($\dot{K} = 10^5$ ksi $\sqrt{in}$/sec) at a constant temperature causes a decrease in the plane strain fracture toughness to a minimum value known as the Dynamic Fracture Toughness 'K_{Id}'. For example, HY-80 steel at a test temperature of - 184 ^{o}C (- 300 ^{o}F) exhibits a K_{Ic} = 67 ksi $\sqrt{in}$ at $\dot{\varepsilon}$ = 5 x 10^{-5} / sec and K_{Id} = 43 ksi $\sqrt{in}$ at $\dot{\varepsilon}$ = 20 / sec.[16].

4.1.2 Specimen Size Requirements:

Some brittle materials exhibit plastic deformation at the crack tip before unstable crack propagation takes place. This is shown by the non-linearity of the load-displacement test records. The question arises, what is the size of the plastic zone that can be allowed while still satisfying the elastic plain strain requirement.

The size of the plastic zone ahead of a crack

can be estimated from the equation for the elastic stress-field distribution at the crack tip (Fig. 4.1) at (r,θ) position in y - direction.

$$\sigma_y = \frac{K_I}{\sqrt{2\pi r}} \cos\frac{\theta}{2} \left(1 + \sin\frac{\theta}{2} \sin\frac{3\theta}{2}\right) \quad .. \quad (4.3)$$

For θ = o, along the x-axis

$$\sigma_y = \frac{K_I}{\sqrt{2\pi r}} \quad ..... \quad (4.4)$$

Considering $\sigma_y = \sigma_{ys}$ = yield strength of the material at the test temperature and strain rate employed, the extent of yielding at the crack tip is

$$r_y = \frac{1}{2\pi} \left(\frac{K_I}{\sigma_{ys}}\right)^2 \quad ..... \quad (4.5)$$

At instability $K_I = K_c$, and therefore the plastic zone size under plane-stress conditions is

$$r_y = \frac{1}{2\pi} \left(\frac{K_c}{\sigma_{ys}}\right)^2 \quad .....(4.6)$$

Under plane strain conditions the plastic zone radius at the center of a plate where the maximum constraintis realized, is equal to $^1/3$ of this value (20), that is

$$r_y = \frac{1}{6\pi} \left(\frac{K_{Ic}}{\sigma_{ys}}\right)^2 \quad ..... \quad (4.7)$$

The major dimensions of the plate specimens for K_{Ic} testing are:

a = crack length

B = thickness

and w-a = uncracked ligament (w = overall depth)

After considerable experimental work [21], the following minimum specimen size requirements have been established to ensure elastic plane-strain behaviour:

$$a, B, w - a \geq 2.5\left(\frac{K_{Ic}}{\sigma_{ys}}\right)^2$$

Thus, it is observed that specimens satisfying the above requirements will have a thickness = 50 times the radius of the plastic zone size.

4.2 Elastic - Plastic Fracture Mechanics

In the previous section, it has been shown that LEFM is applicable only to those situations where crack propagation is accompanied by little or no plastic deformation. Quantitatively this means that the extent of crack tip plasticity should be at least fifty times smaller than the dimensions of the structure including the crack length. Almost all low to medium strength and HSLA structural steels that are used for large complex structures such as bridges, ships, pressure

vessels etc. are of insufficient thickness to maintain the plane strain conditions at the temperature and strain rate of the service conditions. Hence in such applications insufficient constraint is available to maintain plane strain conditions and a large plastic zone forms.

For pipe steels, neither the specimen nor the structure (the pipe) is amenable to LEFM analysis. This is shown clearly in Fig. 4.2 in which are shown typical schematic load-deflection curves for small specimens of various materials. Fig. 4.2 (a) depicts fully linear behaviour which is easily handled by LEFM; Fig. 4.2 (b) shows a "Pop-in" behaviour which characterises the initial crack growth, for a given material, regardless of the specimen thickness. Here, LEFM can also be used to calculate K_{Ic} by the offset procedure as described in the ASTM standard E-399-74;Fig. 42 (c) shows considerable non-linear behaviour in the load-deflection curve prior to sudden failure; while Fig. 4.2 (d) shows the behaviour of a ductile material where sudden failure never occurs. These non-linearities can arise from two sources, plastic deformation at the crack tip and

stable crack extension [22]. Therefore, the test behaviour described in Fig. 4.2 (c) and (d) are the subject matters of Elastic-Plastic Fracture Mechanics (EPFM). In recent years considerable work [16, 22, 24, 28, 30 - 35] has been reported on the development of EPFM analyses as an extension of LEFM analyses.

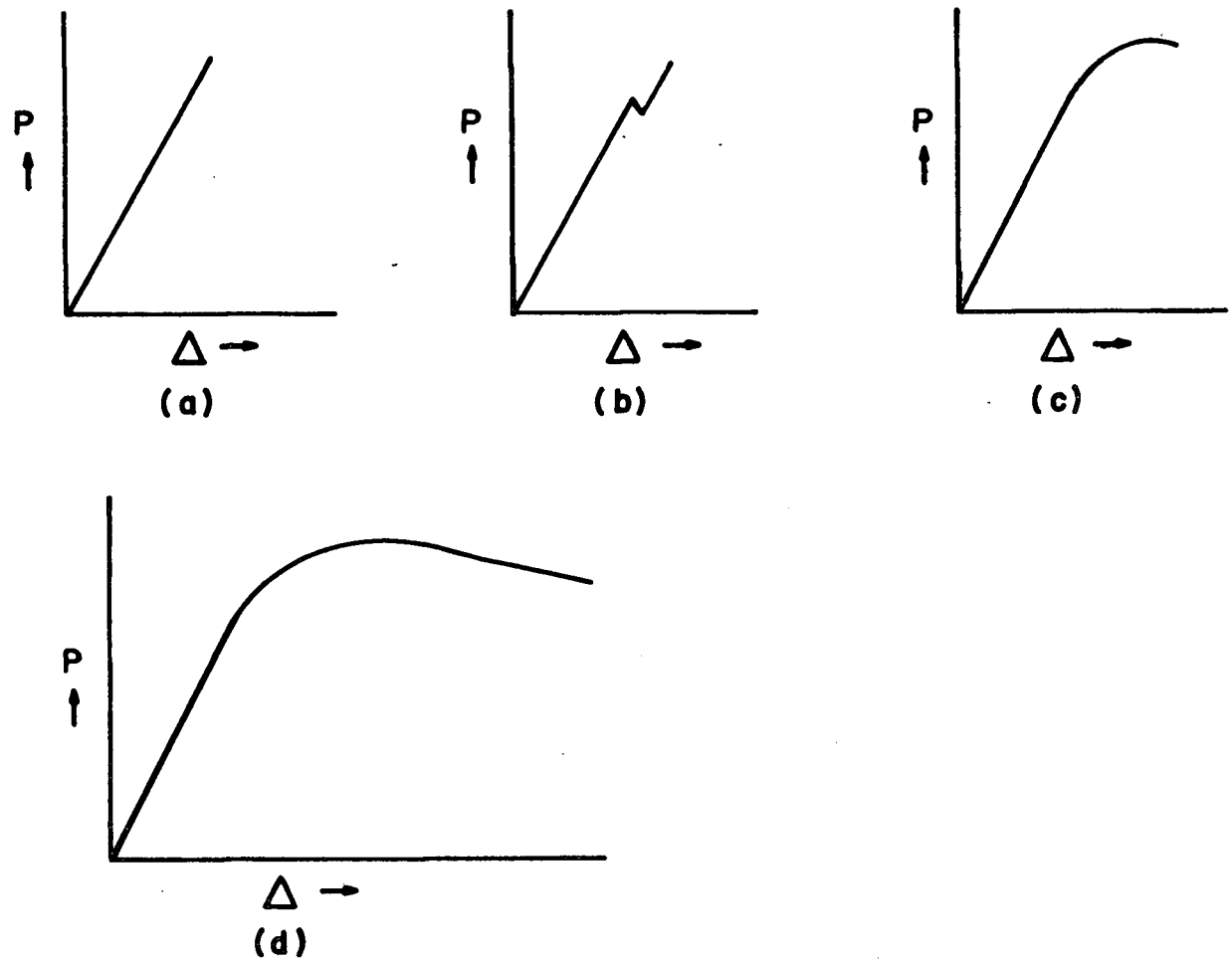

Figure 4.2 Schematic Load (P) vs. Load-point displacement(Δ) curves for
(a) perfectly elastic material.
(b) elastic material with pop-in behaviour.
(c) elastic then plastic behaviour.
(d) ductile material with extensive plasticity prior to failure.

The two most promising and widely accepted techniques for analysing elastic-plastic fracture are

1. The J-Integral Method
2. The crack opening Displacement (COD) Method.

4.2.1 The J-Integral Approach:

The J-Integral, as proposed by Rice [23], is a way of characterising the stress-strain field ahead of a crack tip by an integration path such that

J_1 at a distant field = J_2 at the tip of the crack

where $$J = \int_{\Gamma} w\,dy - Ti \left(\frac{\partial u}{\partial x}\right) ds \quad \ldots\ldots\ldots (4.8)$$

$\Gamma = a$ contour travelling counterclockwise around the crack tip

Ti = the tension vector perpendicular to Γ in an outward direction

Ui = displacement in x - direction

ds = an element of Γ

$w = \int_0^{\varepsilon} \sigma_{ij}\, \varepsilon_{ij}$ (Strain Energy density for elastic materials)

Therefore, even if considerable yielding occurs near the crack tip, the region away from the crack tip can

be analysed and the condition in the crack tip region can be derived.

Later, Hutchinson[24] and Rice and Rosengren[25] described a stress-strain distribution around a crack tip surrounded by a plastic strain field. They developed a model known as the HRR crack tip model which establishes that J is the amplitude of the near field singularity at the crack tip. McClintock[26] has also shown that by combining J with the HRR crack tip model, the near tip values of stress and strain can be expressed as a function of J. This is directly analogus to the stress field equation of LEFM.

Rice[27] has also shown that the J-Integral may be interpreted as the difference in potential energy between two identically loaded bodies with differing crack lengths. This is stated mathematically as

$$J = - \frac{dU}{da} \quad \ldots\ldots\ldots (4.9)$$

where U = the potential energy

where a = crack length

For the linear elastic behaviour and also for small scale yielding, J is therefore equal to G, the strain energy release rate per unit crack extension, i.e. the crack driving force. In cases where the deformation is not reversible that is the general elastic-plastic problem, J loses its physical significance as a crack driving force. Begley and Landes [28] suggest that J is still equal to $-\frac{dU}{da}$ and the physical significance of J for elastic-plastic materials is that J is a measure of the characteristic crack tip elastic-plastic field similar to K in LEFM. They made the additional suggestion that the J_{Ic} fracture criterion applies to crack initiation rather than propagation and is limited to the case of plane strain which is denoted by the subscript I in J_{Ic}.

Later Rice et al [29] developed a simple, single specimen technique for measuring J_I using the expression

$$J_I = \frac{2A}{B\,(w-a)} \quad \ldots\ldots \quad (4.10)$$

where A = Area under the load vs load-point displacement curve

B = Specimen thickness

a = Crack length

In this technique, a bending load is applied to a bar or compact tension specimen containing a deep notch crack $\frac{a}{w} \geq 0.6$ and J_I is determined as a function of the load-point displacement. The critical value of J_I is then J_{Ic} which refers to that value of J_I at which crack initiation takes place.

Once the J_{Ic} value is determined, the corresponding K_{Ic} values can be computed from the relationship between the elastic-plastic and the LEFM parameters [28, 30, 31].

$$J_{Ic} = G_{Ic} = \frac{1 - \nu^2}{E} K_{Ic}^2 \quad \ldots\ldots (4.11)$$

Where ν = Poisson's Ratio

E = Young's Modulus

4.2.1.1 Experimental Technique:

Several experimental techniques have been reported [30 -33] for determining the point of crack initiation in a static J-Integral test. These are

1. Heat Tinting (J-Resistance curve)
2. Compliance

3. Ultrasonic

4. Electrical Potential

5. Resonance Frequency

The heat tinting method is simple and requires less sensitive electronic equipment in comparison with the other test methods. This is the reason why this method has been selected for the present investigation.

This method is also known as the Resistance curve technique. It has been developed by Landes and Begley [30]. Briefly the testing procedure involves:

a) Loading each specimen to a different displacement value

b) Unload each specimen, mark the crack extension by heat tinting the crack. Heat tinting of steels is done by heating the specimen at 320 °C for 10-20 minutes.

c) Pull the specimen apart and measure the crack extension

d) Construct a resistance curve by plotting J for each specimen vs its corresponding crack extension.

In order to find out the J_{IC} value from the resistance curve Landes and Begley suggested the use

of a best fit line to the J vs crack size curve. The point of intersection of this curve with the line $J = 2\ \sigma_{flow}\ \Delta a$ gives the value of J_{Ic},

$$\text{where } \sigma_{flow} = \frac{\sigma\text{yield stress} + \sigma\text{UTS}}{2} \quad \ldots\ (4.12)$$

at the test temperature and loading conditions. This is the most widely used method. The only disadvantage of this method is that it requires several specimens usually 4 to 6 to draw the resistance curve. Currently, ASTM is preparing a standard for J-Integral testing.

4.2.1.2 Validity Criteria:

Landes and Begley [30, 34] have proposed a size requirement which must be satisfied by an elastic-plastic fracture toughness test specimen to obtain valid J_{Ic} data. This size requirement is stated analytically as

$$a,\ B,\ w-a \geq 25\ \frac{J_Q}{\sigma_{flow}} \quad \ldots\ (4.13)$$

If this condition is satisfied, then J_Q becomes J_{Ic}.

4.2.2 The Crack-opening Displacement Method:

For low to medium strength steels extensive

plastic flow takes place before the initiation of the fracture. Under an externally applied load, the two faces of the crack tip move apart without an increase in the length of the crack [36]. The relative movement of the two faces at the crack tip has been termed the Crack-opening Displacement (COD) and has been designated as 'δ' [37].

The consequence of yielding at the crack tip giving rise to physical displacement of the crack surfaces was first applied as a possible fracture criterion by Wells [38].

4.2.2.1 COD as an Extension to LEFM:

For a material that exhibits appreciable crack tip plasticity, it is possible to develop a relationship between the stress intensity factor K and δ near the tip for the crack tip opening displacement. The size of the plane stress plastic zone may be approximated by the relation

$$r_y = \frac{1}{2\pi} \left(\frac{K}{\sigma_{ys}}\right)^2 \quad \ldots\ldots\ldots \quad (4.14)$$

Where r_y = the extent of the plastic zone along the crack plane

σ_{ys} = yield strength of the material in a uniaxial tensile test.

With this corrected crack border model, the y direction displacement, 'η', within the crack at any distance 'r' from its tip may be evaluated using Westergaard's expression [38].

$$\eta = \frac{2K}{E}\sqrt{\frac{2r}{E}} \quad \ldots\ldots\ldots \quad (4.15)$$

Now the displacement at the elastic-plastic interface corresponds to the displacement at the tip of the crack. Therefore, the crack opening displacement near the crack tip is

$$\delta = 2\eta = \frac{4K}{E}\sqrt{\frac{2r_y}{\pi}} \quad \ldots\ldots\ldots \quad (4.16)$$

Combining the equation for ry (4.14), the plastic zone size and the relationship $\frac{K^2}{E} = G$, (4.16) gives rise to

$$\delta = \frac{4G}{\pi\sigma_{ys}} \quad \ldots\ldots\ldots \quad (4.17)$$

This relationship was developed by Wells [38]. He inferred that under local plastic conditions, COD gives a measure of the crack extension force G. Thus the COD can be related to the plane-strain fracture toughness. This also indicates that if the COD is large for a specified value of yield stress such that $\sigma_{ys}\delta$ exceeds the critical crack extension force G, then

fracture follows [39]. Hence the COD measurement in the presence of extensive plastic deformation ahead of the crack tip for elastic-plastic and fully plastic behaviour, is an index of the fracture toughness and is a direct extension of LEFM into yielding materials.

4.2.2.2 Dugdale's Model:

Dugdale [40] proposed a strip yield model as shown in Fig. 4.3. This model describes the extent of yielding ahead of a crack as a function of the external load. A thin sheet containing a straight cut of length $2a$ is loaded in a direction perpendicular to the cut. It is assumed that yielding occurs ahead of the cut by an extent $a_1 - a$ and is confined to a narrow band lying along the line of the cut. This model also suggests that the stresses in the yielded zone may be considered to be a continuous distribution of point loads $\sigma_{ys}.dt$ per unit thickness which act to restrain the crack from opening.

An expression for the restraining stress intensity factor may be obtained by integrating the appropriate Westergaard Stress function for point

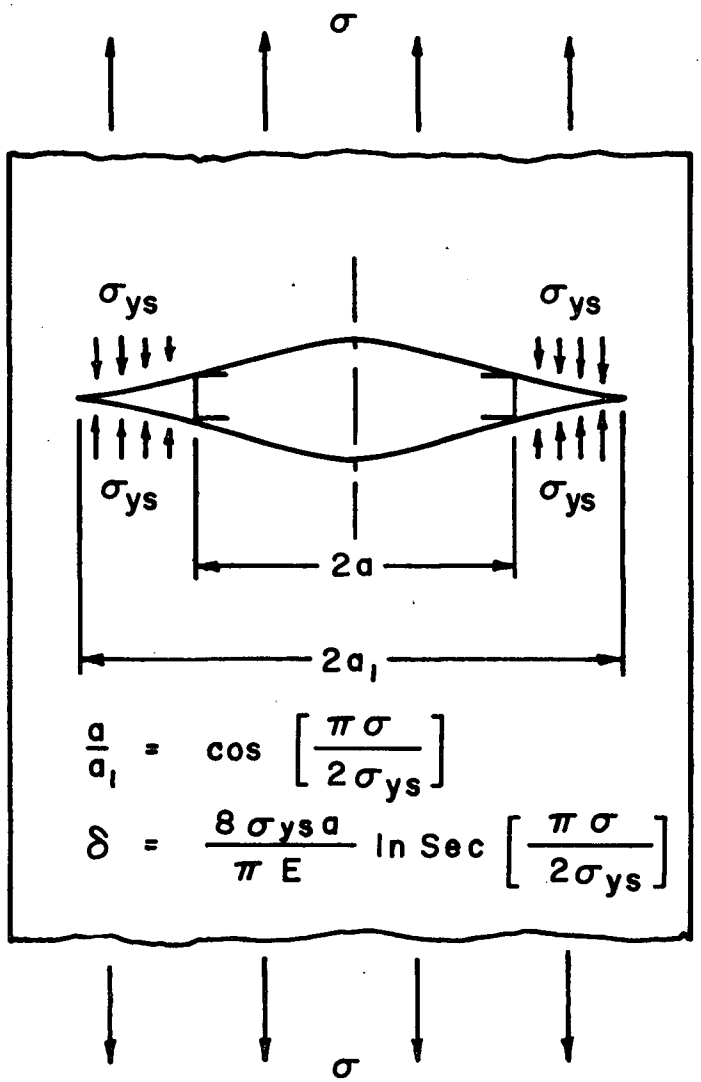

Figure 4.3. Dugdale's Strip Yield Model.

loads in cracks from a to a_1 which gives

$$K = 2\,\sigma_{ys}\left(\frac{a_1}{\pi}\right)^{\frac{1}{2}}\ \mathrm{Cos}^{-1}\ \left(\frac{a}{a_1}\right) \quad \ldots\ldots (4.18)$$

Where the stress intensity factor for the opening of the crack under the applied stress σ and the total crack length a_1 is

$$K = \sigma\sqrt{\pi a_1} \quad \ldots\ldots (4.19)$$

Therefore, the extent of yielding may be given by

$$\frac{a}{a_1} = \mathrm{Cos}\ \frac{\pi\sigma}{2\,\sigma_{ys}} \quad \ldots\ldots (4.20)$$

Dugdale's analysis also suggests that the displacement at the original crack tip, the COD - δ, increases as the crack length increases or as the applied loading increases. Hence an extension of Dugdale's analysis results in the following relationship between COD, the crack length a, and the applied stress :[37,41]

$$\delta = \frac{8\,\sigma_{ys}a}{\pi E}\ \log_e\ \mathrm{Sec}\left(\frac{\pi\sigma}{2\,\sigma_{ys}}\right) \quad \ldots (4.21)$$

Using a standard method of series expansion due to McLaurin[16] this expression gives:

$$\delta = \frac{8\,\sigma_{ys}\,a}{\pi E}\left[\frac{1}{2}\left(\frac{\pi}{2}\,\frac{\sigma}{\sigma_{ys}}\right)^2 + \frac{1}{12}\left(\frac{\pi}{2}\,\frac{\sigma}{\sigma_{ys}}\right)^4 + \frac{1}{45}\,\frac{\pi}{2}\left(\frac{\sigma_{ys}}{\sigma_{ys}}\right)^6 + \ldots\ldots\right] \qquad \ldots\ldots(4.22)$$

For $\sigma/\sigma_{ys} \ll 1$, taking only the first term of the series

$$\delta = \frac{\pi\sigma^2 a}{E\,\sigma_{ys}} \qquad \ldots\ldots (4.23)$$

Since $K_I = \sigma\sqrt{\pi a}$, the above expression can be written as

$$K_I^2 = \delta\, E\, \sigma_{ys} \qquad \ldots\ldots\ldots (4.24)$$

or,
$$\frac{\delta}{\varepsilon_{ys}} = \left(\frac{K_I}{\sigma_{ys}}\right)^2 \qquad \ldots\ldots\ldots (4.25)$$

$$\text{as} \quad E = \frac{\sigma_{ys}}{\varepsilon_{ys}}$$

At the onset of crack instability where K_I reaches K_{Ic}, the COD reaches a critical value, δ_c,

$$\frac{\delta_c}{\varepsilon_{ys}} = \left(\frac{K_{Ic}}{\sigma_{ys}}\right)^2 \qquad \ldots\ldots\ldots (4.26)$$

This expression shows that $\frac{\delta_c}{\varepsilon_{ys}}$ is a measure of the critical crack size in a structure exhibiting elastic-plastic behaviour. Therefore, the crack opening displacement, δ_c, is a material property like K_{Ic} and is a function of the test temperature and loading rate.

The advantages of using the COD approach are:

i) The COD values can be measured throughout the entire span of the plane strain, the elastic-plastic and the fully plastic regions.

ii) A much smaller size test specimen is required. The K_{Ic} values can be measured only under plane strain conditions and often require the use of a prohibitively large size specimen.

4.2.2.3 Experimental Determination of COD:

Several authors [36, 37, 39, 42 - 44] have described different techniques for the experimental determination of COD. However, the British Standards Institution Draft for Development 19:1972 [45] is the only document which gives the details of a recommended procedure for COD testing. The DD19 test method is very similar to the ASTM E399-74 test method for K_{Ic}. Similar specimen preparation, fatigue precracking procedures, and instrumentation and test procedures are followed. The displacement gauge is similar to the one used in K_{Ic} testing and a continuous load-displacement record is obtained during the test.

Egan's [39] evaluation of the fracture

toughness of materials using the COD technique shows that a single specimen test procedure may be used to determine both K_Q and δ_c.

From the load-displacement curve, the critical value of displacement is recorded at the point where a specified amount of crack growth has occurred. In the British Standard Test Procedure, the crack opening displacement is usually calculated by assuming that plastic extension has occurred at the crack tip up to the point of maximum load. This assumes that crack extension initiates at the maximum load. The critical displacement at the tip of the crack δ_c - COD is determined from the critical value of the clip gauge displacement, V_g, as obtained from the P-Δ record. DD19 suggests several methods for obtaining δ_c. All of these methods assume that deformation occurs by a hinge mechanism about a center of rotation at a depth of r(w-a) below the crack tip. The relationship between the clip gauge displacement V_g and δ_c is:

$$\delta_c = \frac{V_g}{1 + \frac{a+z}{r(w-a)}} \qquad \ldots\ldots (4.27)$$

Where Z = Knife edge thickness i.e. the distance above the test piece surface at which point the measurement is made

a = crack length

w = test piece width

r = rotational factor

T. Ingham et. al [46] suggested that on the basis of tests on a wide range of materials and geometries that a fixed value of $r = \frac{1}{3}$ can be used to obtain conservative values of COD. Several works (Robinson and Tetelman [44], R.R.Barret et. al [47]) confirm this viewpoint.

4.2.2.3.1 Determination of δ_c:

The British Standard method of using the maximum load point for calculating the critical COD-δ_c, has been criticised [48]. This may be due to the fact that δ_c is defined as the value of COD which should correspond to the onset of stable crack growth - similar to J_{Ic} in the J-Integral approach. It should be noted that in K_{Ic} testing, the crack initiation load P_Q is taken to be the load corresponding to 2% beyond the yield point.

Several methods have been suggested for detecting the δ_c value associated with the onset of stable crack growth. Smith and Knott's [49] technique involves loading several specimens to various stages on the load-deflection curve followed by unloading. The extent of crack growth in each specimen is then marked by heat tinting. The crack growth value is plotted against crack opening displacement. The displacement associated with the onset of cracking δ_c is obtained by extrapolating the crack extension back to zero. This method is the same as that used in determining J_{Ic}. Diesberg [48] has calculated δ_c on the basis of a maximum stretch zone. He has defined this COD as the crack-opening stretch value, COS. with the help of the relations

$$\delta_c = COS = \frac{8\ \sigma_{ys} a}{\Pi E} \log_e \text{Sec} \left(\frac{\Pi\sigma}{2\sigma_{ys}}\right) \quad \ldots(4.28)$$

$$\frac{a}{a+\nabla a_c} = COS \frac{\Pi\sigma}{2\sigma_{ys}} \quad \ldots\ldots\ldots(4.29)$$

and $$J_{Ic} = 2\ \sigma_{flow}\ \Delta a_c \quad \ldots\ldots\ldots\ldots(4.30)$$

and experimental values of J_{Ic}, he has determined the COS value. His COD values were much lower than those obtained by assuming that the crack initiated at the

point of maximum load.

4.2.2.3.2 Evaluation of an Equivalent K_{Ic} from COD:

From linear elastic fracture mechanics

$$G = \frac{K_{Ic}^2}{E}(1 - \nu^2) \qquad \text{.....(4.31}$$

and from Well's treatment for the critical value of COD

$$\delta_c = \frac{4}{\Pi}\frac{G}{\sigma_{ys}} \qquad \text{.....(4.17)}$$

Equation 4.17 can be written as

$$G = \lambda\ \delta_c\ \sigma_{ys} \qquad \text{.....(4.32)}$$

Where λ = a constant.Several theoretical analyses predict different values of λ e.g. 1, $\Pi/4$, 1.27, 1.48, 2 and 2.4. This variation in λ values may be due to the differences in the definition of the COD values. However, calculations by Burdekin and Stone [37], Bilby et. al [41], Rice and Rosengren [25] all yielded results identical with experiment for λ = 1.

Therefore, using $\lambda = 1$ and equating G from equations (4.31) and (4.32), the following expression results

$$\frac{K_{Ic}^2}{E} (1 - \nu^2) = \delta_c \sigma_{ys} \quad .... \quad (4.33)$$

This in turn gives rise to an equivalent K_{Ic} from the critical COD values

$$K_{Ic} = \sqrt{\frac{E \delta_c \sigma_{ys}}{1 - \nu^2}} \quad .... \quad (4.34)$$

5. EXPERIMENTAL

5.1 Test Materials:

Sections of spiral welded pipe from production heats were supplied by two Canadian Steel Manufacturers for the test program. Both of the pipe products were 42 inch (107 cm) outside diameter, with a 0.54-inch (13.7 mm) wall thickness and were rated as an x-70 grade steel (minimum yield strength of 70 ksi). The chemical compositions of these steels are given in table.

Table No. 5.1

Steel Compositions

	C	Mn	Mo	Nb	Si	Al	S	P	Cu	Ni	Cr	Sn	Ti	Ce
AF-1	0·05	1·93	0·26	·063	0·03	—	·023	·012	0·24	0·10	0·04	0·02	—	—
AF-2	0·06	1·82	0·45	0·05	0·26	·045	·006	·006	·037	·027	·068	·005	·002	·034

The AF-2 steel composition indicates that it is fully killed and rare earth treated. The AF-1 steel contains

considerably more S and is a semi killed steel.

5.2 Specimen Preparation:

Samples of the AF-1 steel were cut from sections of the pipe. Samples of the AF-2 steel were cut from smaller sections of the pipe obtained by acetylene cutting. In both cases specimens were cut using an automatic hack saw; no specimens were cut any closer than 50 mm from a flame cut edge.

The test samples were cut so that the through-thickness machined notch could have one of three different orientations.

1) Parallel to the pipe axis.

2) Parallel to the rolling direction.

3) Transverse to the rolling direction.

The rolling direction was at an angle of 63^{o} to the pipe axis for the AF-1 pipe and 45^{o} to the pipe axis for the AF-2 pipe.

5.3 Specimen Configuration and Dimensions:

5.3.1 Compact Tension Specimen:

Compact tension specimens were used for all of the fracture toughness tests, the K_{IC} test, the J-Integral test as well as the COD test. Since the pipe wall thickness was 0.54 inch (13.7 mm), the maximum fabricated specimen thickness was 0.50 inch. Fig. 5.1 illustrates the size of the compact tension specimen used in this study. The specimen dimensions conform to the specimen requirements described in the ASTM E399-74 standard for plane strain fracture toughness testing.

The three test directions were examined for the following reasons[15].

i) Crack parallel to pipe axis: This is considered to be the most important orientation because full scale burst tests indicate that failures do propagate along the pipe axis[50, 51]. The maximum operating stress in pipelines is the hoop stress which tends to open cracks parallel to the axis of the pipe.

ii) Crack parallel to Rolling Direction: Although toughness specifications require testing only in the pipe axis orientation, it is important to determine the effect of the distribution and spacing

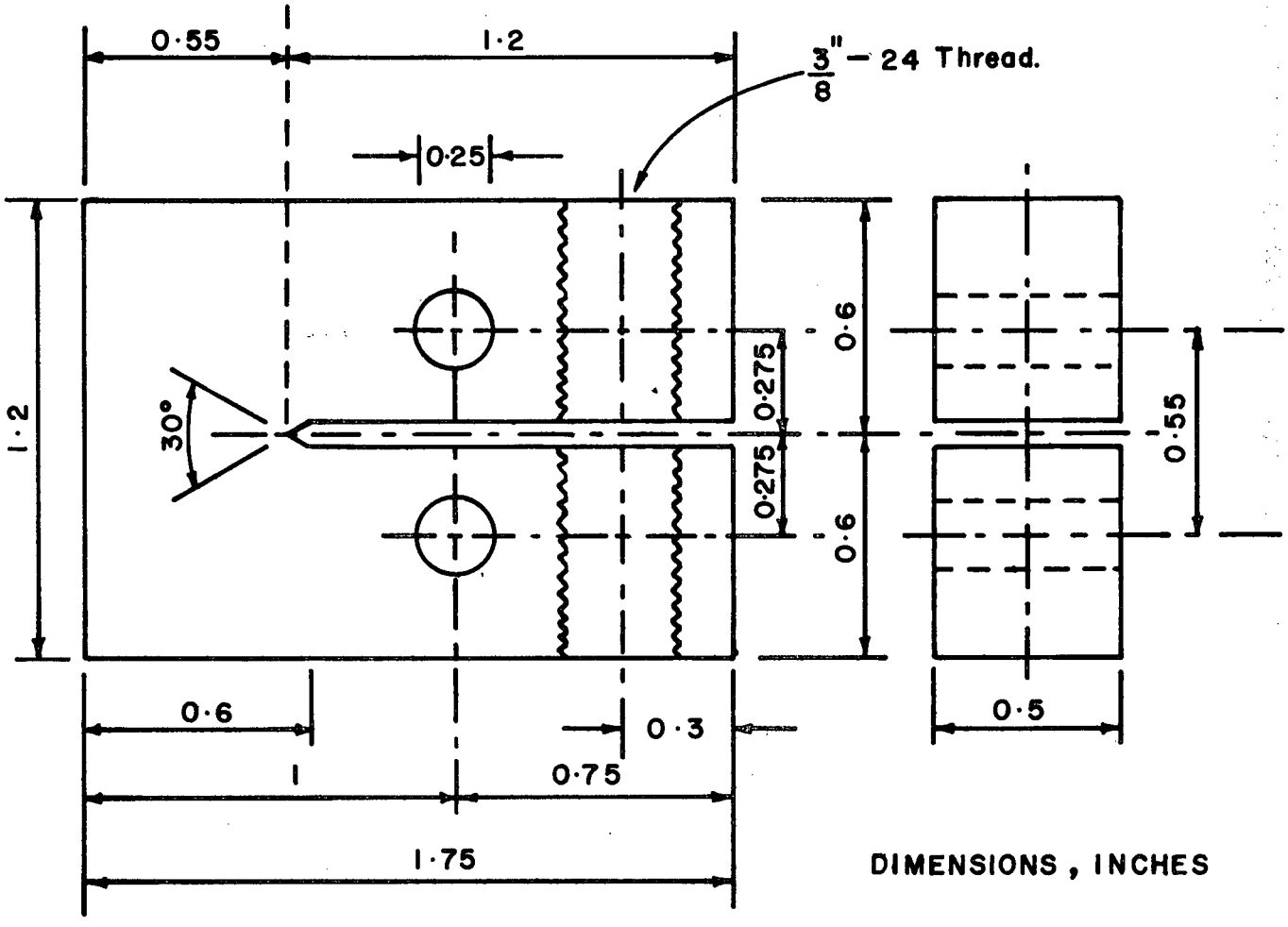

FIG. 5.1. 0·5 inch Thick Compact Tension Specimen.

of non-metallic inclusions etc. For this reason samples were cut with the crack running parallel to the rolling direction; these were designated as T-L orientation and it is expected to be the weakest direction of a material after rolling.

iii) Crack transverse to rolling direction: This orientation is designated as the L-T orientation. The pipe is known to possess a maximum upper shelf energy along this orientation [52]. This direction was included to determine the maximum toughness attainable in the structural component.

5.3.2 Tensile Specimens:

In order to assess the fracture toughness validity criteria and the equivalent K_{Ic} data from COD measurements at the test temperature and strain rate conditions for each specimen orientation, it is necessary to know the yield strength of the material. The orientation of the tensile specimen with respect to the axis of the compact tension specimen and the specimen dimensions are presented in Fig. 5.2.

The flow stress of both the steels for all

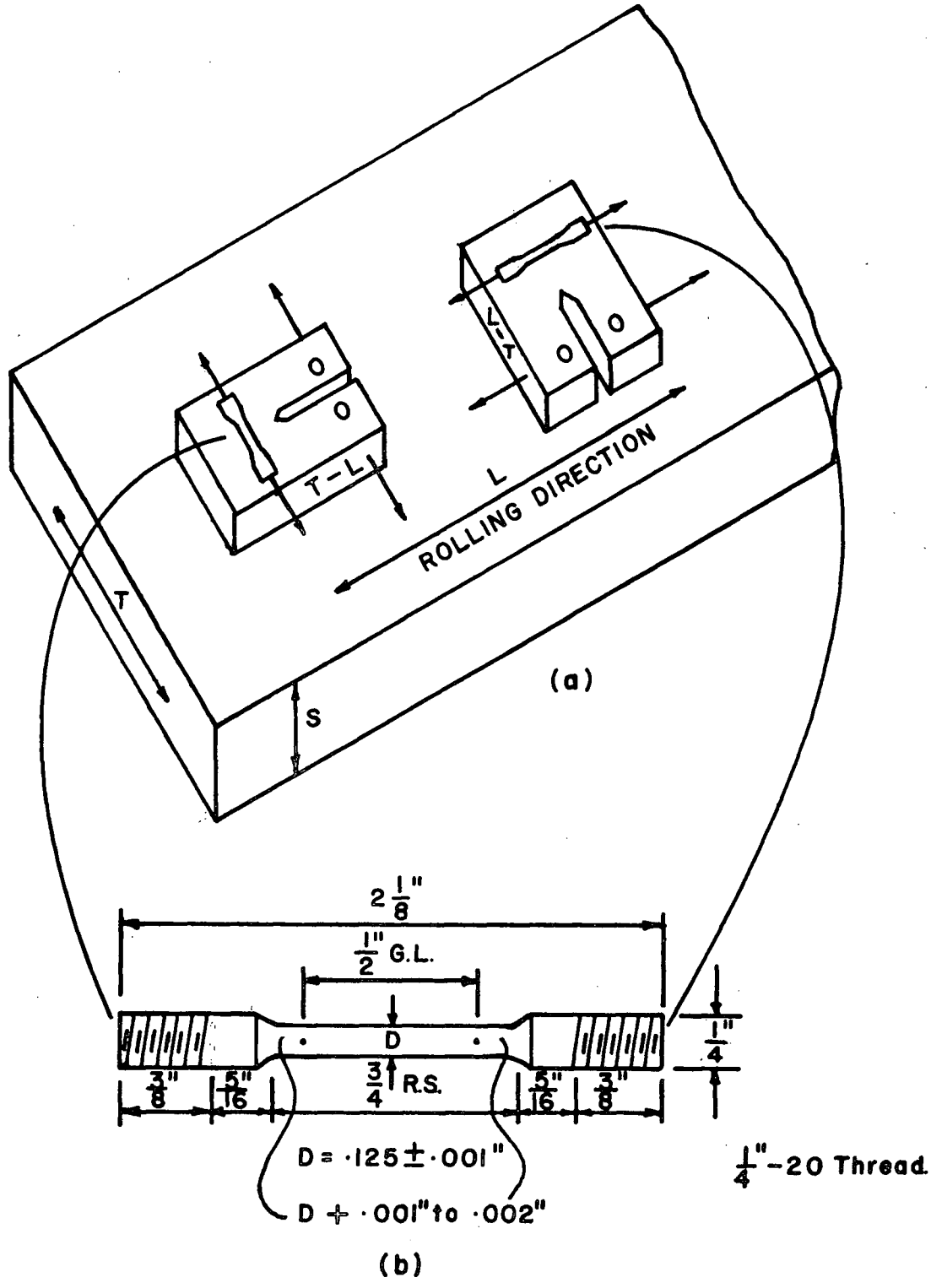

Figure 5.2. (a) Orientation of CT specimens with respect to Rolling Direction of the plate.

(b) Dimensions of the tensile specimen.

orientation and test conditions are also required to calculate the J_{Ic} values. Therefore, appropriate tensile tests were conducted along with fracture toughness tests.

Substandard sized tensile specimens having dimensions proportional to the standard were used to enable testing at sub-zero temperatures; it was necessary to immerse the specimen and the testing fixtures into a temperature controlled bath and to complete the test in this environment.

5.4 Fatigue Precracking:

The compact tension specimens were fatigue precracked before testing. This was necessary for the following reasons:

1) The validity of the K_{Ic}, δ_c and J_{Ic} values are dependent upon the establishment of a sharp crack at the tip of the machined notch.

2) The fatigue crack simulates a sharp internal crack which might exist inside the material as a result of processing and would remain undetected by standard NDT techniques.

The notched specimens were cleaned and degreased. The surface of each specimen was polished to a 600 grit emery paper; the 600 grit polishing lines running transverse to the notch. The maximum extension of the fatigue crack during the pre-cracking operation was readily visible on either surface.

Fatigue pre-cracking was performed using a Sonntag Fatigue Testing Machine, Model SF-1-U, operated with a manual preload. This equipment introduces a cyclic load which is symmetrical with relation to the notch.

5.4.1 ASTM Standard for Precracking:

The ASTM standard for determining the plane strain fracture toughness of metallic materials stipulates certain important prerequisites for fatigue precracking which are listed below..

i) The fatigue crack is to be extended from the notch at least 0.05 inch (1.3 mm).

ii) The ratio of the maximum stress intensity of the fatigue cycle to the Young's Modulus $K_{f(max)}/E$ shall not exceed 0.002 $in^{\frac{1}{2}}$ (0.0032 $m^{\frac{1}{2}}$).

iii) $K_{f(max)}$ must not exceed 60% of the K_Q value.

iv) When fatigue cracking is conducted at a temperature T_1 and testing at a temperature of T_2, $K_{f(max)}$ must not exceed $0.6\left|\frac{\sigma_{ys_1}}{\sigma_{ys_2}} K_Q\right|$

Where σ_{ys_1} and σ_{ys_2} are the yield strengths of the material at the respective temperatures.

5.4.2 Precracking Stress Intensity $K_{f(max)}$:

The previous fracture toughness data on these steels from IIT tests [15] indicated that the K_Q values obtained at ambient temperature may be greater than 88 ksi$\sqrt{in}$ (96.71 MPa$\sqrt{m}$). In this investigation, for precracking K_Q was assumed to be 100 ksi$\sqrt{in}$ (110 MPa$\sqrt{m}$). Considering $\frac{a}{w} = 0.50$ and $K_{f(max)}$ = 10 to 20% K_Q, the stress cycle to be employed was calculated. A sample calculation and $P_{f(max)}$ (in lbs) for corresponding $K_{f(max)}$ values are shown in Appendix - I.

In this work, a value of $K_{f(max)}$ = 15 to 18% K_Q was found to be adequate to generate fatigue

precracking in the specimens. This lower value of the stress intensity factor was used to minimize the plastic deformation ahead of the crack tip.

For the K_Q and COD tests, fatigue precracking was done such that $0.45 \leq \frac{a}{w} \leq 0.55$

For the J- Integral tests, the specimens were deeply notched to attain $\frac{a}{w} \geq 0.6$. Normally, $0.6 \leq \frac{a}{w} \leq 0.7$ was obtained.

The time required for precracking the K_Q and COD specimens varied from approximately 15 to 20 minutes; in the case of the J-Integral specimens, approximately double the time was needed. The details of the precracking are indicated in Appendix-II.

5.5 K_{Ic} Test Procedure:

K_{Ic} fracture toughness testing was aimed at:

a) Obtaining a load (P) vs. load-point displacement (Δ) curve.

b) Establishing the notch-toughness behaviour of the materials in the transition temperature range.

c) Obtaining an accurate measurement of the load-point displacement so as to obtain the critical value of the crack-opening displacement.

Therefore, one test technique was used to obtain the K_{IC} and the COD data. The critical value of the load (P) from the P-Δ record was utilised to calculate the K_Q or K_{IC} values and the critical value of displacement (Δ) was used to calculate the COD values.

5.5.1 Test Fixtures and Displacement Gauge:

To measure the load-point displacement at room temperature and also at sub-zero temperatures down to the liquid nitrogen temperature (-196^{o} C), the following fixture was designed and constructed. Two concentric, closely fitting brass tubes, were attached to the loading pins in such a way that when the pins

moved apart, the inner tube moved with respect to the outer one. For displacement measurements, a 50% - 1 inch extensometer was clamped to these tubes. Eccentricity of loading due to misalignment of the loading pins with the holding fixture was averted by applying a minor load of approximately 10 - 20 lbs prior to experimentation. The design and dimensions of the tubes and the experimental set-up are shown in Fig. 5.3.

5.5.2 Test Details:

Static K_{IC} tests were carried out using the INSTRON machine. Almost all of the tests were conducted at a full scale load of 5000 lbs (22.25KN), with the strain gauge preamplifier setting at the 2x range, a chart speed of 1 inch per minute and a cross-head speed of 0.05 inch per minute. Using these settings 10 inches of chart is equivalent to a displacement of 0.05 inch. Therefore, 1-inch of chart gives a measurement of 0.005 inch and 1 division, 0.0005 inch.

To establish the notch toughness transition behaviour of the materials, tests were conducted over

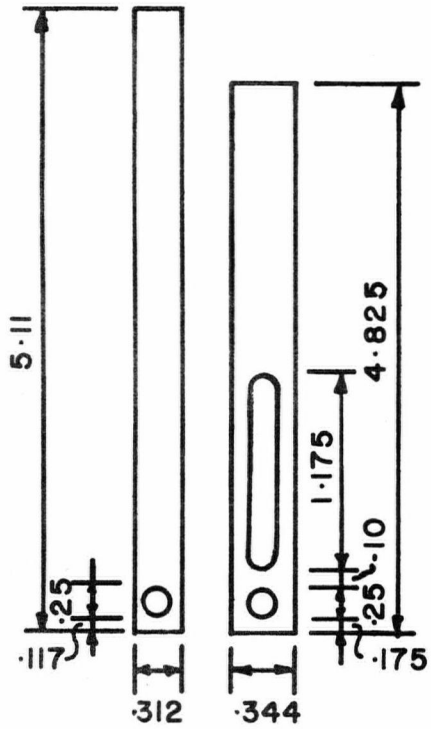

(a)

DIMENSIONS , INCHES

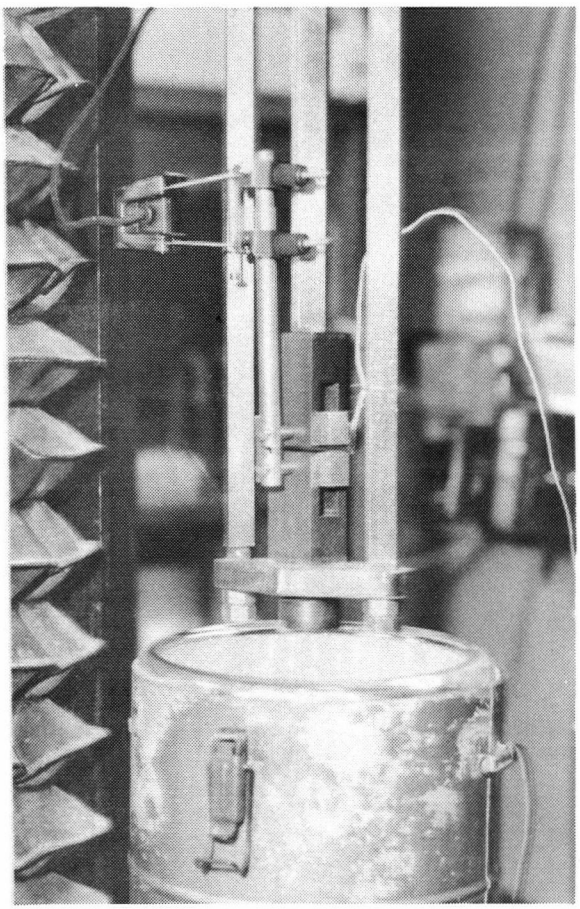

(b)

Figure 5.3(a) Dimensions of Brass Tubes.

(b) Photograph of the Experimental Set-up.

a range of temperatures extending from 20°C to 25°C (RT) to -40°C, -60°C, -80°C, -100°C, -110°C, -130°C, -150°C and -196°C. Initially, it was thought that tests to -100°C would establish the transition behaviour, but the results down -80°C did not deviate appreciably from the upper shelf toughness level. Therefore, to get toughness values in the transition range, experiments were carried out below -100°C and tests at -60°C were discontinued.

5.5.3 Low Temperature Tests:

Low temperature tests were conducted using different baths depending upon the temperature desired. The tests were carried out keeping the specimen, the specimen holding fixture, the loading pins and the brass tubes immersed inside the constant temperature bath as shown in Fig. 5.3.

The strain gauge was kept above the level of the bath in all experiments.

Tests down to -80°C were done using a bath of either denatured alcohol or a 60-40 ethanol-methanol

mixture. Tests at -100°C, -110°C and some tests at -130°C were also carried out using the 60-40 mixture. The tests at -150°C were carried out in an isopentane (Dimethyl Butane, Freezing Point = -160°C) bath.

All low temperature experiments were done keeping the specimen inside the bath for a minimum time of 20 minutes. The temperature of the specimen was measured by placing a chromel-alumel thermocouple junction adjacent to the sample. The bath temperature was controlled to an accuracy of $\pm$ 1°C.

In all of the experiments (RT as well as low temperature), the strain gauge was monitored until the maximum load was attained. The gauge was then disconnected and the test was continued until the specimen was broken into two halves for measurement purposes and to allow examination of the fracture surfaces. For the tests at -130°C and below, the specimens became so brittle that the fracture was always unstable and the specimens always broke into two pieces.

5.5.4 Test Records:

Test records of an autographic plot of the output of the load-sensing transducer vs. the output of the displacement gauge were obtained. Typical test records are shown in Fig. 5.4(a) and (b).

5.5.5 Measurements of the Test Piece Dimensions and Crack Length:

Before carrying out the experiments B, W, L, of the specimens were measured to the nearest 0.001 inch (.025 mm). L was the total length of the specimen.

After fracture, the crack length was measured at 25, 50 and 75% B (a_1, a_2, a_3,).

$$\text{Therefore, } a = \frac{a_1 + a_2 + a_3}{3}$$

In all specimens, the fatigue crack tip remained in a single plane. In all cases the a/w ratio was found to be $0.45 \leq \frac{a}{w} \leq 0.55$.

5.5.6 Analysis of the Experimental Data:

The RT and $-40^{\circ}C$ P-Δ record (Fig. 5.4(a))

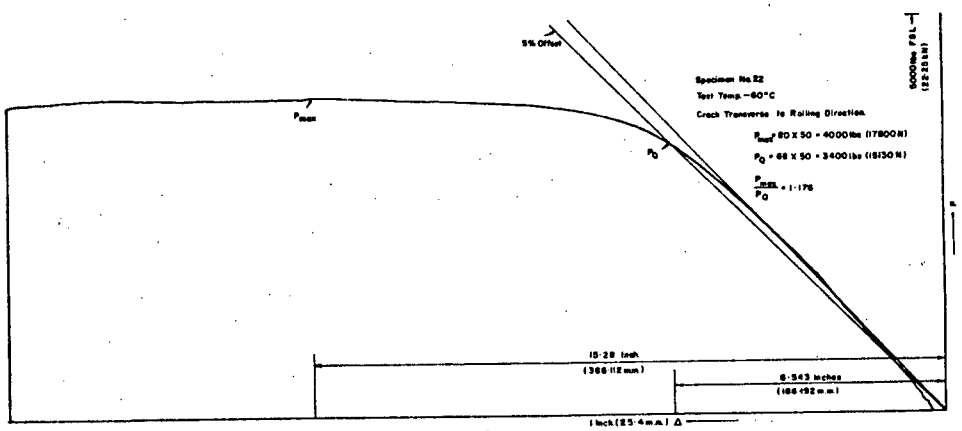

Fig. 5.4(a) Actual P - Δ Test Record for AF-1 Steel at - 60°C.

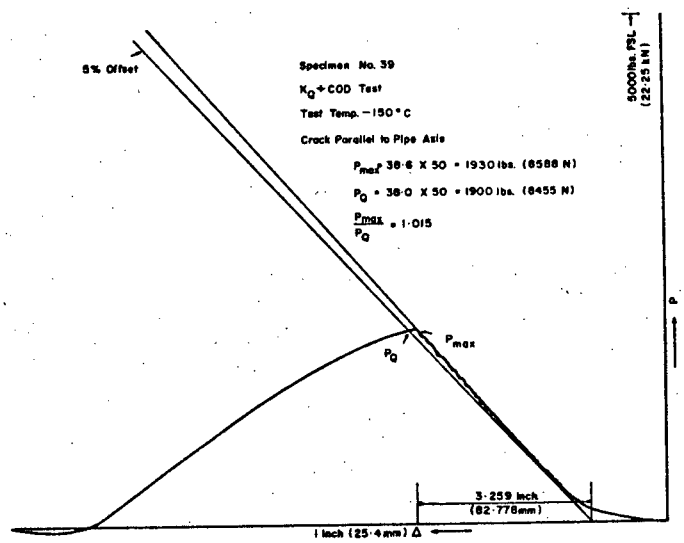

Fig. 5.4(b) Actual P - Δ Test Record for AF-1 Steel at - 150°C.

were typical of ductile behaviour indicating a high level of notch toughness, whereas the P-Δ test records at temperatures - 130 °C and below were characteristic of brittle plane strain behaviour. The test records resembled type - III as given in the ASTM E399-74 standard as shown in Fig. 5.4 (b).

In all cases, the 5% secant offset procedure was adopted to measure the P_Q load value. The $\frac{P_{max}}{P_Q}$ ratio was observed to be greater than 1.10 for RT, - 40 °C and - 60 °C tests and less than 1.10 for tests conducted at lower temperatures.

Through the linear elastic portion of the P-Δ curve, a best fitting straight line was drawn cutting the Δ-axis. A 5% offset line was then drawn through this point on the Δ-axis. The point where the offset cuts the curve was taken as the P_Q value.

From the a/w ratio, f(a/w) was calculated using the table for compact tension specimens. K_Q in psi $\sqrt{in}$ (MPa$\sqrt{m}$) was then calculated with the help of the relation.

$$K_Q = \frac{P_Q}{B_w^{1/2}} f(a/w) \quad \ldots\ldots \quad (5.1)$$

Finally the validity criterion for K_{IC} testing was calculated using the relation

$$B > 2.5\left|\frac{K_Q}{\sigma_{ys}}\right|^2 \quad \ldots\ldots \quad (5.2)$$

Where σ_{ys} = 0.2% offset yield strength at the respective test temperature and strain rate.

5.6 COD Test Details:

Since COD tests and K_{IC} tests are essentially the same, a single test was conducted to obtain both types of data. At each test temperature a minimum of two compact tension specimens were tested. In certain cases, where COD results or K_{IC} results showed a wide scatter, up to 4 specimens were tested.

5.6.1 Assessment of Test Data:

Some judgment was necessary to determine the critical value of displacement associated with the onset of unstable fracture.

For the smooth curves obtained at RT and

- 40 °C, the critical displacement value was taken as that occurring at the maximum load, including elastic-plastic components. This value of displacement is termed V_m and indicates the displacement of the loading pins. For comparison purposes and also to understand the basic mechanism of crack initiation a displacement value corresponding to P_Q was measured and reported. This displacement reading was termed V_Q. In low temperature tests, $V_Q > V_m$; hence the measurement V_Q was discontinued. Since 1 inch of chart corresponded to 0.005 inch displacement, V_Q and V_m values were obtained by multiplying chart readings by 0.005 inch.

5.6.2 Calculation of δ_c:

Having obtained the critical values of strain gauge displacements (V_m and V_Q), it was necessary to convert these to the true critical COD($\delta_c - \delta_m$ or δ_Q) at the crack tip.

V_c values were converted to the corresponding δ_c value using the generalised relationship

$$\delta_c = \frac{V_c}{1 + \frac{a + z}{r(w - a)}}$$

Where r = rotational factor 0.33

z = knife edge thickness

In the present experimental technique adopted z = o.

Therefore,

$$\delta_c = \frac{V_c\ (w - a)}{w + 2a}$$

correspondingly,

$$\delta_m = \frac{V_m\ (w - a)}{w + 2a} \quad \text{and} \quad \delta_Q \quad \frac{V_Q\ (w - a)}{w + 2a}$$

5.6.3 Calculation of Equivalent K_{Ic}:

Once the critical value of COD at the crack tip is obtained, an equivalent value of K_{Ic} was calculated using the relationship

$$G_{Ic} = \frac{K_{Ic}^2}{E}(1-\nu^2) = \sigma_{ys}\,\delta_{Ic} \quad (44,54)$$

which gives

$$K_{Ic} = \sqrt{\frac{E.\ \sigma_{ys}.\ \delta_{Ic}}{1-\nu 2}}$$

The value of the equivalent K_{Ic} is obtained in ksi$\sqrt{in}$ and is converted to MPa$\sqrt{m}$ unit multiplying by 1.099

5.7 J-Integral Test Details

5.7.1 Testing Parameters:

The heat tinting technique which is the same as the Resistance curve test technique developed by Landes and Begley was adopted in this investigation. CT specimens 0.5 inch thick having crack lengths $0.6 \leq a/w \leq 0.7$ were used. For RT and -40^{o} c temperature tests a full resistance curve was developed. For tests at -80^{o} C and below, a full resistance curve was not necessary as the slope of the J - Δa curve tends to become zero due to the ductile-brittle transition. Therefore, for RT and -40^{o} C tests 5 to 6, CT specimens were used and for other temperatures a minimum of two specimens were used.

Each specimen was loaded, with increasing displacement, then unloaded and heat tinted at 316^{o} C for 15 - 20 minutes to tint the cracked area. Then the specimens were pulled to failure in the Instron. As the rate of oxidation at the fatigue precracking segment was different from that of the crack growth zone, the crack growth zone was easily detectable by visual inspection.

Typical P - Δ records for J-Integral tests for AF-2 steel at - 40 ^{o}C and - 130 ^{o}C are shown in Fig. 5.5 (a) and (b) respectively.

5.7.2.1. Measurement of Specimen Dimensions and Crack Growth (Δa):

Using techniques similar to those employed in the K_{Ic} or COD tests, B, L, W were measured to the nearest 0.001 inch prior to experimentation. From the fractured specimens after heat tinting, the crack parameters were measured at three positions and an average of the three readings was used as the crack length 'a'. As previously mentioned, all specimens had a a/w ratio between 0.65 to 0.70.

The crack growth or crack extension, Δa, ahead of the fatigue precrack was also measured to an accuracy of 0.001 inch. The minimum value of crack growth measured was 0.004 inch and the maximum value, 0.16 inch.

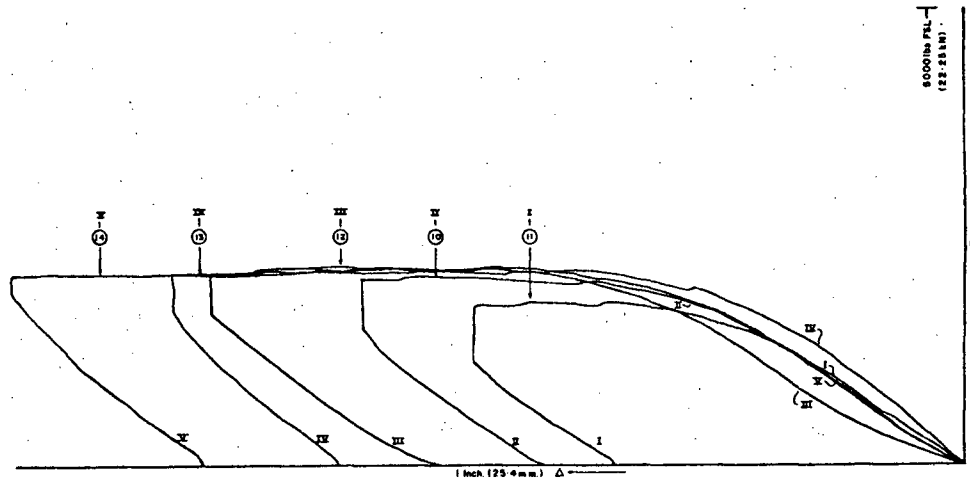

Fig. 5.5(a) J-Integral Test Record of AF-2 Steel with Crack Transverse to Rolling Direction. Test Temp. - 40°C.

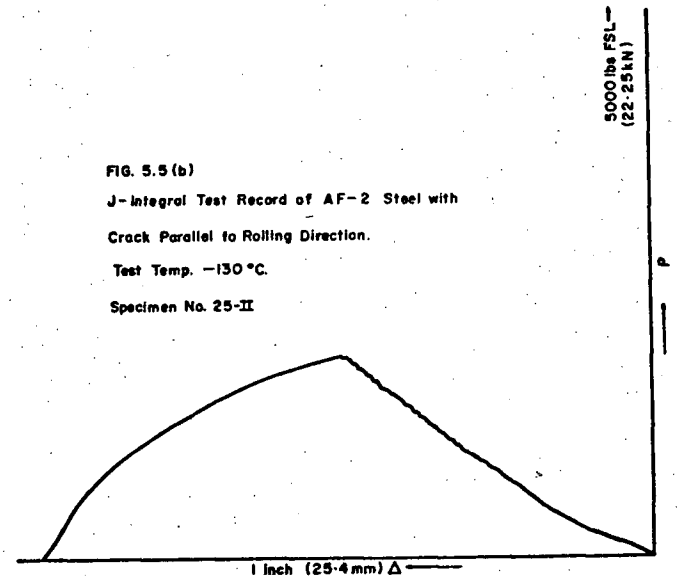

5.7.2.2 Measurement of the area (A) under the P - Δ Record:

For each specimen the area under the P - Δ record consisting of both the elastic and plastic deformation was measured with the help of a compensating type polar planimeter (33661 Made in Japan). Keeping the position of the vernier on the tracer bar at 143.8, individual areas were measured. An average of 3 to 4 readings of each area was taken. The mean value of the readings was multiplied by 0.015 to give the area in square inches. One square inch in the record denotes an equivalent energy of 2.5 in-lb since Y - axis, load = 50 lbs / inch of chart

X - axis, Δ = 0.005 inch / inch of chart.

Therefore for each specimen, the amount of energy expended for crack extension was measured by the area A under the P - Δ record in in - lb.

5.7.3 Calculation of J for RT and - 40 ^{o}C tests:

J-Integral tests at RT and - 40 ^{o}C resulted in different values of area (A) with a corresponding Δa for each individual specimen. J for each specimen

was then calculated using the relationship (29 - 33, 35).

$$J = \frac{2A}{B\ (w - a)} \quad \text{in - lb / in}^2$$

Therefore, for a single specimen Δa and a corresponding J value were obtained. Since 5 to 6 specimens were used at a particular temperature, 5 to 6 sets of J vs Δa values were obtained. As each specimen differed from each other by an increasing amount of Δa J values also increased in magnitude. Hence, 5 to 6 sets of increasing order J and Δa values were plotted to construct a curve. The best fitting line was drawn through these points to generate the resistance curve.

5.7.4 Determination of J_{Ic} Value:

It was pointed out in Section 4.2.11 that the critical value of J_{Ic} should be obtained by extrapolating the resistance curve backward to the point of zero crack extension due to actual material separation. Hence a line $J = 2\ \sigma_{flow}\ \Delta a$ was constructed on the resistance curve. The σ_{flow} value of each orientation for each steel at each testing temperature was calculated from the yield strength and the UTS values. The J_{Ic} value was determined where

the line $J = 2\sigma_{flow}\,\Delta a$ cuts the resistance curve.

For tests at -80^{o}C and below a "single specimen" test technique could be used to obtain a J_{Ic} value. This was verified by a minimum of 2 specimens in each case.

It was also verified in the case of the AF-2 steel with specimens having cracks running parallel to the rolling direction at the -80^{o}C test temperature; specimen No. 17 extended 0.001 inch less than specimen No. 16 and did not indicate any crack growth as revealed by the heat tinting technique. Therefore J calculated for specimen No. 16 is the J_{Ic} value.

5.7.5 Calculation of Equivalent K_{Ic}:

From the J_{Ic} value corresponding K_{Ic} values were calculated from the relationship between elastic-plastic and linear elastic fracture mechanics parameters [30, 31, 54].

$$J_{Ic} = G_{Ic} = \frac{K_{Ic}^2}{E}(1-\nu^2)$$

which gives

$$K_{Ic} = \sqrt{\frac{E \cdot J_{Ic}}{1-\nu^2}}$$

Where ν = Poisson's ratio = 0.3

E = Young's Modulus = 30×10^6 psi.

5.7.6 Verification of Validity Criterion:

For valid J_{IC} results, the following size requirement must be met by an elastic-plastic fracture toughness specimen (28, 30 - 32, 34, 35).

$$a, B, w - a \geq 25 \frac{J_Q}{\sigma_{flow}}$$

It was verified that for all test results the criteria were satisfied. Therefore, all J_Q values obtained were valid J_{IC} values.

5.8 Tensile Test Details:

Tensile tests were conducted for the purposes already mentioned in section 5.3.2.

At each test temperature, a minimum of two specimens were used. Yield strength and UTS values were calculated and the average values were reported. The σ_{flow} stress was calculated as

$$\sigma \text{ flow} = \frac{\sigma \text{ yield stress} + \sigma \text{UTS}}{2}$$

6. RESULTS AND DISCUSSIONS

6.1 Tensile Properties:

The increase in the yield strength as well as the flow strength with decreasing temperature are presented in Figures 6.1 to 6.4 for the AF-1 steel and in Figures 6.5 to 6.8 for the AF-2 steel. The increase in the flow strength and yield strength on decreasing the temperature from RT to -100°C is less than 30% of the RT value. However, for temperatures below -100°C, the yield strength and the flow strength increase markedly; at -150°C an increase of approximately 80% is observed while at -196°C the yield strength and the flow strength are approximately double the values measured at room temperature. It is well established that the tensile properties of most metals are governed by the thermally activated motion of dislocations. Where this is the predominant mechanism, the yield stress and flow stress decrease with increasing temperature (55).

For the AF-1 steel, the RT yield strength varied from 71,000 psi (489 MPa) along the axis

transverse to the pipe axis to 80,000 psi (551 MPa) along the axis transverse to the rolling direction. Surprisingly, the RT yield strength was the same 80,000 psi (551 MPa) on the rolling direction and transverse to the rolling direction. For the tests conducted at -196 °C, the yield strength varied from a minimum of 144,000 psi (993 MPa) transverse to the pipe axis to a maximum of 157,000 psi (1082 MPa) transverse to the rolling direction. The yield strengths along the pipe axis and the rolling direction were comparable throughout the temperature range examined.

In terms of the yield strength, the AF-1 plate is strongest along an axis transverse to the rolling direction, weakest along an axis transverse to the pipe axis and exhibits an intermediate strength along the pipe axis and the rolling direction.

The yield strength of the AF-2 steel at RT varied from 73,000 psi (503 MPa) to 88,000 psi (606 MPa), being a minimum along the axis transverse to the rolling direction and a maximum along the axis transverse to the pipe axis. In contrast, the yield

strength at -196°C varied from 150,000 PSi (1034 MPa) to 160,000 psi (1103 MPa) being a minimum along rolling direction and a maximum along the axis transverse to the rolling direction. Above -150°C, the plate is strongest along an axis transverse to the pipe axis, exhibits an intermediate strength along the pipe axis and the rolling direction and exhibits its lowest strength along an axis transverse to the rolling direction. In contrast, below -150°C, the plate is strongest along an axis transverse to the rolling direction; shows an intermediate strength along an axis transverse to the pipe axis and is weakest along the pipe axis as well as the rolling direction.

In comparing the tensile properties of the AF-1 and the AF-2 steels, it is observed that the AF-2 steel is stronger than the AF-1 steel.

Both steels exhibit anisotropic strength properties, but the properties of the AF-1 steel are more anisotropic than those of the AF-2 steel. The better tensile properties e.g. higher yield strength and more isotropic behaviour of the AF-2 steel may be the result of rare earth additions and of the lower

sulphur content. However, Lyckx et. al [5] suggested that rare earth additions did not have any effect on the tensile properties of the steel. The AF-1 steel possesses inferior tensile properties, that is, a lower yield strength and greater anisotropy. This may be due to the higher sulphur content of this steel. The higher sulphur content results in the presence of more second phase particles in the form of sulphides. The yield strength of a material decreases as the volume of the second phase particles increases. This is because the second phase particles enhance the process of void nucleation and growth. The decrease in yield strength and greater anisotropy of the AF-1 steel can be attributed to the deleterious effect of the sulphur content on the true strain to fracture as reported by W.G. Wilson and G.S. Klems [61].

AF-I STEEL

SPECIMEN TRANSVERSE TO ROLLING DIRECTION

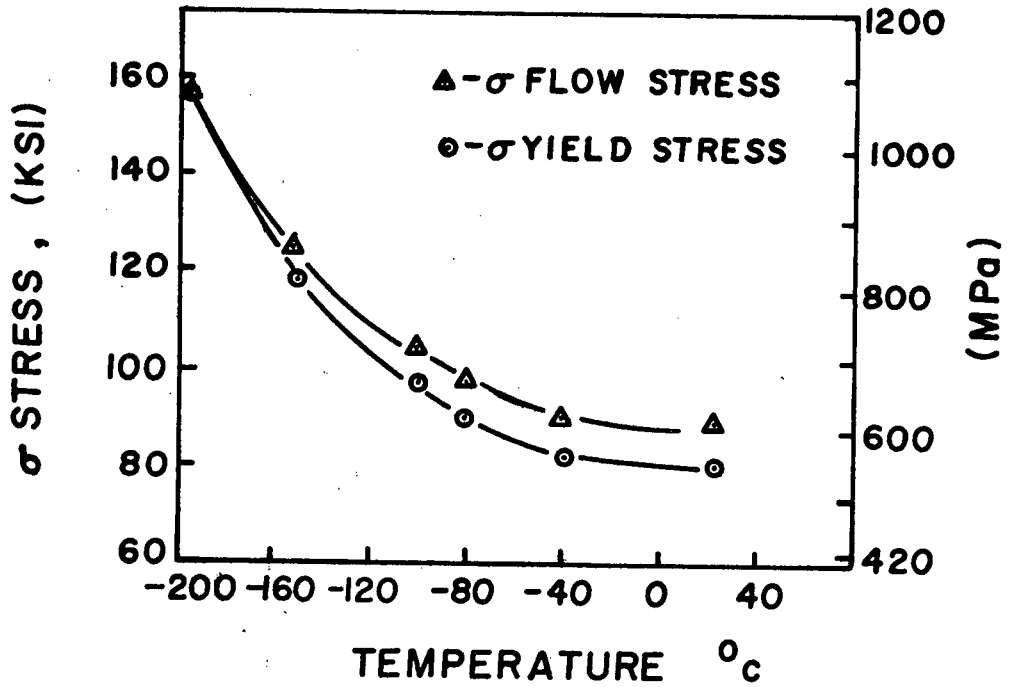

FIG. 6.1

AF-I STEEL

SPECIMEN TRANSVERSE TO PIPE AXIS

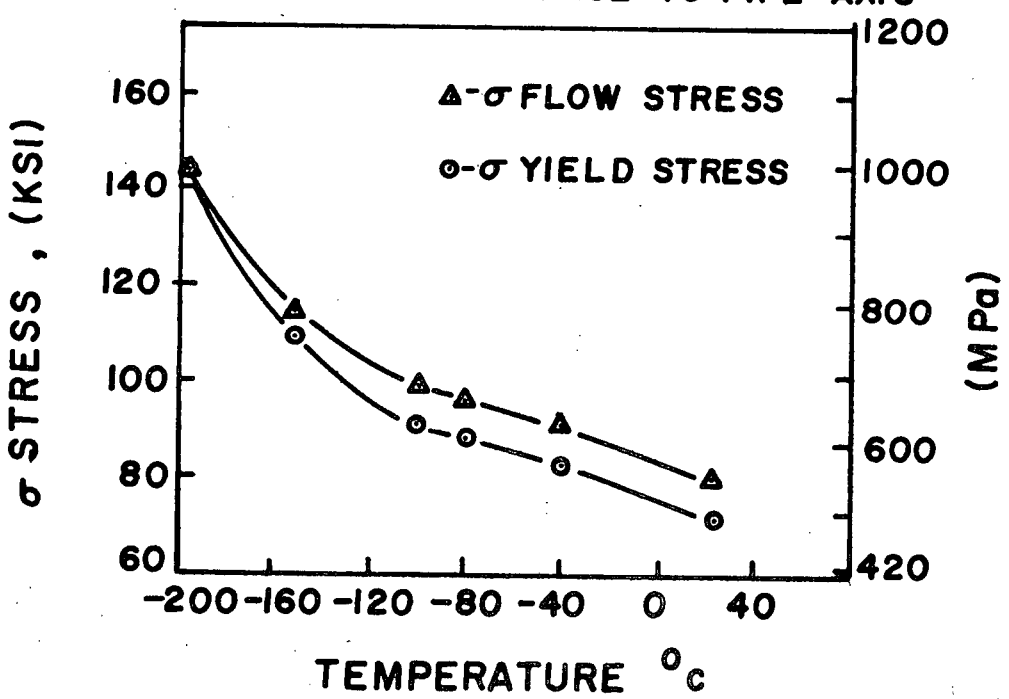

FIG. 6.2

AF-1 STEEL

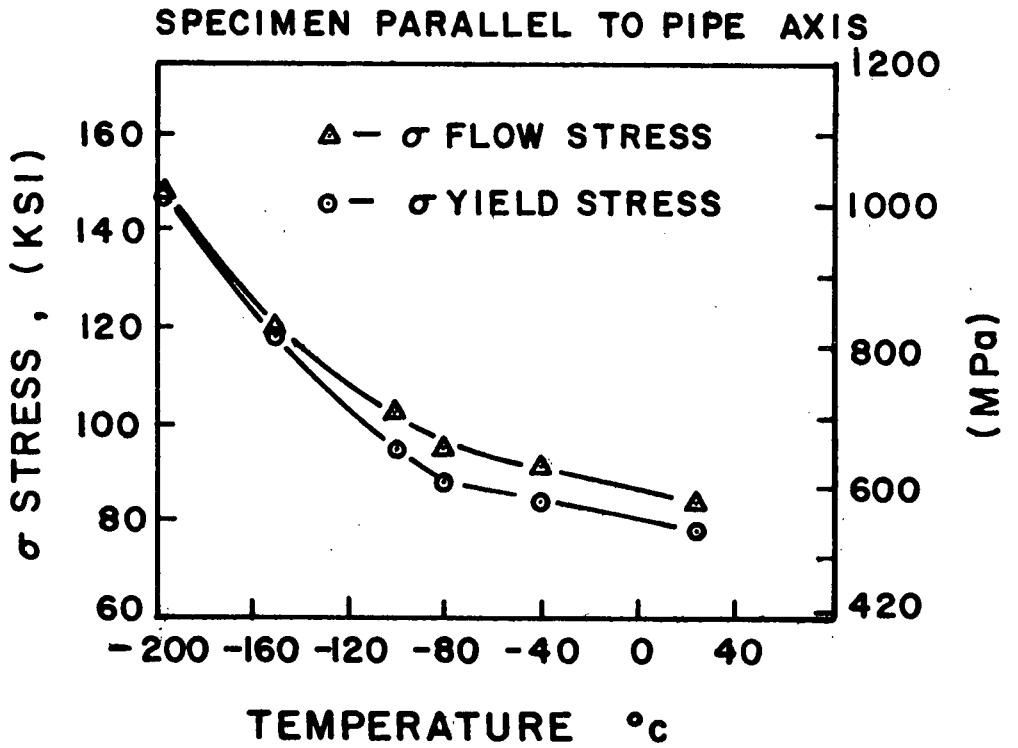

FIG. 6.3

AF-1 STEEL

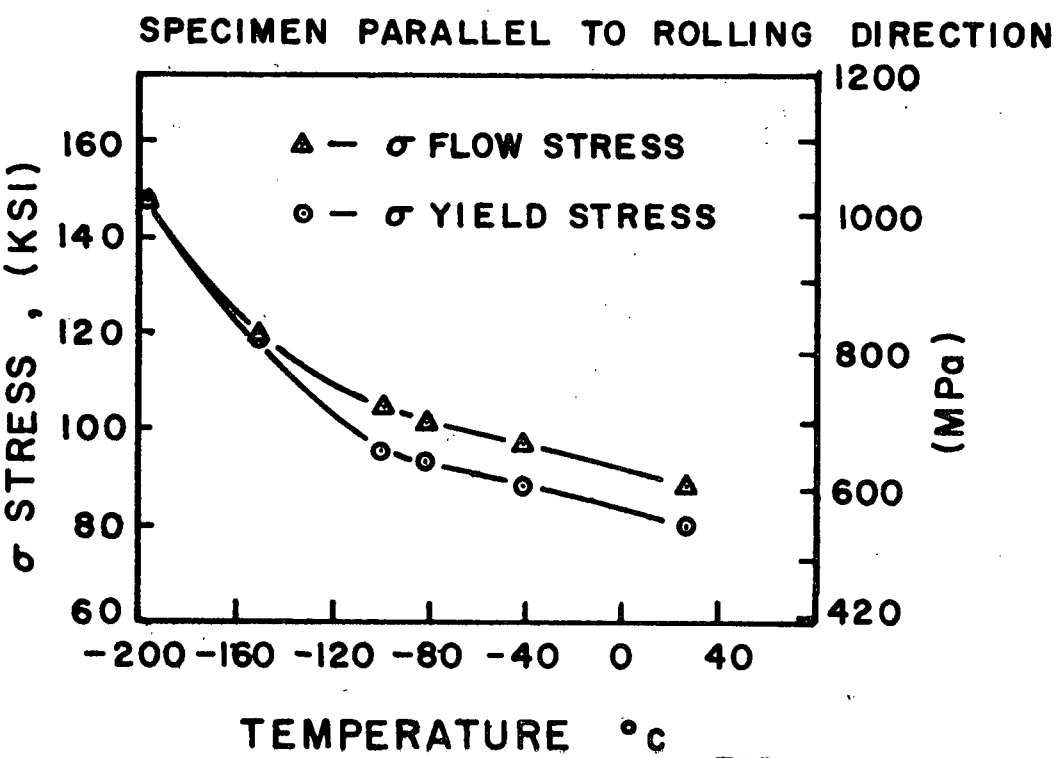

FIG. 6.4

AF-2 STEEL

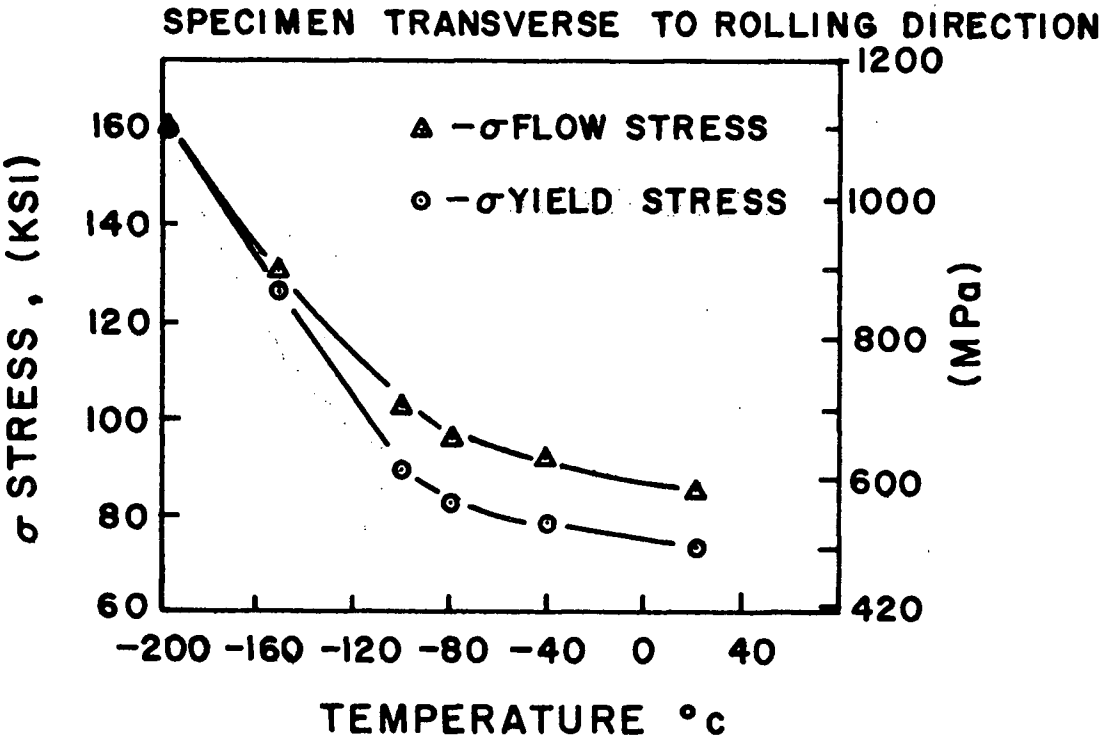

FIG. 6.5

AF-2 STEEL

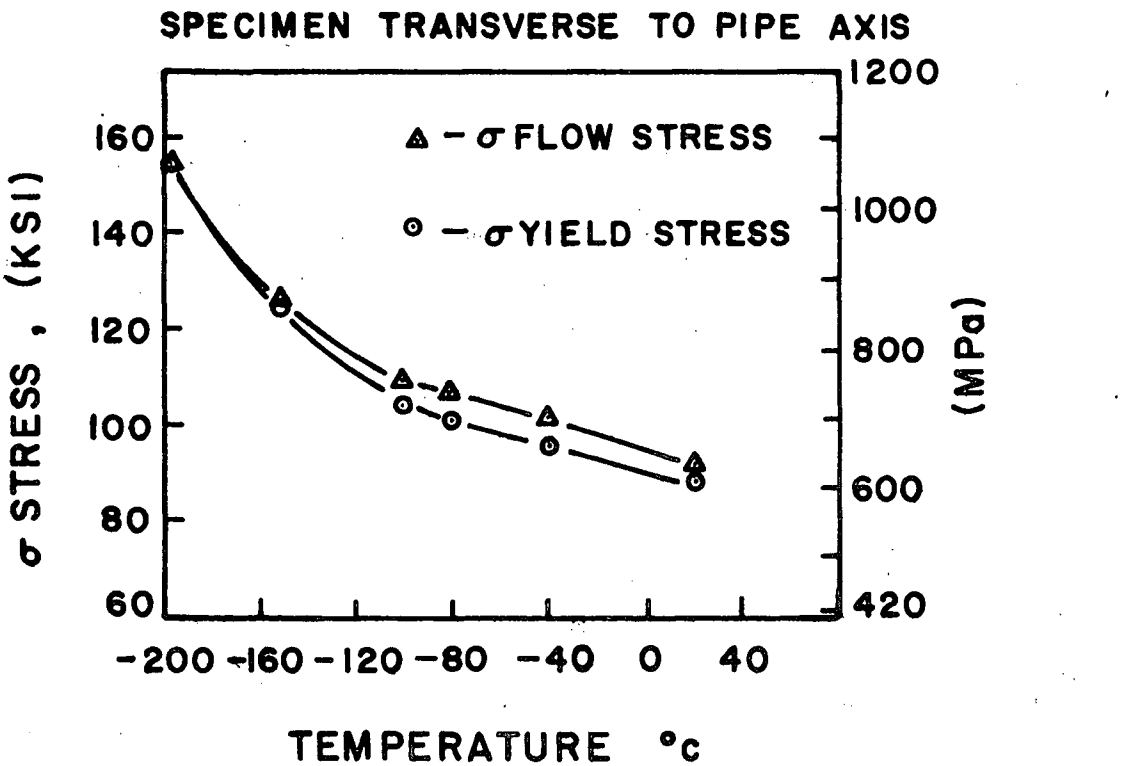

FIG. 6.6

AF - 2 STEEL

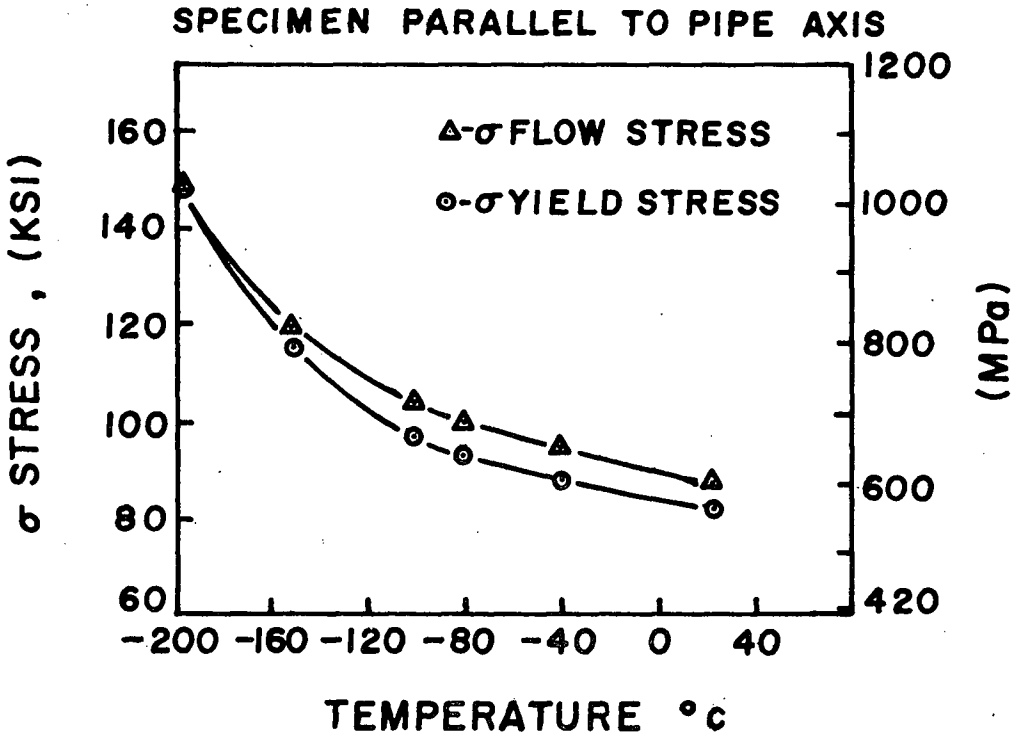

FIG. 6.7

AF - 2 STEEL

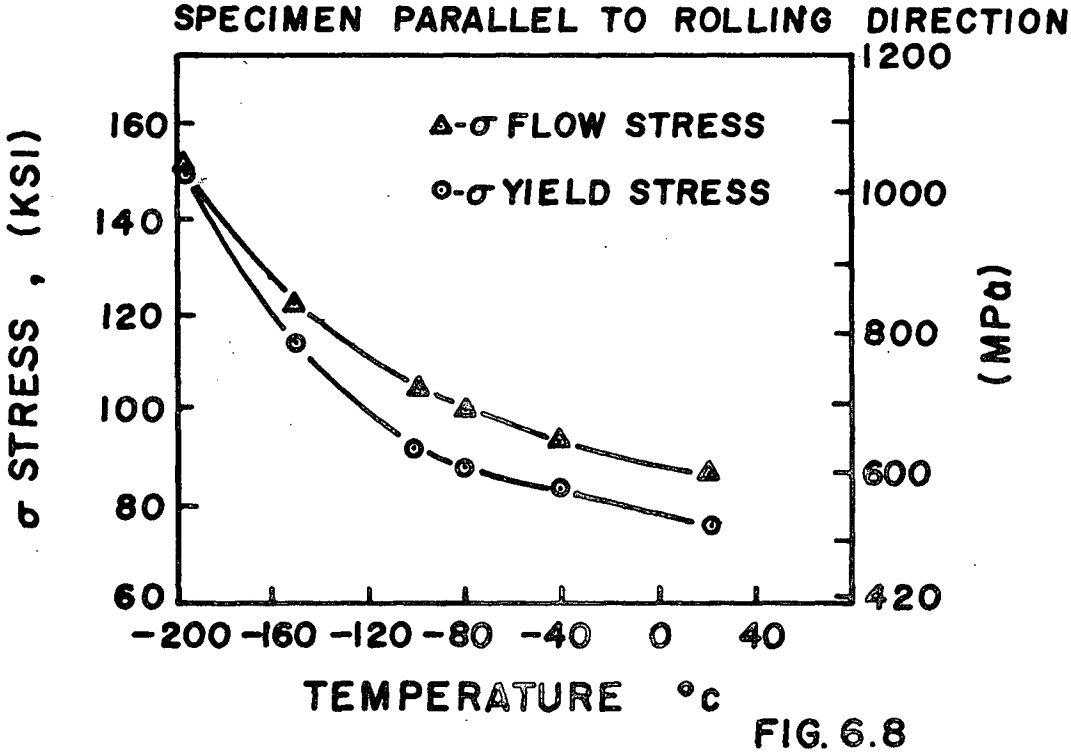

FIG. 6.8

6.2 Fracture Toughness:

6.2.1 K_Q Test Results:

The fracture toughness values (K_Q or K_{IC}) for the AF-1 steel as obtained by the K_{IC} tests, are reported in Tables 6.1, 6.2 and 6.3 for cracks parallel to the rolling direction, cracks parallel to the pipe axis and cracks transverse to the rolling direction respectively. The comparable results for the AF-2 steel are shown in Tables 6.4, 6.5 and 6.6. In general the K_Q values for both steels decrease in each test direction with decreasing temperatures as can be seen in Figures 6.9.1, 6.9.2, 6.9.3.

This decrease in fracture toughness with decreasing temperature is expected in strain rate sensitive materials* and is related to the increase in yield stress with decreasing temperature. The increase in yield strength allows a higher level of tensile stress to be present in the plastic zone ahead of the crack and ensures crack tip triaxiality. Cleavage failure occurs when the stress attained over a distance of one or two grain diameters ahead of

---

* Strain rate sensitive materials exhibit a marked variation in yield strength with variations in the test temperature and strain rate (56). The low carbon structural steels are more strain rate sensitive than high strength aluminum and high strength alloy steels. (56,57)

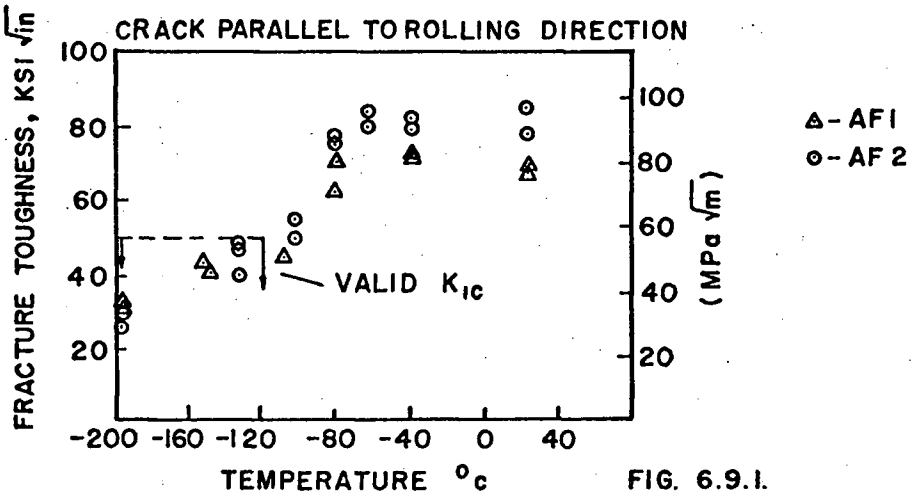

FIG. 6.9.1.

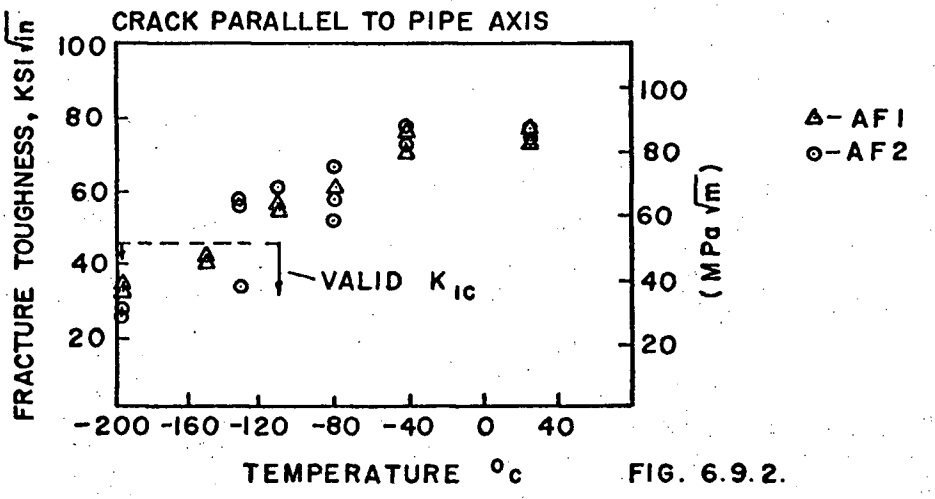

FIG. 6.9.2.

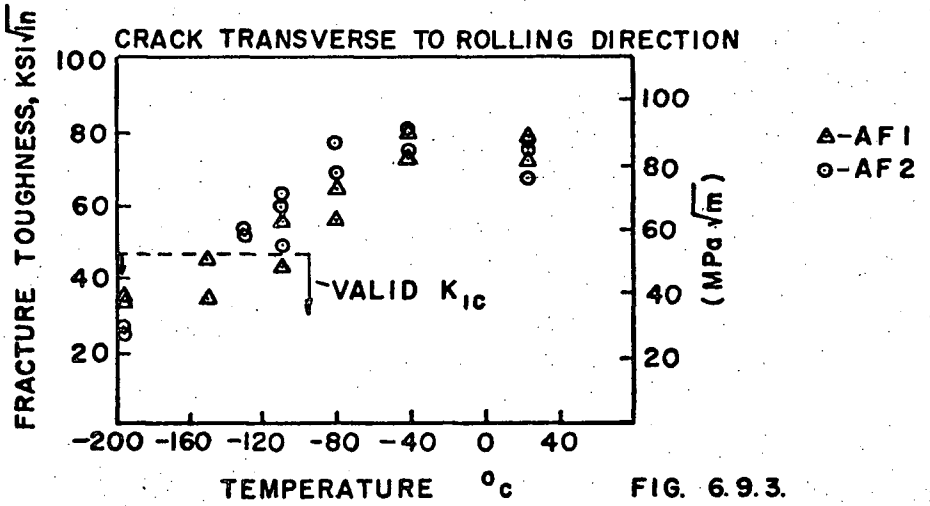

FIG. 6.9.3.

the material [58]. As the temperature increases the yield stress decreases until the cleavage stress is no longer achieved and the material tears instead [54]. The tearing mode of failure occurs predominantly by a process of void initiation and coalescence [55].

It should be noted that there are two possible transitions in fracture behaviour with temperature, namely:

1) A K_{Ic} transition (Plane Strain transition)
2) A Plane-strain to Plane-stress transition commonly called the 'Elastic-Plastic Transition'.

Although Wessel [59] suggested that the failure mechanism in K_{Ic} tests was cleavage over the whole temperature range, Barsom and Rolfe's [60] fractographic analyses established that the K_{Ic} transition is associated with the onset of a change in the microscopic fracture mode. At low temperatures, the fracture is 100% cleavage or quasi-cleavage whereas at the transition or intermediate temperatures, the fracture surface exhibits a combination of quasi-cleavage and tear dimples. At higher temperatures above the transition region, the fracture surface

consists of 100% tear dimples.

The test results as obtained using the ½ inch thick compact tension specimens indicate that valid K_{Ic} values are obtained at - 130°C and below for both steels in all test directions; in the rolling direction the AF-2 steel is the exception. The AF-2 steel exhibits a lower yield strength in this direction and therefore valid K_{Ic} data is not obtained until the temperature is below - 130°C. Thus, the test values obtained at - 130°C, - 150°C, and - 196°C lie on the lower shelf of the fracture toughness transition curve. The data obtained at - 40°C and RT lie on the upper shelf and are K_Q values. The results for - 80°C, - 100°C and - 110°C lie in the transition zone and are also K_Q values.

Fig. 6.10.1 shows the fracture surface of the AF-2 steel after testing at RT, - 40°, - 80°, - 110°, - 130° and - 196°C with the crack parallel to the pipe axis. The fracture surfaces obtained at RT and - 40°C are gray and fibrous, typical of ductile failure. In fact, the RT specimen exhibited a fracture extending at 45° to the specimen axis. In

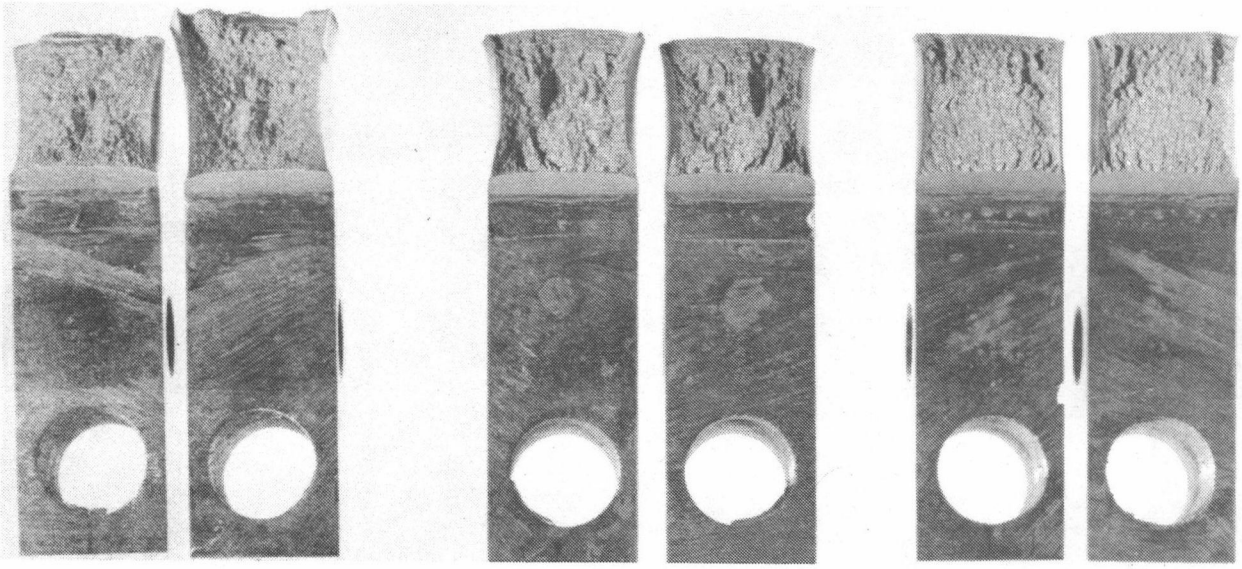

R.T. -40°C -80°C

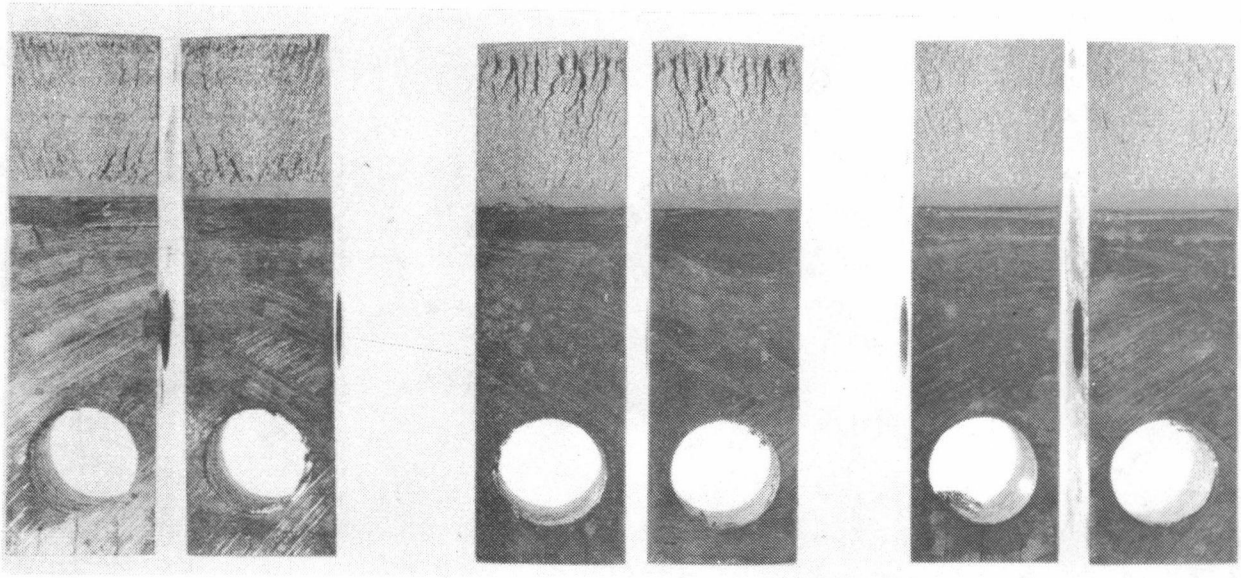

-110°C -130°C -196°C

Figure 6.10.1. Fracture surfaces of K_{IC} specimens of Af-2 steel with crack parallel to pipe axis at various temperatures.

contrast the fracture surfaces on specimen tested at $-130^{o}C$ and below are bright and granular, indicative of brittle failure. The fracture surfaces obtained at -80^{o} and $-110^{o}C$ consist of both fibrous and granular structure; 40% fibrous and 60% granular at $-80^{o}C$, 20% fibrous and 80% granular at $-110^{o}C$.

The test results indicate that the plane strain to plane stress transition occurs above $-130^{o}C$ with increasing temperature. This is due to the fact that as the temperature increases, the yield strength of the material decreases. This in turn reduces the through thickness constraint at the crack tip although a triaxial state of stress exists. As a consequence the plane strain condition no longer prevails.

The fracture surface study established that even in the case of samples tested in the elastic-plastic transition, the micro-mode of fracture remains the same as with Plane Strain transition, that is, 100% cleavage at low temperature, 100% ductile tear at higher temperature and a combination of both in the transition temperature range.

Considering the directionality of the toughness behaviour of the AF-2 steel, the test results as shown by the transition curves in Fig. 6.9.1, 6.9.2, 6.9.3 do not indicate much deviation from one orientation to another orientation. In other words, the AF-2 steel exhibits essentially isotropic fracture toughness behaviour. The same is not true for the AF-1 steel; for tests with the crack parallel to the rolling direction a lower toughness value is obtained in the upper shelf region in comparison to the other two test directions.

In comparing the K_Q and K_{Ic} results of the AF_1 and the AF_2 steel the following observations can be made.

1. In the upper shelf region, for a crack parallel to the rolling direction, the AF-1 steel possesses a significantly lower toughness than the AF-2 steel. The K_Q values of both steels are comparable in the other two test directions.

2. In the transition region, both the AF-1 and AF-2 steels show steeper transition behaviour for the crack parallel to the rolling direction; but the transition temperature range remains the same for each

steel in all three test directions.

3. Both steels exhibit comparable fracture toughness in all test directions in the valid K_{Ic} range.

The more isotropic nature of the fracture toughness behaviour of the AF-2 steel and its higher fracture toughness values along the transverse direction (T - L) in comparison to the AF-1 (containing more sulphur) clearly reveals the beneficial effects of rare earth addition during the steel making process.

6.2.2 J-Integral Test Results:

The J-Integral test results for the AF-1 and the AF-2 steel are shown as J-resistance curves in Figure:

6.11.1 - for the crack parallel to the rolling direction (T-L)

6.11.2 - for the crack parallel to the pipe axis

6.11.3 - for the crack transverse to the rolling direction (L-T)

6.12.1 - for the crack parallel to the rolling direction (T-L)

6.12.2 - for the crack parallel to the pipe axis

6.12.3 - for the crack transverse to the rolling direction (L-T) respectively. The J-resistance curve for the AF-1 steel tested at - 80 °C with the crack transverse to the rolling direction as shown in Fig. 6.11.3 confirms the fact that the slope of the J-Δa curve approaches zero with decreasing test temperature and the J_{IC} value remains constant independent of the crack growth (Δa) at these low temperatures. Therefore, this curve verifies that for tests done at temperatures < - 80 °C, a full resistance curve is not obtainable or necessary.

To indicate how J increases with crack growth, Fig. 6.13.1 shows the fracture surfaces of the AF-2 steel specimens which were tested at RT and were used

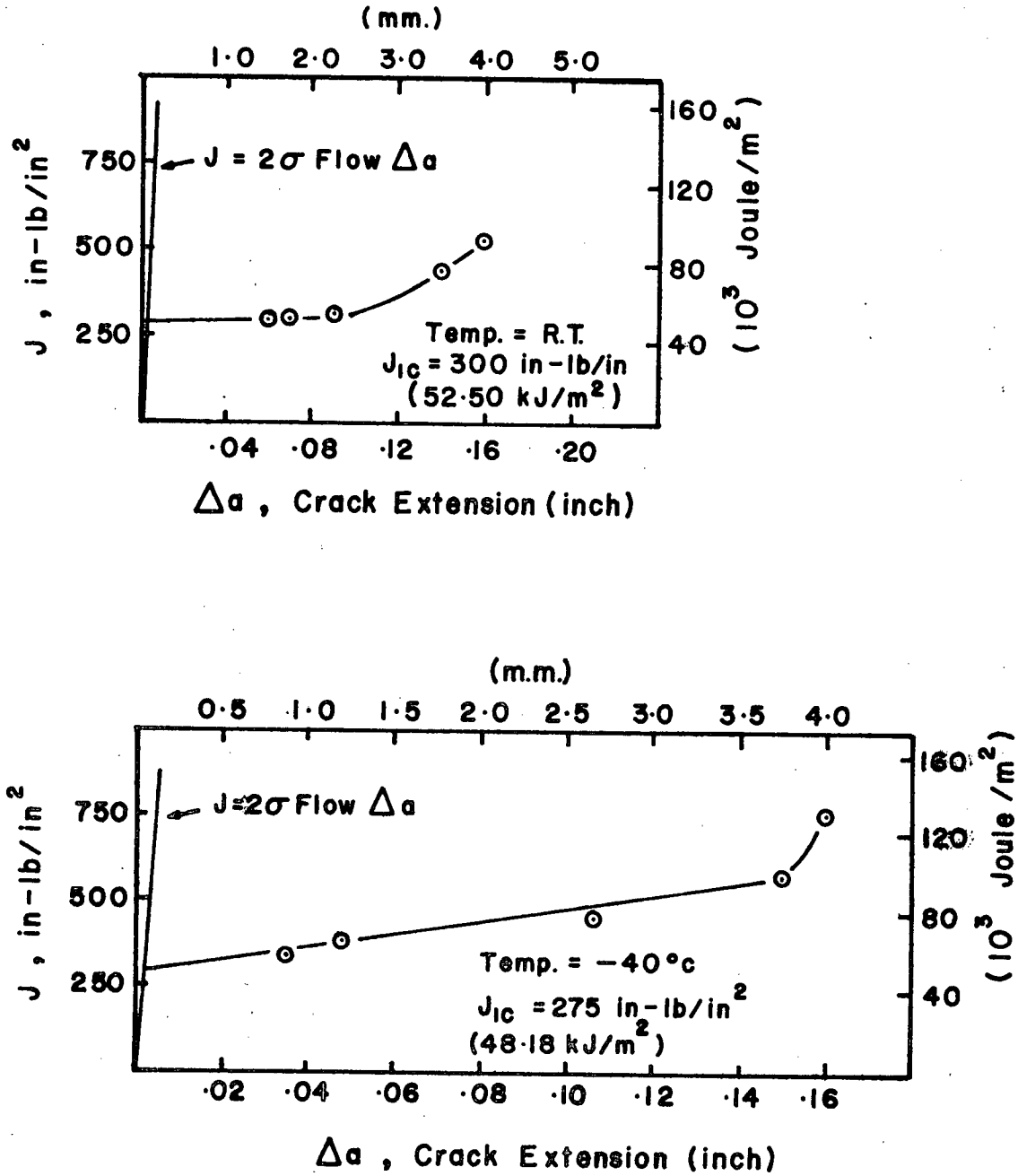

FIG. 6.11.1.
J - resistance curve for AF-1 steel with crack parallel to rolling direction at R.T & −40 °c

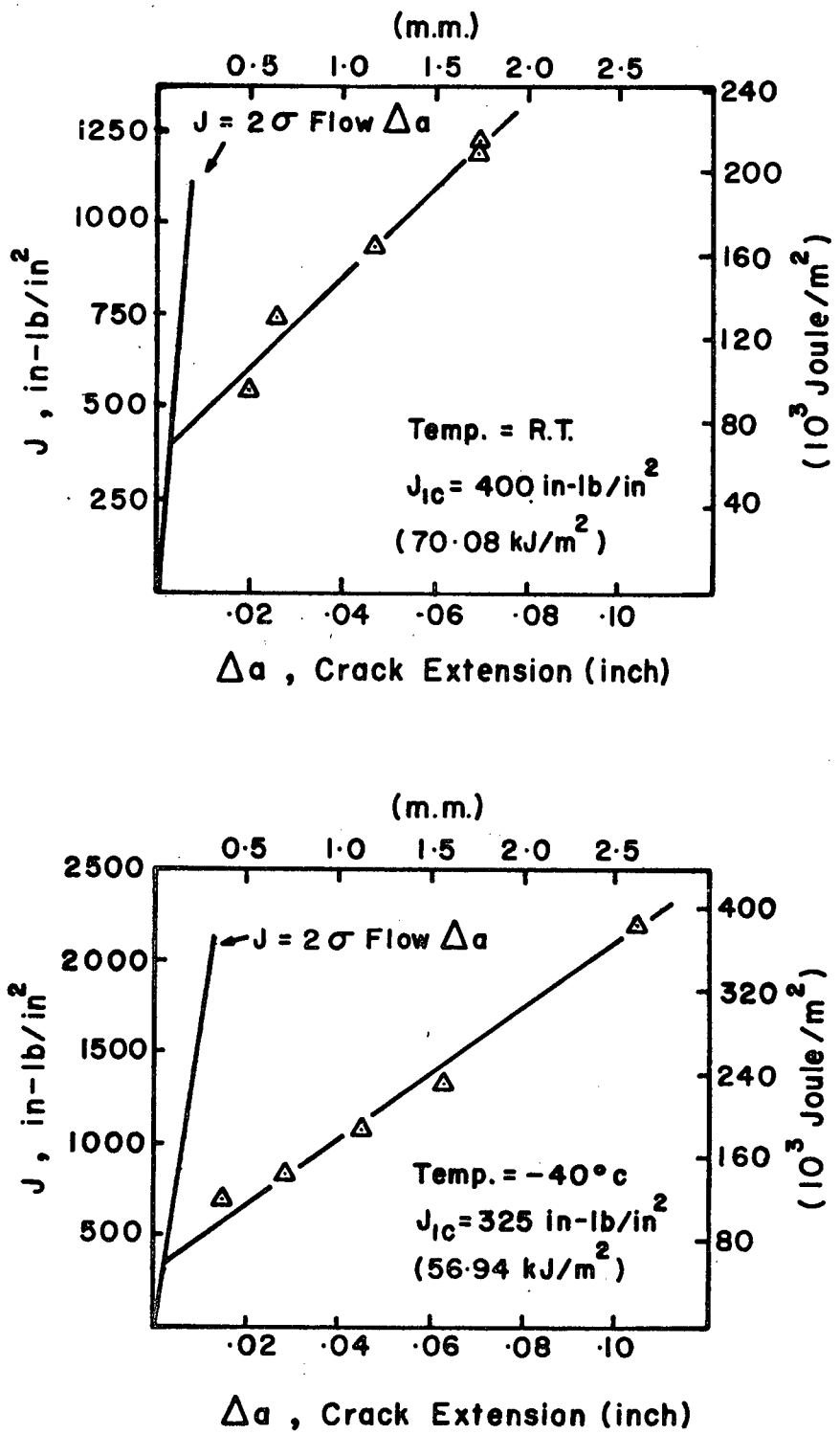

Figure 6.11.2. J-Resistance curve for AF-1 steel with crack parallel to Pipe Axis at RT & -40°C.

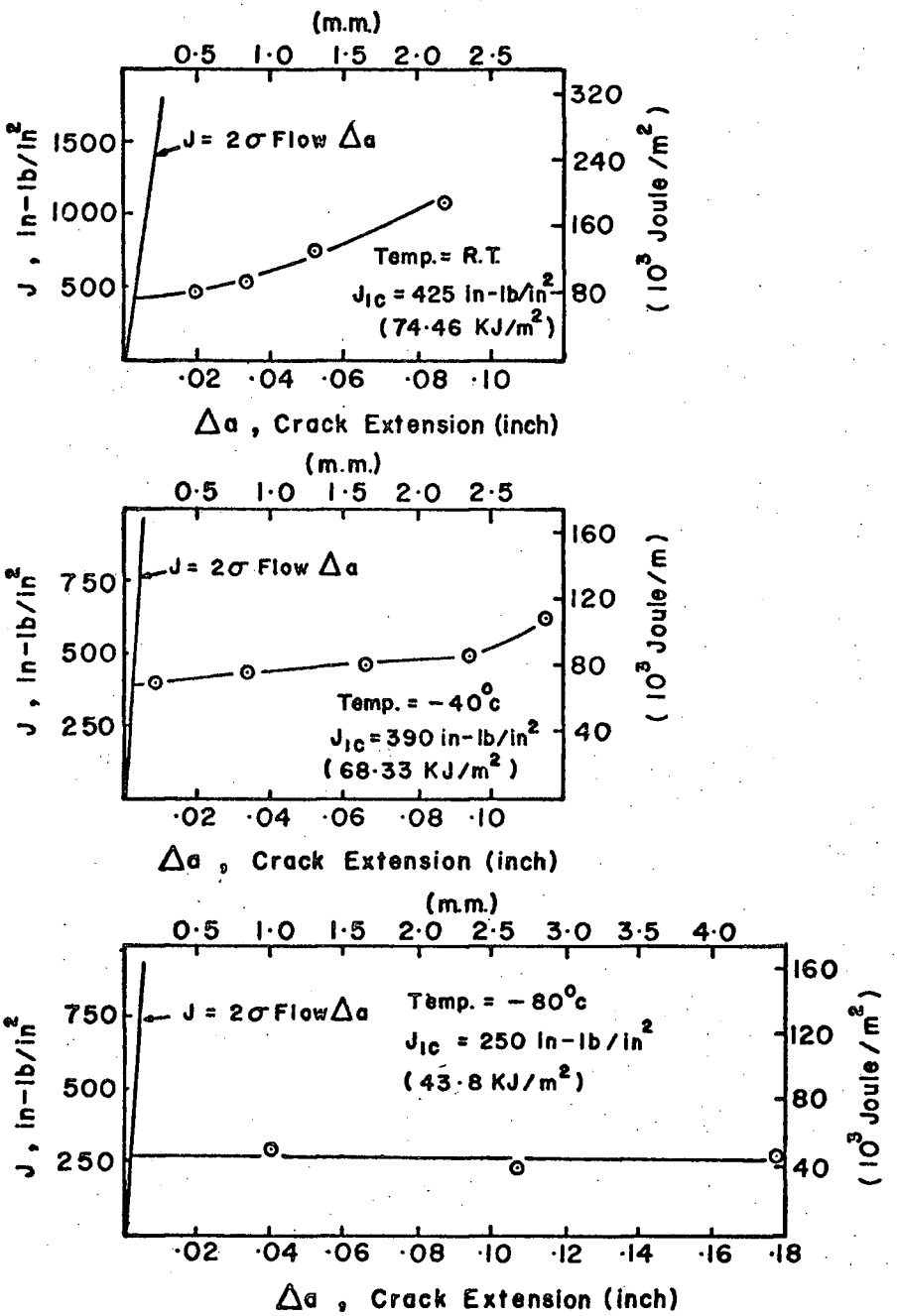

FIG. 6.11.3.
J-resistance curve for steel AF-1 with crack transverse to rolling direction at R.T., −40°c & −80°c.

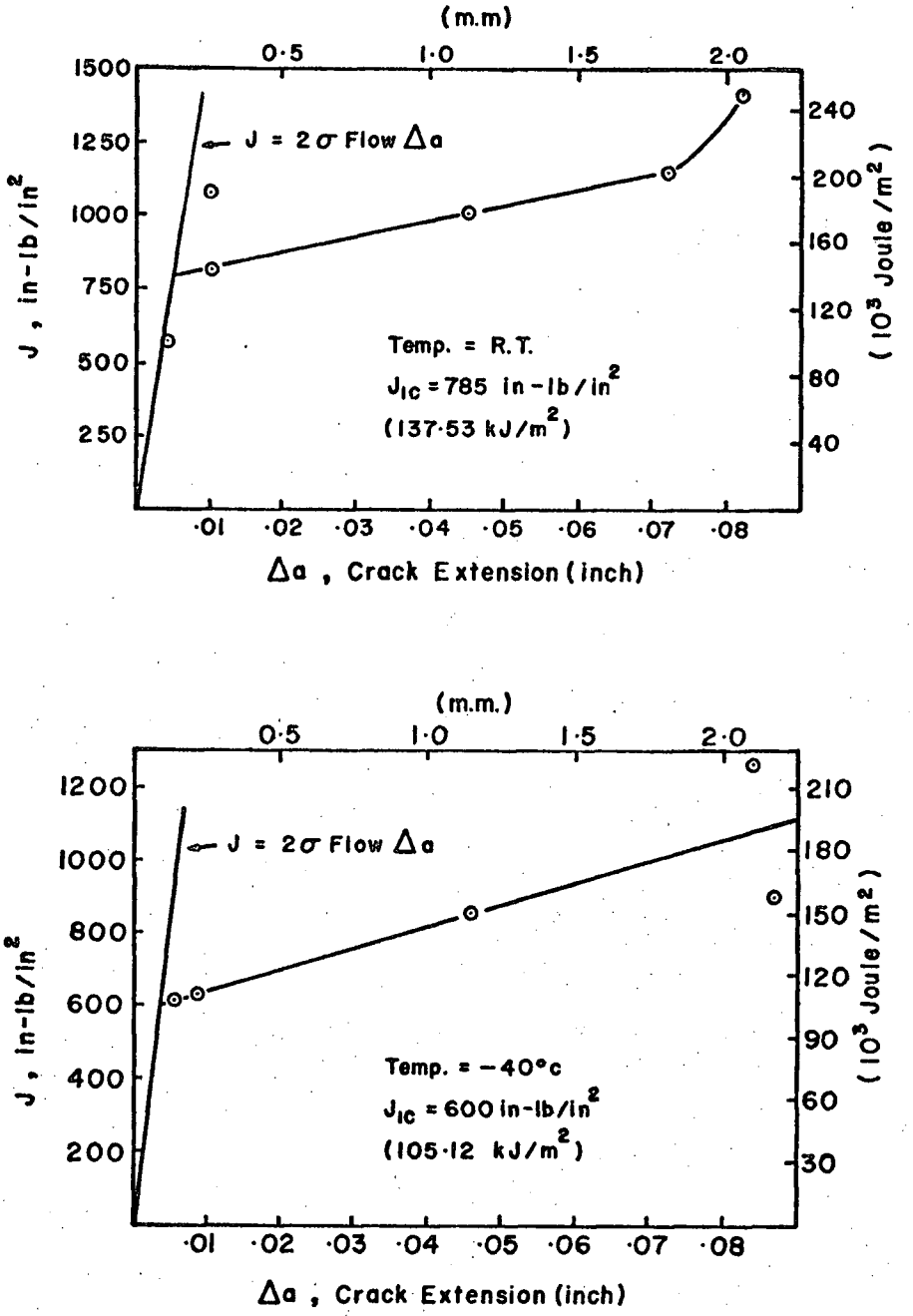

Figure 6.12.1. J-Resistance curve for Af-2 Steel - with crack parallel to Rolling Direction at RT and -40°C.

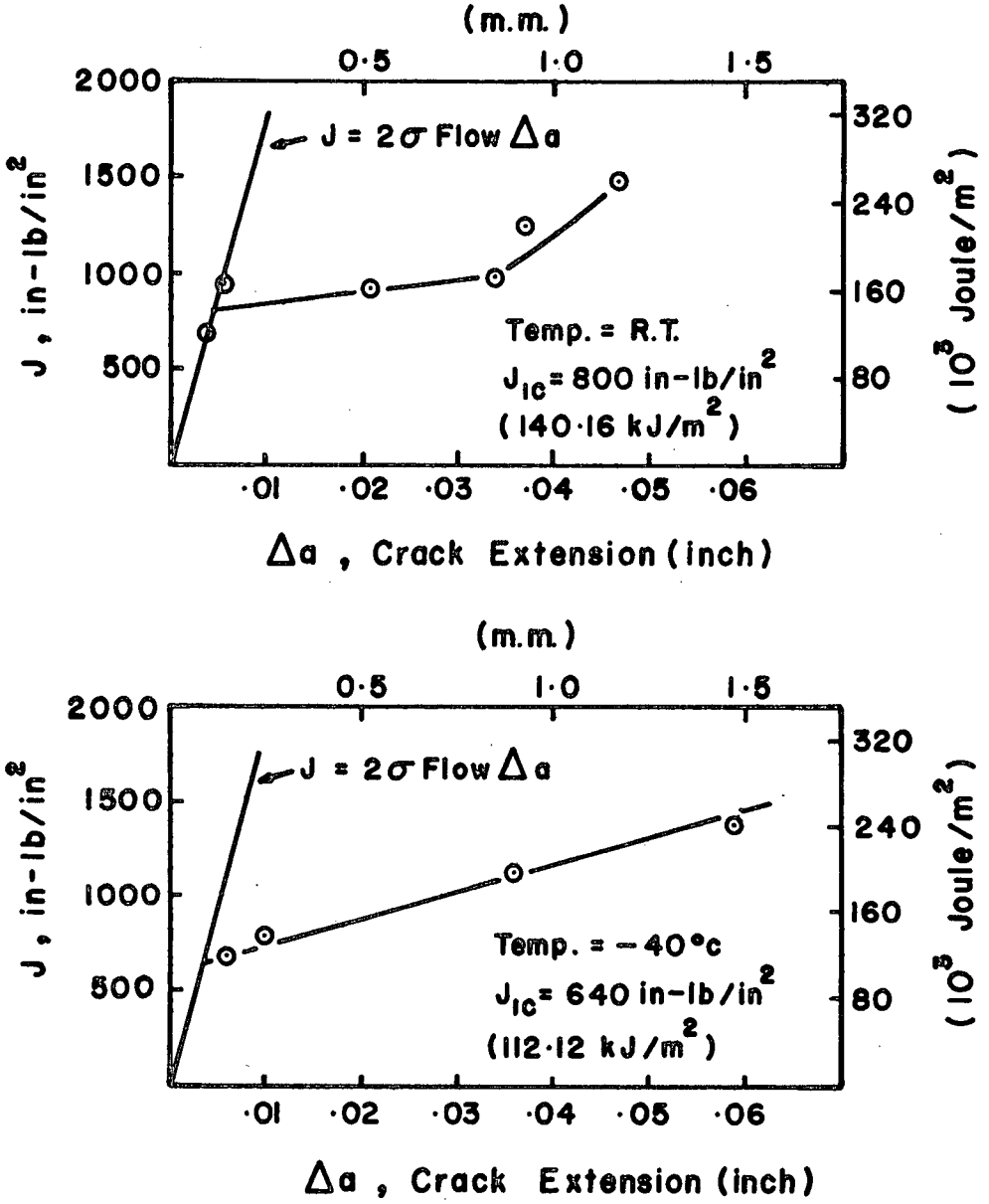

Figure 6.12.2. J-Resistance curves for AF-2 steel with crack parallel to Pipe Axis at RT and -40°C.

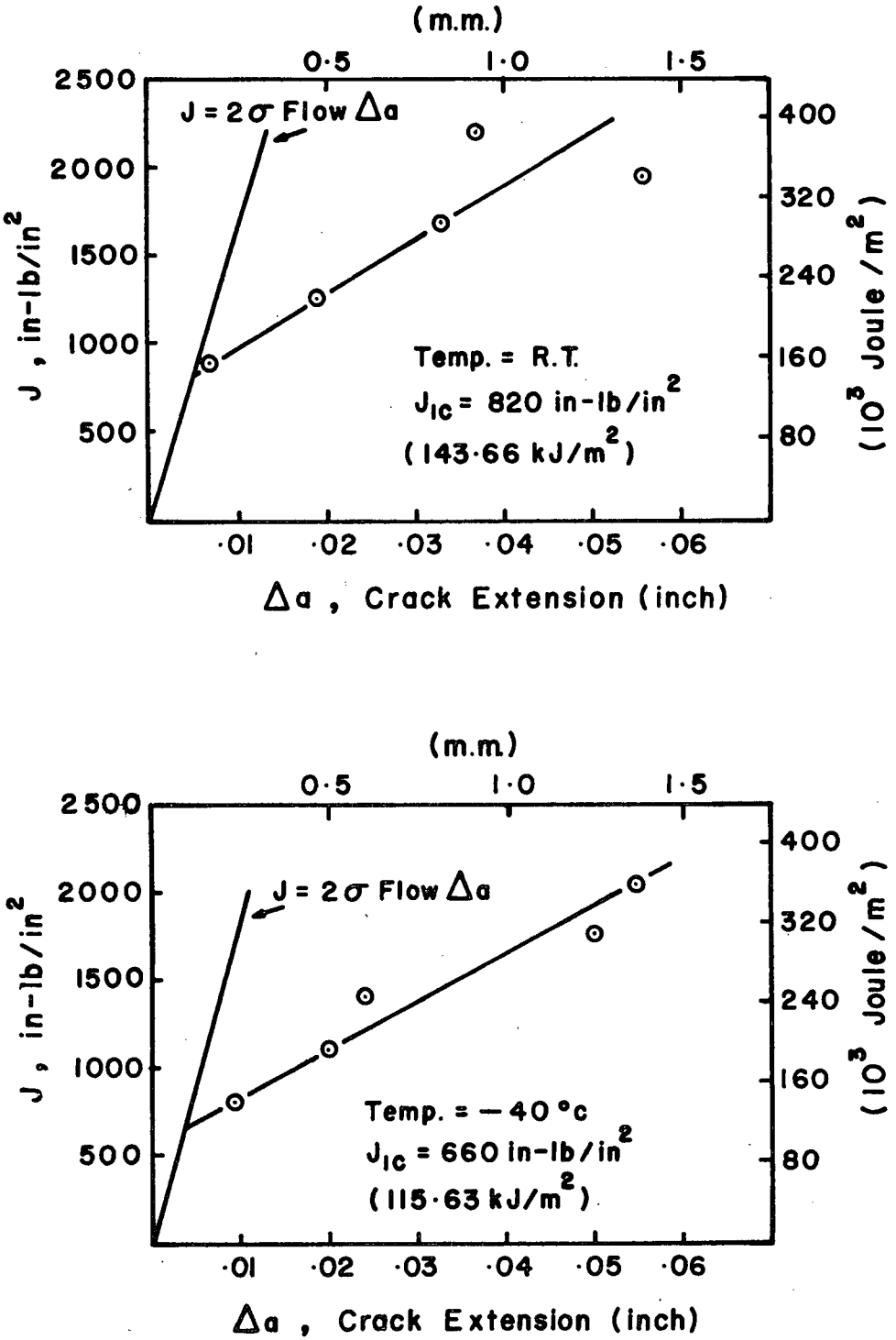

Figure 6.12.3. J-Resistance curves for AF-2 steel with crack Transverse to Rolling Direction at RT & -40°C.

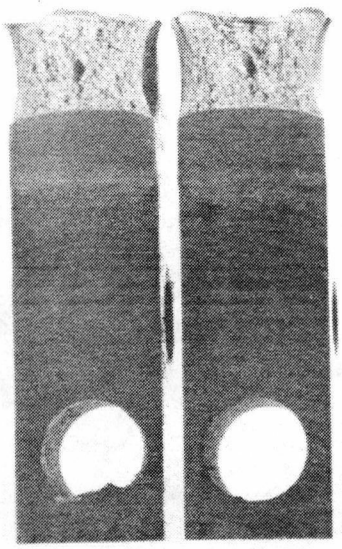

No. 33-V
R.T.

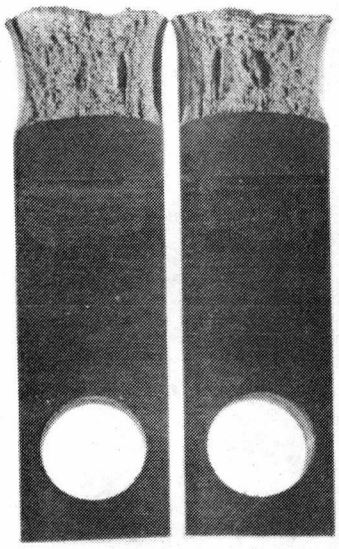

No. 29-I
R.T.

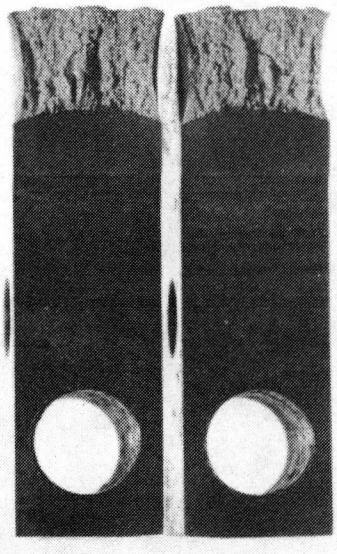

No. 30-II
R.T.

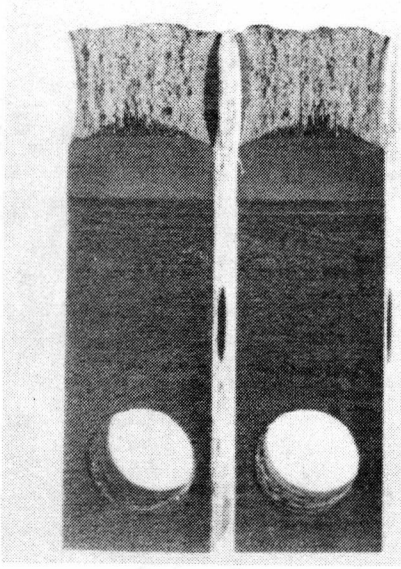

No. 32-IV
R.T.

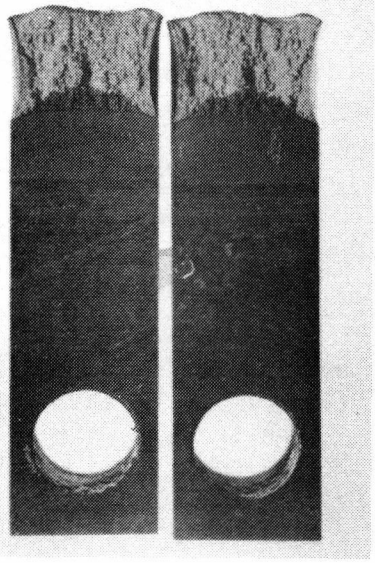

No. 31-III
R.T.

Figure 6.13.1 Fracture surfaces of AF-2 steel specimens with crack parallel to Rolling direction, tested at R.T. Arranged in order of increasing crack extension.

to construct the J-resistance curve in Fig. 6.12.1.

The specimens in Fig. 6.13.1 are kept in the order of increasing crack extension. Heat-tinting clearly distinguishes the crack extension experienced by each specimen.

The fracture toughness value, J_{Ic}, the critical value of J obtained for each of these curves for temperatures - 40 °C and RT and the direct values from the tests conducted at other temperatures are reported in Tables 6.1, 6.2, 6.3 for the AF-1 steel and in Tables 6.4, 6.5, 6.6 for the AF-2 steel.

The J-Integral tests confirmed that with increasing temperature, the fracture toughness of a material increases. This is demonstrated for both steels in Figs. 6.14.1, 6.14.2 and 6.14.3.

The test results show a similar fracture toughness transitional behaviour as was observed in the K_{Ic} tests. Fig. 6.15.1 compares the K_Q and J data for both steels and shows that for the crack parallel to the rolling direction the results at - 130 °,

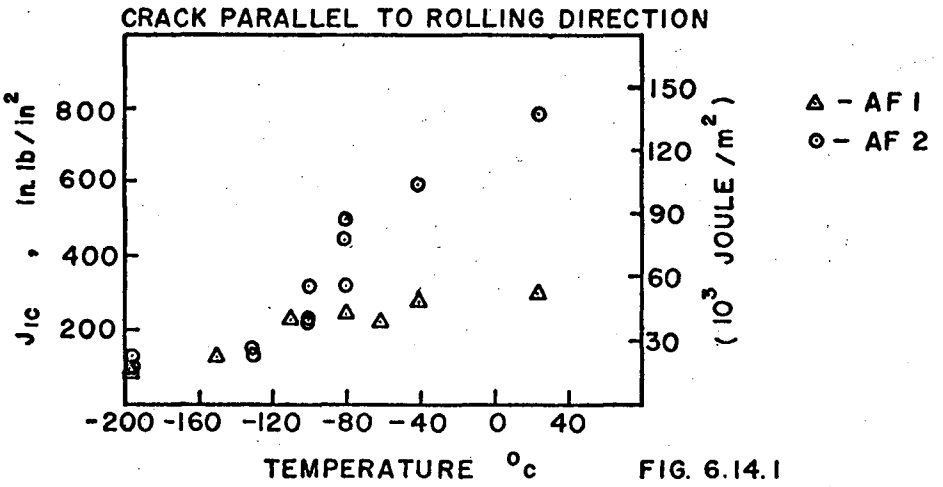

FIG. 6.14.1

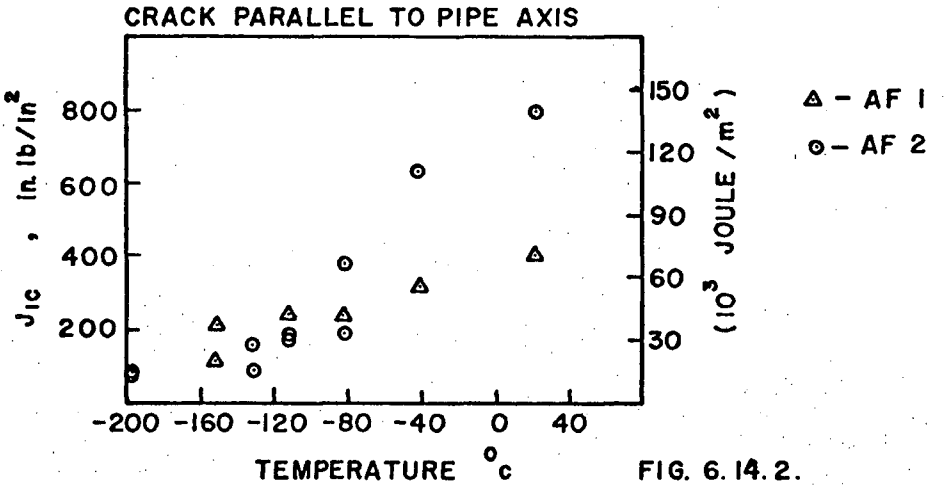

FIG. 6.14.2.

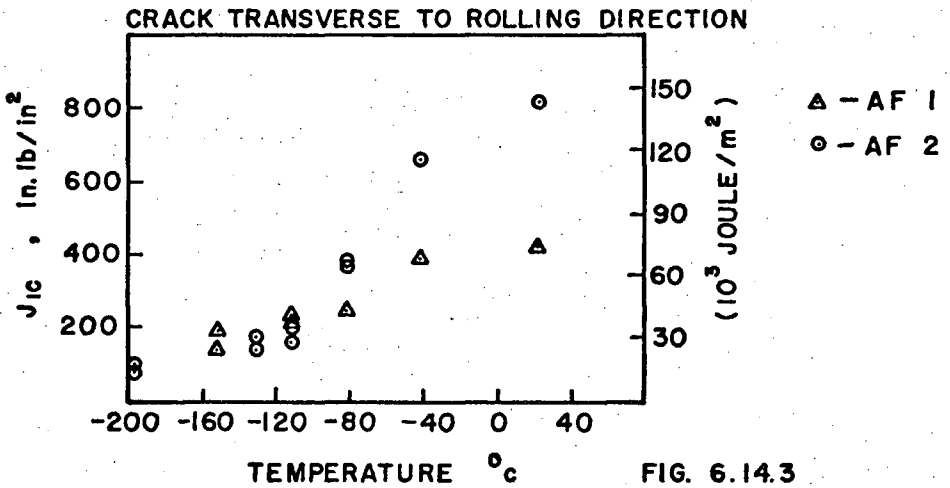

FIG. 6.14.3

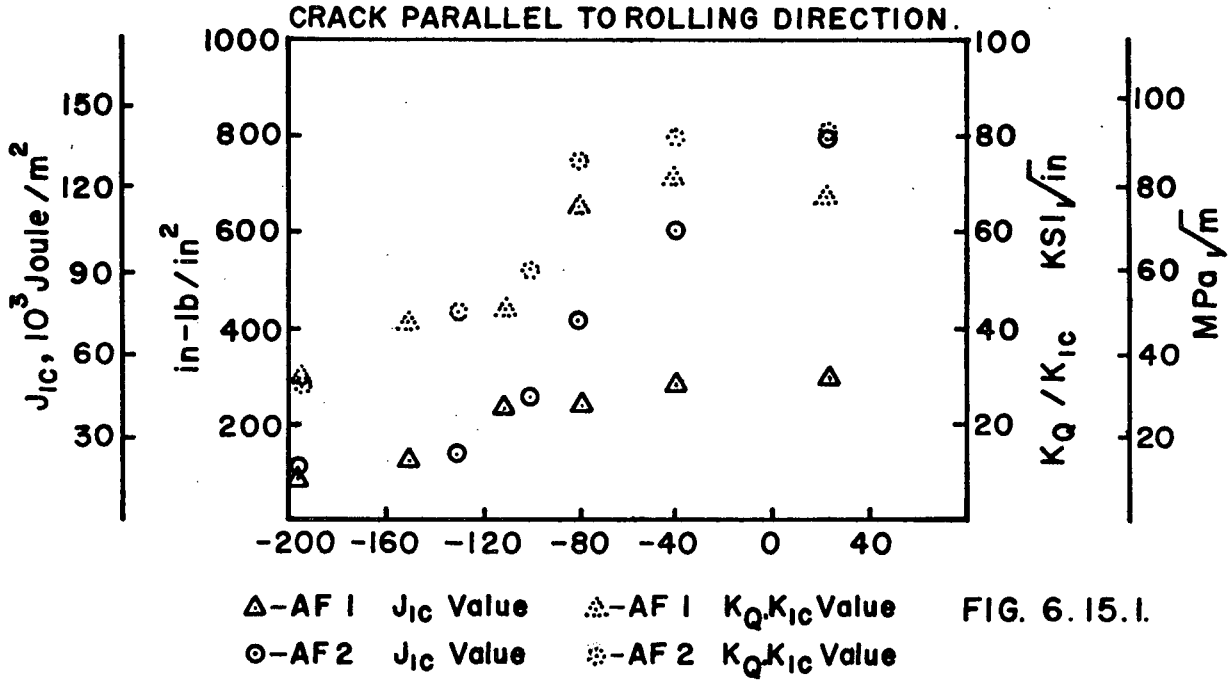
CRACK PARALLEL TO ROLLING DIRECTION.
J_{IC}, 10^3 Joule/m^2
in-lb/in^2
K_Q / K_{IC} KSI$\sqrt{in}$
MPa$\sqrt{m}$
150
120
90
60
30
1000
800
600
400
200
100
80
60
40
20
100
80
60
40
20
-200 -160 -120 -80 -40 0 40
△-AF 1 J_{IC} Value
⊙-AF 2 J_{IC} Value
△-AF 1 K_Q.K_{IC} Value
⊙-AF 2 K_Q-K_{IC} Value

FIG. 6.15.1.

-150^{o}, and -196^{o}C lie in the lower shelf, -40^{o}C and RT in the upper shelf region and -80^{o}, -100^{o}C and -110^{o}C lie in the transitional range. This is true for both of the steels for all three test directions. It should be noted that the J_{Ic} values are valid over the whole temperature range - and that this fracture toughness transitional behaviour depicts the J_{Ic} transitional pattern; whereas in the K_Q - K_{Ic} testing, the plane strain to plane stress transition (K_{Ic} to K_Q) was observed and not a K_{Ic} transition.

For the AF-1 steel, the J_{Ic} transitional curves do show anisotropic behaviour; the highest toughness is realised in specimens in which the crack propagates transverse to the rolling direction. This is quite usual as along this longitudinal (L-T) direction a material would be expected to possess its highest toughness. The minimum upper shelf toughness is realized for the crack growing parallel to the rolling direction (T-L). This indicates that the material possesses its minimum toughness along the transverse (T-L) direction. However, the lower shelf J_{Ic} values are similar in magnitude in all three test directions.

In the case of the AF-2 steel, the J_{Ic} transition curves do not show any marked anisotropy in fracture toughness behaviour. These J_{Ic} curves clearly show that the AF-2 steel is much tougher than the AF-1 steel in the transition and upper shelf temperature range. At RT, the AF-2 steel tested with the crack parallel to the pipe axis exhibits a J_{Ic} value of 800 in-lb/in^2 (140.16 KJ/m^2), whereas for the same test direction, the AF-1 steel shows approximately 400 in-lb/in^2 (70.08 KJ/m^2). This is shown in Table 6.7.

Table: 6.7 Comparative J_{Ic} values of AF-1 and AF-2 Steels along crack parallel to rolling direction (T-L) and crack parallel to pipe axis

Test Temperature °C	Crack Parallel to Rolling Direction				Crack Parallel to Pipe Axis			
	AF-1		AF-2		AF-1		AF-2	
	J_{Ic} in-lb/in^2	J_{Ic} KJ/m^2	J_{Ic} in-lb/in^2	J_{Ic} KJ/m^2	J_{Ic} in-lb/in^2	J_{Ic} KJ/m^2	J_{Ic} in-lb/in^2	J_{Ic} KJ/m^2
RT	300	52.56	785	137.53	400	70.08	800	140.16
-40	275	48.18	600	105.12	325	56.94	640	112.12
-80	250	43.80	418	73.23	240	42.05	379	66.40
-100	-	-	264	46.25	-	-	-	-
-110	237	41.52	-	-	284	49.75	176	30.83
-130	-	-	142	24.87	-	-	124	21.72
-150	127	22.25	-	-	161	28.20	-	-
-196	82	14.36	118	20.67	54	9.46	80	14.01

For the tests conducted at - 40 °C along the same orientations, the AF-2 steel exhibits a J_{Ic} toughness of 640 in-lb/in^2 (112.12 KJ/m^2) whereas the AF-1 steel gives only 325 in-lb/in^2 (56.94 KJ/m^2).

The greatest difference in toughness between the AF-1 and the AF-2 steels is observed for specimens tested with the crack parallel to the rolling direction (T-L) (Table 6.7). For example, at RT, the AF-2 steel exhibits a J_{Ic} toughness of 785 in-lb/in^2 (137.53 KJ/m^2) whereas the AF-1 steel gives only 300 in-lb/in^2 (52.56 KJ/m^2). The data shown in Table 6.7 also suggests that in the design consideration for pipelines, the fracture toughness of a pipe should be considered not only along the pipe axis but also parallel to the rolling direction, the (T-L) direction of the plate since the material is weakest along this orientation. It is the combination of the stress and the toughness that will influence failure. Even though the Hoop stress is the maximum operating stress, high residual welding stresses can exist parallel to the lower toughness rolling direction (T-L).

The high toughness J_{Ic} values reported for

the AF-2 steel are thought to be due to the beneficial effect of the low sulphur content of the steel and the sulphide shape control [5]. The rare earth sulphides that are present in the AF-2 steel are spherical in shape, have a high melting point and do not elongate to form stringers in the direction parallel to the rolling direction as is the case for the AF-1 steel. Hence, the lower non-metallic inclusion content and the beneficial effect of the rare earth additions [61] have resulted in the high toughness for the AF-2 steel.

6.2.3 COD Test Results:

The critical COD values (δ_m and δ_Q) are shown in Tables 6.1, 6.2, 6.3 for the AF-1 steel and Tables 6.4, 6.5, 6.6 for the AF-2 steel.

The variation of δ_c in terms of δ_m and δ_Q with temperature for all of the test specimens is also shown in Figures 6.16.1, 6.16.2, 6.16.3 for the δ_m values and in Figures 6.17.1, 6.17.2 and 6.17.3 for the δ_Q values.

The general trends and characteristics of

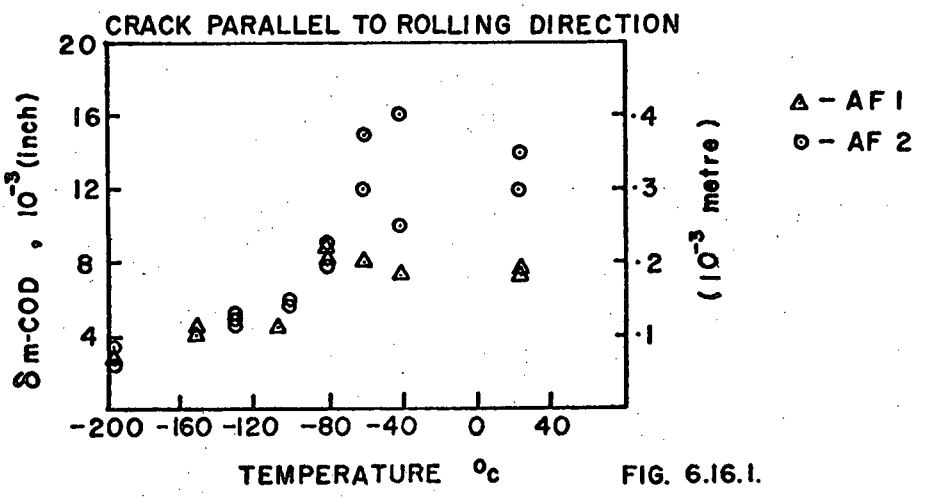

FIG. 6.16.1.

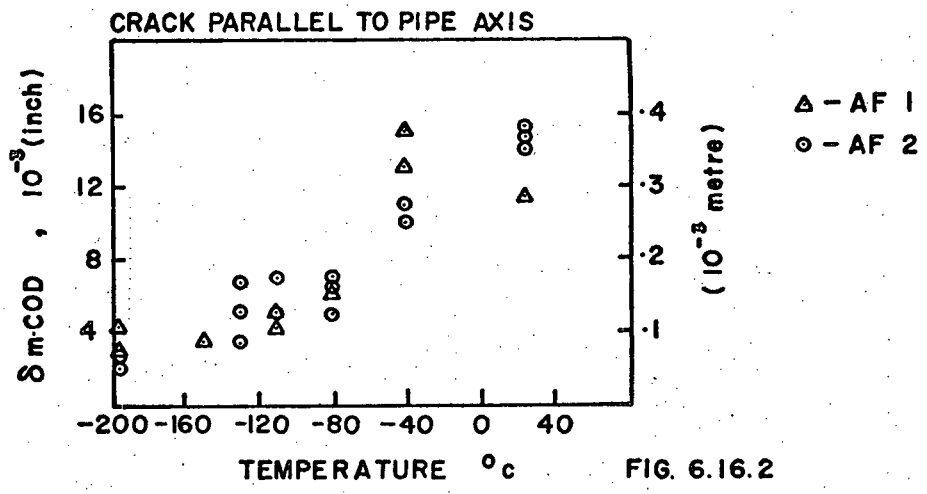

FIG. 6.16.2

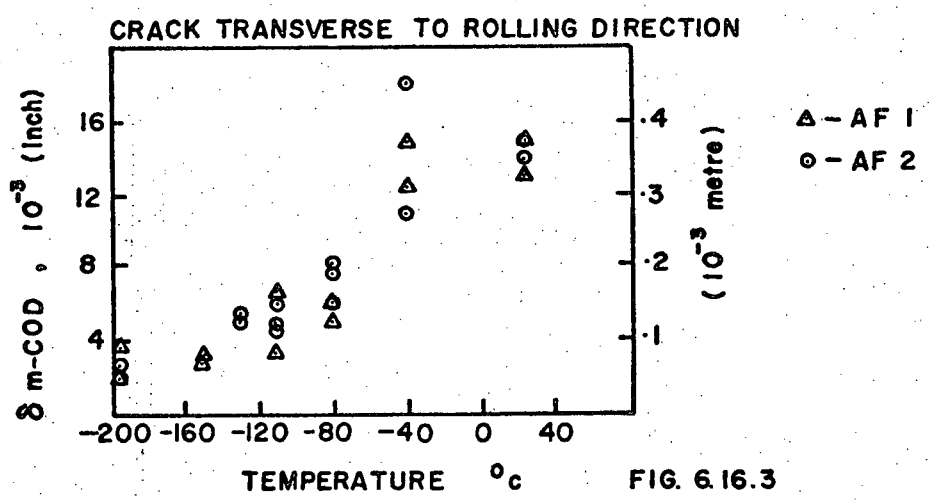

FIG. 6.16.3

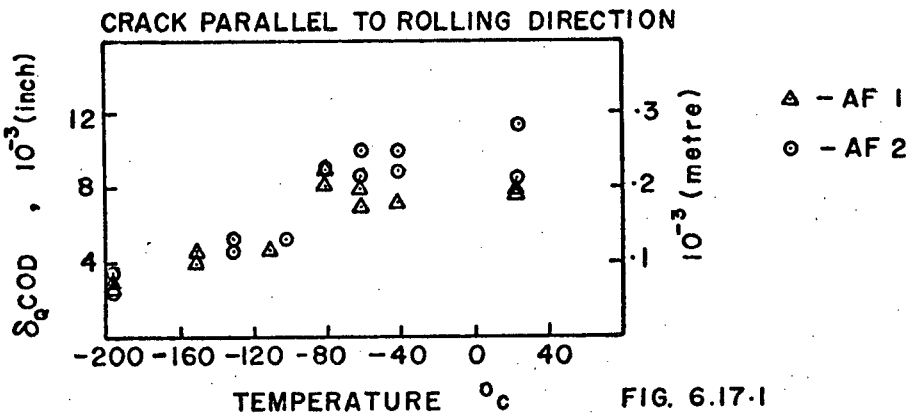

FIG. 6.17.1

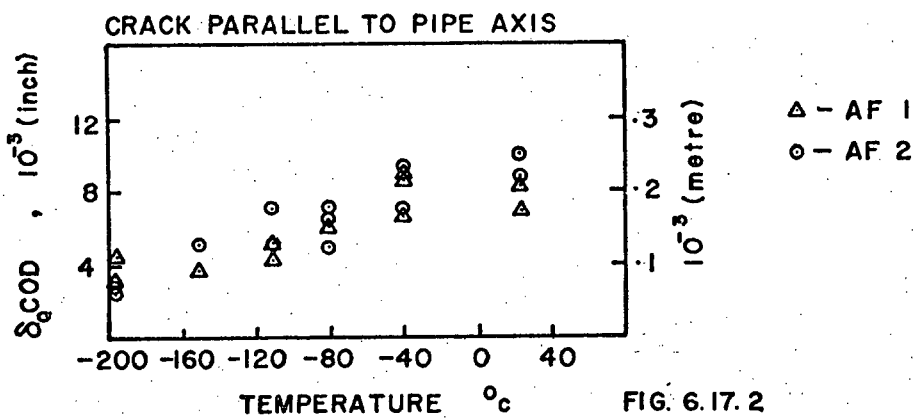

FIG. 6.17.2

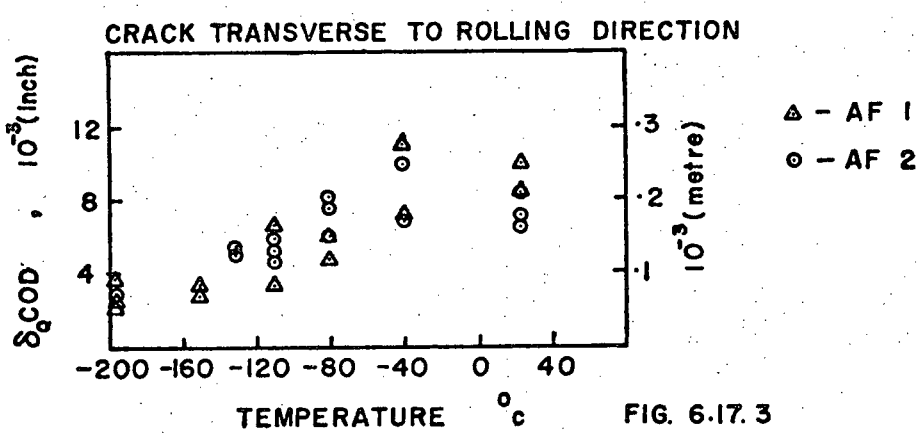

FIG. 6.17.3

the COD transition curves remain similar to those of the J_{Ic} or K_Q - K_{Ic} curves. But the COD data exhibits much more scatter than the data obtained from the other two methods.

From the δ_m vs. T data (Fig. 6.16.1 to 6.16.3) it is obvious that the δ_m values of both steels are comparable at - 80°C and below, this being the lower temperature portion of the transition temperature range and the lower shelf condition. In the upper shelf region, the AF-2 steel possesses a much higher δ_m value than does the AF-1 steel for the crack running parallel to the rolling direction (T-L orientation). The same is found to be true if the δ_Q value of both steels are considered (refer to Fig. 6.17.1). In contrast, the δ_m and the δ_Q values of both steels do not differ significantly in the other two test directions. The δ_m vs T transition curves clearly show that the COD properties of the AF-2 steel are more isotropic than those of the AF-1 steel.

Therefore, the COD test results also verify that the AF-1 steel which contains more sulphur than the AF-2 steel possesses a minimum upper shelf

toughness for the crack running parallel to the rolling direction (the T-L orientation). Similar observations have been reported in various works (5, 49, 61)

6.3 Comparison of Fracture Toughness from K_{Ic}, J-Integral and COD Tests:

The fracture toughness values, K_Q and K_{Ic}, from the K_{Ic} tests and the equivalent K_{Ic} values from the J_{Ic} and COD tests are compared in the transition curves shown in Figures 6.18.1, 6.18.2, 6.18.3 for the AF-1 steel and in Figures 6.19.1, 6.19.2, 6.19.3 for the AF-2 steel. The respective data are summarized in Tables 6.1 to 6.6.

It should be noted that K_Q values at temperatures - 130 °C and below are valid and hence represent the linear elastic fracture toughness K_{Ic} values.

In general, the three approaches to determine the temperature dependence of fracture toughness reveal:

1) that the fracture toughness of the two

acicular ferrite steels increases with increasing temperature

2) that the COD elastic-plastic fracture toughness values lie above the J_{Ic} elastic-plastic fracture toughness and that the J_{Ic} values lie above the K_Q values at higher temperatures and above the K_{Ic} values at lower temperatures

3) that δ_m - K_{Ic} data obtained from the COD tests are much higher in magnitude than the K_{Ic} values predicted by the other test results; the values are approximately twice the magnitude of the J-Integral values over the entire temperature range of the tests.

4) that the K_{Ic} data obtained from the J-Integral test is larger in magnitude than the K_Q or K_{Ic} data; the magnitude of the difference between two sets of data generally increases with increasing temperature. The difference is most pronounced for the AF-2 steel at the higher temperatures for the three test directions examined.

5) that in one case for the AF-1 steel with the crack propagating parallel to the pipe axis, very good agreement was obtained between the linear elastic, K_{Ic}, and the elastic-plastic, J_{Ic}, fracture

toughness results.

At higher temperatures, the COD and the J_{Ic} values indicate a large increase in toughness which is not reflected in the K_Q values. This has been explained by Egan [39] as the inability of the K-type analyses to take account of the increase in the size of the plastic zone; the larger plastic zone would have required more work than if the same load value (P_Q) had been reached by linear elastic loading. Therefore, at higher temperatures, where K_Q tests do not give valid K_{Ic} results, a more meaningful and representative toughness level is indicated by the COD and J_{Ic} test results.

A wide difference between the valid K_{Ic} data and the equivalent K_{Ic} from δ_m - COD and J_{Ic} tests is observed at lower shelf temperatures. The equivalent K_{Ic} data from δ_m - COD at low temperatures indicate that the fracture toughness of both steels increased at - 130 ^{o}C and below. This is misleading in that if the experimental COD data at - 130 ^{o}C and lower temperature for both steels is considered (refer Fig. 6.16.1 to 6.16.3). The equivalent K_{Ic} from δ_m - COD

was obtained using the following relationship

$$K_{Ic} \text{ equivalent} = \sqrt{\frac{E\ \delta_m\ \sigma_{ys}}{1 - \nu^2}}$$

Where σ_{ys} = yield strength of the material at test temperature and strain rate

E = Young's Modulus

ν = Poisson's Ratio

At higher temperatures, the conversion of δ_m - COD to K_{Ic} gives reasonable agreement, whereas at low temperates, - 130 ^{o}C and below, the conversion results in an increase in fracture toughness with decreasing temperature. This apparent increase in equivalent K_{Ic} from δ_m - COD may be due to the high yield strength of the material at low temperature. Therefore, the conversion relationship for δ_m - COD to equivalent K_{Ic} does not seem to be applicable at the lower temperature range.

The difference between the two estimates of the elastic-plastic fracture toughness as indicated by the equivalent K_{Ic} data obtained from δ_m or δ_Q values and J_{Ic} values, particularly at upper shelf temperatures,

can be explained as follows. The linear elastic fracture toughness values, that is, the K_{Ic} or K_Q values are based on a 2% effective crack growth which includes the effect of plastic zone formation. Therefore, the critical COD- δ_Q value represents a 2% effective crack growth condition. Hence in this case, δ_Q represents a 0.01" (0.2 x 0.5 = 0.01 inch) inch crack growth on a 0.5 inch ligament on a 0.5 inch thick compact tension specimen. In contrast, the δ_m - COD value represents a much higher crack growth condition as this displacement is obtained for the maximum load.

In comparing the COD values with the J-Integral values, it should be recalled that the corresponding J_{Ic} value is based on crack initiation only, that is, zero crack growth due to actual material separation.

Consider the following example in which is examined the difference between the J_{Ic} value and the δ_Q value at - 40 °C for the crack parallel to the pipe axis for the AF-2 steel (Fig. 6.19.2 or Table 6.5): J_{Ic} = 145 ksi$\sqrt{in}$ (159.35 MPa$\sqrt{m}$) whereas δ_Q Average = 162 ksi$\sqrt{in}$ (178.03 MPa$\sqrt{m}$). Using - 40°C the J-resistance curve data for the AF-2 steel with the

crack parallel to the pipe axis (Fig. 6.12.2), Δa = .01 inch gives J = 775 in-lb/in^2, (135.78 KJ/m^2). The corresponding value of K_{Ic} is 158.84 ksi$\sqrt{in}$ (175.66 MPa$\sqrt{m}$). This equivalent K_{Ic} value agrees with the δ_Q value of 162 ksi$\sqrt{in}$ (178.03 MPa$\sqrt{m}$) shown in the Fig. 6.19.2. Therefore, it is apparent that in the upper shelf temperature region, the difference between the equivalent K_{Ic} as obtained from the J_{Ic} data and the K_{Ic} obtained from the δ_Q - COD data is insignificant provided an appropriate correction for crack growth is taken into account. The large deviation between the equivalent K_{Ic} from δ_m COD data and the equivalent K_{Ic} from J_{Ic} data in the upper shelf temperature region, where $K_{Ic} = \delta_m$ is approximately twice the $K_{Ic} - J_{Ic}$, is not surprising. The simplest explanation is that the $K_{Ic} - J_{Ic}$ stands for NIL CRACK GROWTH whereas $K_{Ic} - \delta_m$ stands for EXTENSIVE CRACK GROWTH CORRESPONDING TO MAXIMUM LOAD.

In the transition temperature region, the large difference between the $K_{Ic} - J_{Ic}$ and K_{Ic} δ_m or δ_Q can be attributed to two effects:

i) the definitions of K_{Ic} and δ_m fracture toughness are based upon different crack growth criteria

ii) the increase in yield strength at low temperatures.

The tendency of equivalent K_{Ic} values from J_{Ic} data to be larger in magnitude than the K_{Ic} values even at the low temperatures where both the test procedures involve ½ inch thick compact tension specimens and both the test samples experience 100% cleavage fracture is thought to be due to the smaller energy expended in fracturing J_{Ic} specimens in comparison to that required to fracture K_{Ic} specimens. The ligament length in the K_{Ic} specimen is approximately .45 to .50 W, whereas the ligament length in the J_{Ic} specimen is approximately .35 to .30 W; where W is the specimen depth.

TABLE - 6.1

AF-1 Steel crack Parallel to Rolling Direction

(T-L Orientation)

	K_Q		J_{Ic}		COD				Equivalent K_{Ic}					
					δ_m		δ_Q		J_{Ic}		COD-δ_m		COD-δ_Q	
Temp. °C	ksi$\sqrt{in}$	MPa$\sqrt{m}$	in-lb/in^2	KJ/m^2	inch	mm	inch	mm	ksi$\sqrt{in}$	MPa$\sqrt{m}$	ksi$\sqrt{in}$	MPa$\sqrt{m}$	ksi$\sqrt{in}$	MPa$\sqrt{m}$
RT	68.88	75.70	300.00	52.56	0.0078	0.1981	0.0078	0.1981	99.44	109.28	144.00	158.25	144.00	158.25
	66.00	72.53			0.0076	0.1930	0.0074	0.1879			141.69	155.71	139.80	153.64
- 40	72.25	79.40	275.00	48.18	0.0075	0.1905	0.0070	0.1778	95.21	104.63	143.18	157.35	138.32	152.01
	72.30	79.45			0.0075	0.1905	0.0070	0.1778			143.18	157.35	138.32	152.01
- 60	71.99	79.11	220.00	38.54	0.0081	0.2057	0.0072	0.1828	85.16	93.59	152.91	168.04	143.95	158.20
	74.99	82.41			0.0081	0.2057	0.0079	0.2006			152.73	167.85	150.37	165.25
- 80	70.73	77.73	250.00	43.80	0.0082	0.2082	0.0082	0.2082	90.78	99.76	153.96		153.96	169.20
	62.18	68.33			0.0091	0.2311	0.0091	0.2311			162.19		162.19	178.24
- 110	44.33	48.71	236.86	41.49	0.0046	0.1168			88.36	97.10	123.99			
- 150	39.74	43.67	127.12	22.27	0.0046	0.1168			64.73	71.13	135.24			
	42.05	46.21			0.0041	0.1041					127.25			
- 196	30.25	33.24	83.53	14.63	0.0028	0.0711			52.47	57.66	122.39			
	31.28	34.37	80.94	14.18	0.0029	0.0736			51.65	56.76	122.91			

TABLE - 6.2

AF-1 Steel crack Parallel to Pipe Axis

Temp.	K_Q		J_{Ic}		COD				Equivalent K_{Ic}					
					δ_m		δ_Q		J_{Ic}		COD-δ_m		COD-δQ	
°C	ksi$\sqrt{in}$	MPa$\sqrt{m}$	in-lb/in^2	KJ/m^2	inch	mm	inch	mm	ksi$\sqrt{in}$	MPa$\sqrt{m}$	ksi$\sqrt{in}$	MPa$\sqrt{m}$	ksi$\sqrt{in}$	MPa$\sqrt{m}$
RT	73.05	80.28	400.00	70.08	0.0115	0.2921	0.0084	0.2133	114.83	126.19	171.00	187.92	146.00	160.45
	76.70	84.29			0.0115	0.2921	0.0068	0.1727			171.00	187.92	132.00	145.06
- 40	76.20	83.74	325.00	56.94	0.0134	0.3403	0.0087	0.2209	103.50	113.74	177.24	194.78	136.52	150.03
	70.70	77.69			0.0113	0.2870	0.0066	0.1676						
	70.70	77.69			0.0150	0.3810	0.0092	0.2336			204.34	224.56	160.55	176.44
- 80	59.00	64.84	240.00	42.04	0.0061	0.1549			88.94	97.74	133.14	146.32		
- 110	55.83	61.35	328.94	57.63	0.0042	0.1066			104.13	114.43	115.12	126.51		
	54.18	59.54	239.33	41.93	0.0051	0.1295			88.82	97.61	126.30	138.80		
- 150	41.60	45.71	211.20	37.00	0.0036	0.0914			83.44	91.70	113.99	125.27		
	40.39	44.38	111.28	19.49	0.0037	0.0939			60.57	66.56	116.03	127.51		
- 196	32.89	36.14	50.68	8.87	0.0032	0.0812			40.87	44.91	124.49	136.81		
	34.07	37.44	57.97	10.15	0.0044	0.1117			43.72	48.04	146.30	160.78		

TABLE 6.3

AF-1 Steel crack Transverse to Rolling Direction

(L-T orientation)

Temp.	K_Q		J_{Ic}		COD				Equivalent K_{Ic}					
					δ_m		δ_Q		J_{Ic}		COD-δ_m		COD-δ_Q	
°C	ksi$\sqrt{in}$	MPa$\sqrt{m}$	in-lb/in^2	KJ/m^2	inch	mm	inch	mm	ksi$\sqrt{in}$	MPa$\sqrt{m}$	ksi$\sqrt{in}$	MPa$\sqrt{m}$	ksi$\sqrt{in}$	MPa$\sqrt{m}$
RT	71.93	79.05	425.00	74.46	0.0130	0.3302	0.0084	0.2133	118.36	130.07	185.31	203.65	148.96	163.70
	77.91	85.62			0.0153	0.3886	0.0105	0.2667			201.04	220.94	166.86	183.37
- 40	73.24	80.49	390.00	68.32	0.0126	0.3200	0.0072	0.1828	113.38	124.60	191.87	210.86	144.58	158.89
	80.63	88.61			0.0148	0.3759	0.0115	0.2921			207.29	227.81	183.43	201.58
- 80	55.90	61.43	250.00	43.80	0.0050	0.1270	0.0048	0.1219	90.78	99.76	127.37	139.97	125.84	138.29
	64.71	71.11			0.0061	0.1549	0.0060	0.1524			140.70	154.62	139.47	153.27
- 110	42.12	46.28	222.56	38.99	0.0034	0.0863			85.65	94.13	106.01	116.50		
	55.68	61.19	243.90	42.73	0.0066	0.1676			89.67	98.54	146.26	161.83		
- 150	33.77	37.11	141.13	24.72	0.0027	0.0685			68.21	74.96	103.23	113.44		
	44.69	49.11	190.72	33.41	0.0032	0.0812			79.29	87.14	111.50	122.53		
- 196	33.39	36.69	83.77	14.67	0.0037	0.0939			52.55	57.75	135.42	148.82		
	32.39	35.59	107.19	18.77	0.0021	0.0533			59.44	65.32	101.81	111.88		

TABLE - 6.4

AF-2 Steel crack Parallel to Rolling Direction

(T-L orientation)

Temp.	K_Q		J_{Ic}		COD				Equivalent K_{Ic}					
					δ_m		δ_Q		J_{Ic}		COD-δ_m		COD-δ_Q	
°C	ksi$\sqrt{in}$	MPa$\sqrt{m}$	in-lb/in^2	KJ/m^2	inch	mm	inch	mm	ksi$\sqrt{in}$	MPa$\sqrt{m}$	ksi$\sqrt{in}$	MPa$\sqrt{m}$	ksi$\sqrt{in}$	MPa$\sqrt{m}$
RT	78.12	85.85	785.00	137.53	0.0119	0.3022	0.0084	0.2133	160.86	176.78	168.91	185.63	142.62	156.73
	85.72	94.20			0.0142	0.3606	0.0114	0.2895			184.73	203.01	165.33	181.69
- 40	79.59	87.46	600.00	105.12	0.0109	0.2768	0.0089	0.2260	140.64	154.56	168.03	184.66	151.84	166.87
	83.40	91.65			0.0166	0.4216	0.0107	0.2717			207.60	228.15	166.82	183.33
- 60	80.90	88.90			0.0125	0.3175	0.0106	0.2692			182.63	200.71	168.20	184.85
	84.64	93.01			0.0150	0.3810	0.0087	0.2209			199.96	219.75	152.71	167.78
- 80	71.65	78.74	446.24	78.18	0.0098	0.2489	0.0091	0.2311	121.00	132.97	163.47	179.65	157.14	172.69
	76.53	84.10	492.51	86.28	0.0087	0.2209			127.42	140.03	154.14	169.39		
	78.67	86.45	317.83	55.68	0.0085	0.2159			102.36	112.49	152.19	167.36		
- 100	55.00	60.44	236.21	41.38	0.0058	0.1473			88.24	96.97	130.76	143.70		
			323.67	56.70					103.29	113.51				
	49.90	54.84	233.00	40.82	0.0057	0.1447			87.64	96.31	130.28	143.17		
- 130	46.52	51.12	135.62	23.76	0.0054	0.1371			66.86	73.47	140.75	154.68		
	48.18	52.94	149.50	26.19	0.0050	0.1270			70.20	77.15	135.07	148.44		
	40.32	44.31			0.0048	0.1219			132.13	145.21				
- 196	30.76	33.80	124.50	21.81	0.0026	0.0660			64.06	70.40	118.62	130.36		
	25.86	28.42	113.02	19.80	0.0036	0.0914			61.04	67.08	137.92	151.57		

TABLE - 6.5

AF-2 Steel crack Parallel to Pipe Axis

Temp.	K_Q		J_{Ic}		COD				Equivalent K_{Ic}					
					δ_m		δ_Q		J_{Ic}		COD-δ_m		COD-δ_Q	
°C	ksi$\sqrt{in}$	MPa$\sqrt{m}$	in-lb/in^2	KJ/m^2	inch	mm	inch	mm	ksi$\sqrt{in}$	MPa$\sqrt{m}$	ksi$\sqrt{in}$	MPa$\sqrt{m}$	ksi$\sqrt{in}$	MPa$\sqrt{m}$
	74.46	81.83			0.0148	0.3759	0.0103	0.2616			207.66	228.21	173.29	190.44
RT	74.98	82.40	800.00	140.16	0.0142	0.3706	0.0087	0.2209	162.39	178.46	203.34	223.47	159.34	175.11
	77.43	85.09			0.0152	0.3860	0.0103	0.2616			210.69	231.54	173.47	190.64
	76.96	84.57			0.0104	0.2641	0.0092	0.2336			181.40	199.35	171.09	188.02
- 40	69.76	76.66	640.00	112.12	0.0107	0.2717	0.0070	0.1778	145.25	159.62	184.27	202.51	149.47	164.26
	71.98	79.10			0.0109	0.2768	0.0089	0.2260			185.62	203.99	167.86	184.47
	57.72	63.43	382.52	67.01	0.0072	0.1828			112.29	123.40	155.69	171.10		
- 80	52.15	57.31	193.95	33.98	0.0051	0.1295			79.96	87.87	131.02	143.99		
	66.83	73.44	376.50	65.96	0.0066	0.1676			111.41	122.43	148.86	163.59		
	55.14	60.59	188.77	33.07	0.0054	0.1371			78.88	86.68	138.63	152.35		
- 110														
	61.04	67.08	163.00	28.55	0.0071	0.1803			73.30	80.55	158.91	174.64		
	55.53	61.02	165.31	28.96	0.0067	0.1701			73.82	81.12	160.56	176.45		
-130	34.11	37.48	83.35	14.60	0.0037	0.0939					119.09	130.87		
	57.92	63.65			0.0053	0.1346			52.42	57.60	142.19	156.26		
	26.09	28.67	93.97	16.46	0.0022	0.0558			55.66	61.17	106.47	117.01		
- 196														
	26.39	29.00	67.27	11.78	0.0027	0.0685			47.09	51.75	118.61	130.35		

TABLE - 6.6

AF-2 Steel crack Transverse to Rolling Direction

(L-T orientation)

Temp.	K_Q		J_{Ic}		COD				Equivalent K_{Ic}					
					δ_m		δ_Q		J_{Ic}		COD-δ_m		COD-δ_Q	
°C	ksi$\sqrt{in}$	MPa$\sqrt{m}$	in-lb/in^2	KJ/m^2	inch	mm	inch	mm	ksi$\sqrt{in}$	MPa$\sqrt{m}$	ksi$\sqrt{in}$	MPa$\sqrt{m}$	ksi$\sqrt{in}$	MPa$\sqrt{m}$
RT	73.58	80.86	820.00	143.66	0.0149	0.3784	0.0064	0.1625	164.41	180.68	192.35	211.39	126.07	138.55
	76.53	84.10			0.0140	0.3556	0.0071	0.1803			186.48	204.94	133.47	146.68
- 40	81.07	89.09	660.00	115.63	0.0182	0.4622	0.0103	0.2616	147.50	162.10	224.80	246.05	169.22	185.97
	74.23	81.57			0.0113	0.2870	0.0069	0.1752			177.08	194.61	138.99	152.75
- 80	77.03	84.65			0.0077	0.1955	0.0069	0.1752			150.00	164.85	142.22	156.29
	69.55	76.43	364.86	63.92	0.0082	0.2082			109.67	120.52	154.32	169.59		
	76.48	84.05	379.39	66.47	0.0078	0.1981			111.83	122.90	150.76	165.68		
- 110	49.85	54.78			0.0046	0.1168			74.54	81.91	121.66	133.70		
	63.37	69.64	168.56	29.53	0.0049	0.1244					125.12	137.50		
	60.10	66.05	194.07	34.00	0.0059	0.1498			79.98	87.89	137.72	151.35		
- 130	51.82	56.95	173.56	30.40	0.0050	0.1270			75.64	83.12	132.60	145.72		
	52.81	58.03	146.35	25.64	0.0054	0.1371			69.46	76.33	137.36	150.95		
- 196	24.97	27.44	73.03	12.79	0.0022	0.0558			49.07	53.92	105.62	116.07		
	26.97	29.64	85.99	15.06	0.0029	0.0736			53.24	58.51	120.93	132.90		

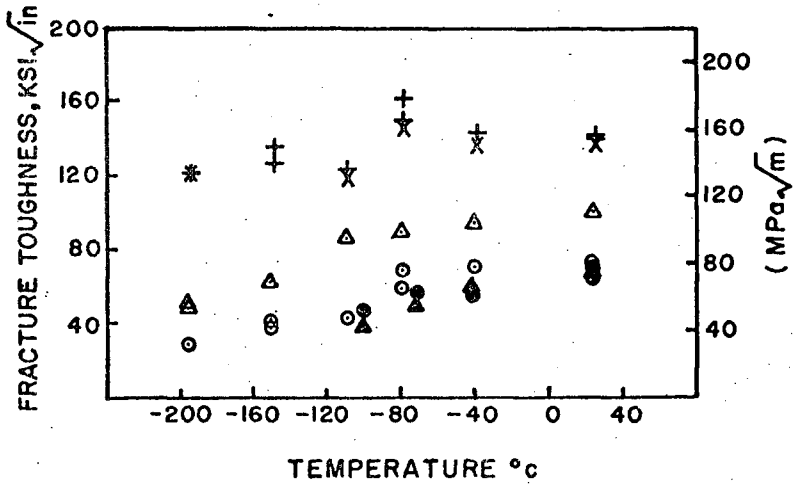

Figure 6.18.1. Temperature dependence of fracture toughness of AF-1 steel along crack parallel to Rolling Direction.

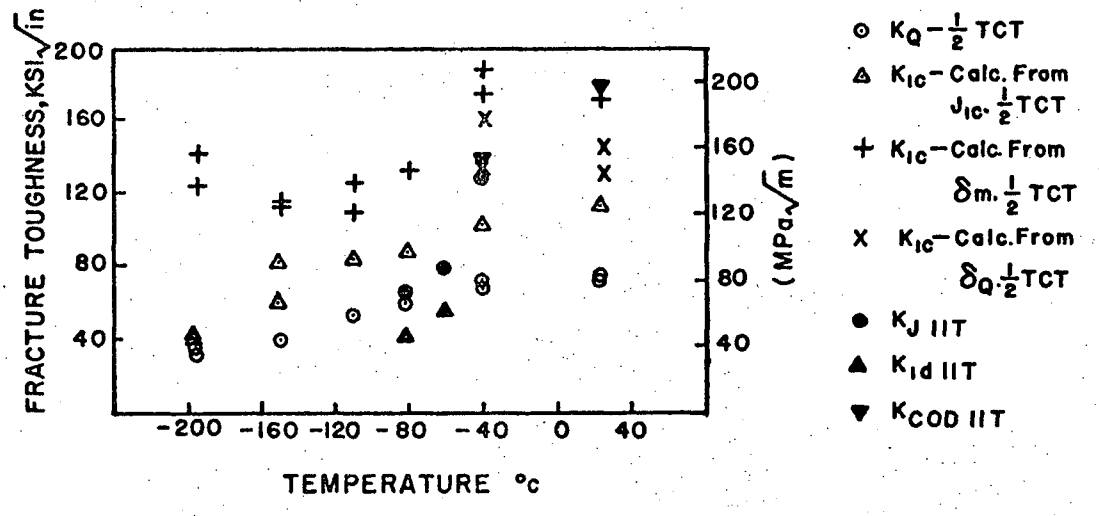

Figure 6.18.2. Temperature dependence of fracture toughness of AF-1 steel along crack parallel to Pipe Axis.

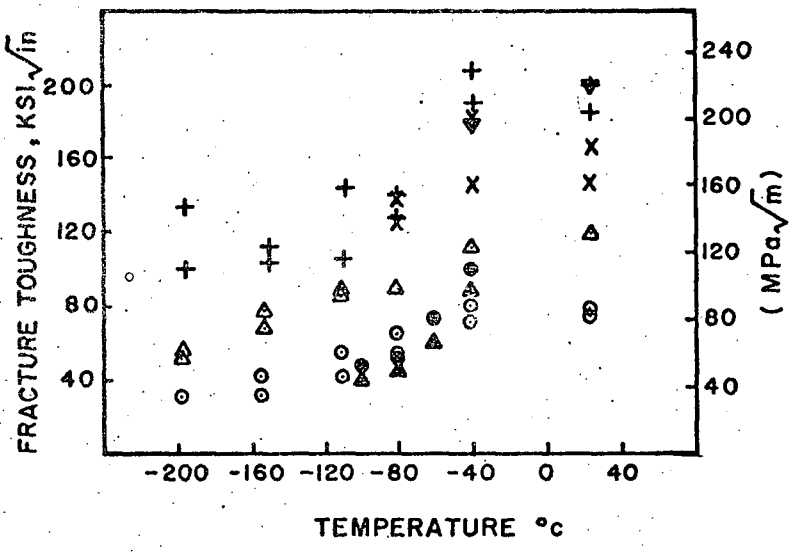

Figure 6.18.3. Temperature Dependence of Fracture toughness of AF-1 steel along crack transverse to Rolling Direction.

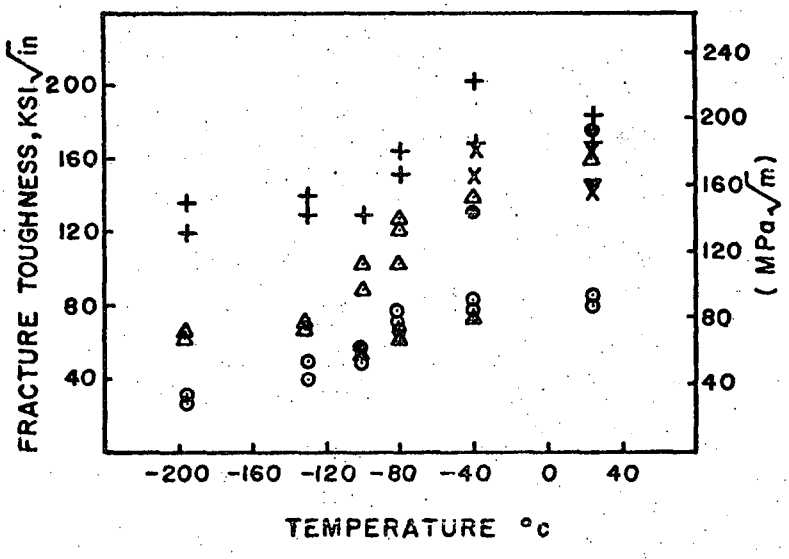

Figure 6.19.1. Temperature Dependence of Fracture Toughness of AF-2 steel along crack parallel to Rolling Direction.

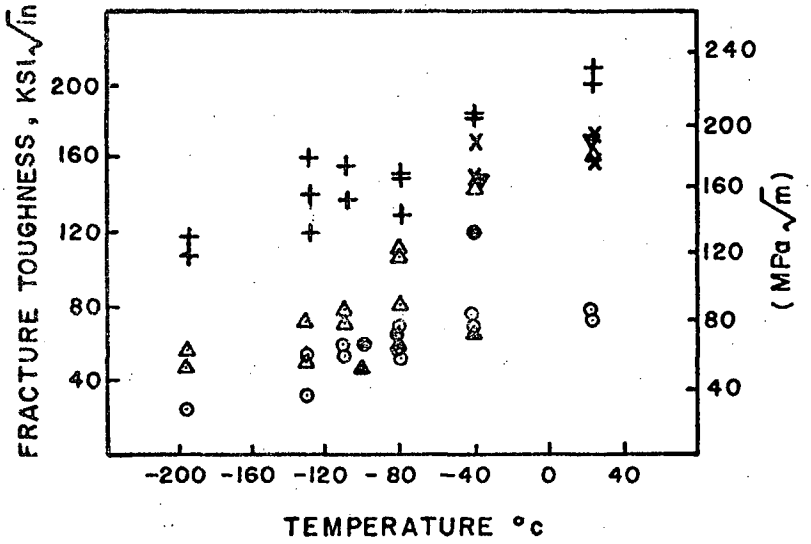

Figure 6.19.2. Temperature Dependence of Fracture Toughness of AF-2 steel along crack parallel to Pipe Axis.

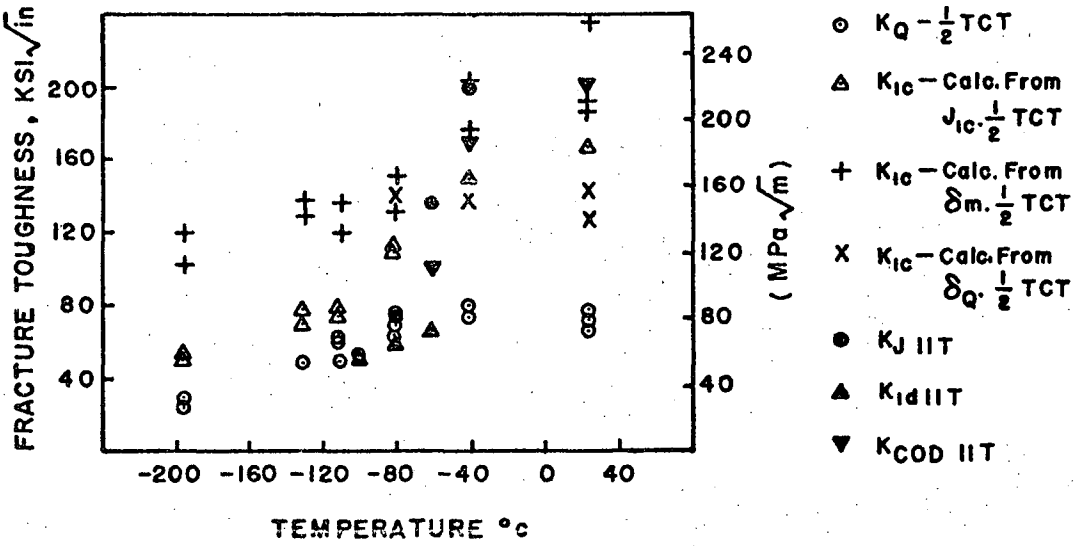

Figure 6.19.3. Temperature dependence of fracture toughness of AF-2 steel along crack transverse to Rolling Direction.

6.4 Comparison of Static and Dynamic Fracture Toughness:

In this section, an attempt is made to compare the static fracture toughness data of the AF-1 and the AF-2 steel as obtained in the present investigation (K_{Ic}, J_{Ic}, COD) with dynamic, equivalent fracture toughness values obtained from the Instrumented Impact Tests conducted by Paul McConnell (15)

Static and Dynamic fracture toughness data are superimposed on the following figures: For the AF-1 steel a) Fig. 6.18.1 shows fracture toughness data for the crack parallel to the rolling direction (the T-L orientation); b) Figure 6.18.2 shows fracture toughness data for the crack parallel to the pipe axis; and c) Fig. 6.18.3 shows fracture toughness data for the crack transverse to the rolling direction (the L-T orientation). A similar comparison for the AF-2 steel is shown in Fig. 6.19.1, 6.19.2 and 6.19.3. The average dynamic fracture toughness data were calculated and are shown in the figures; dynamic data were available only for temperatures down to - 100 ^{o} C.

The data for the AF-1 steel with the crack running parallel to the rolling direction (Fig. 6.18.1) indicates that a very good correlation exists between the K_Q static data, the $K_{J\ 11T}$ and the $K_{Id\ 11T}$ data for test temperatures from RT down to - 100 ^{o}C. The magnitude of the $K_{J\ 11T}$ and $K_{Id\ 11T}$ results is much smaller than the results obtained for the J_{Ic}, δ_m, δ_Q, COD static data.

If the static J_{Ic} and δ_m, δ_Q COD are considered representative fracture toughness properties of the steel for temperatures above - 130 ^{o}C, where K_{Ic} becomes invalid, then it is obvious that dynamic fracture toughness is less than the static fracture toughness for the same test temperature. It is clear that an equivalent K_{Ic} obtained from δ_m or δ_Q COD data is a poor indication of the fracture toughness over the whole temperature range. This is due to the fact that δ_m corresponds to a COD for the maximum load where extensive crack extension has occurred.

For samples of the AF-2 steel having the same crack orientation, the static and dynamic fracture toughness data are shown in Fig. 6.19.1. This diagram

shows that at - 100°C and - 80°C, static K_Q, K_J 11T, and K_{Id} 11T are comparable; the dynamic data have a much smaller magnitude than the respective static J_{Ic}, δ_m and δ_Q COD values. At - 40°C the K_{Id} 11T value is comparable to the K_Q; but the K_J 11T value is comparable to the J_{Ic} value, J_{Ic} being much higher than the K_Q value. At RT the magnitude of the dynamic K_J 11T and K_{COD11T} results are comparable to the J_{Ic}, δ_m and δ_Q COD value.

In the case of the AF-1 steel with the crack running parallel to the pipe axis (Fig. 6.18.2), at - 60°C and - 80°C, the K_J 11T and K_{Id} 11T results are comparable to the K_Q data. At - 40°C, the K_{COD} 11T and K_J 11T results are comparable to the δ_Q - COD and are higher than the J_{Ic} value. At RT the K_{COD} 11T value is comparable to the δ_m - COD value. For a similar specimen orientation of the AF-2 steel, Fig. 6.19.2 indicates that a good correlation exists between the K_Q data and K_J 11T and K_{Id} 11T results obtained at - 80°C and below. For - 40°C and higher temperatures, the K_{COD} 11T data are comparable to J_{Ic}, δ_m and δ_Q COD values. However, at - 40°C, the K_{Id} 11T value is comparable to the K_Q value, K_J 11T lies much

above the K_Q values but below the J_{Ic} data.

For the AF-1 steel with the crack running transverse to the rolling direction (Fig. 6.18.3) it can be seen that at -40° C and below there is a good correlation between the K_Q data and the $K_{J\ 11T}$ and $K_{Id\ 11T}$ results. At temperatures of -40° C and above, a good correlation exists between $K_{COD\ 11T}$ and δ_m, δ_Q COD values. For the AF-2 steel with the same specimen orientation (Fig. 6.19.3) the K_Q data is comparable to the $K_{Id\ 11T}$ and $K_{J\ 11T}$ results at -80° C and below. At -40° C and RT the $K_{COD\ 11T}$ results are comparable to δ_Q - COD and J_{Ic} values; whereas at -40° C, the $K_{J\ 11T}$ data is comparable to δ_m - COD value.

In summary, it may be stated that:

i) the $K_{COD\ 11T}$ value is comparable to the δ_m and the δ_Q COD static data in the upper shelf temerature range.

ii) At -60° C and below, the $K_{J\ 11T}$ and $K_{Id\ 11T}$ values are comparable to the K_Q data.

iii) At temperatures $> -60^{\circ}$ C, the $K_{J\ 11T}$ data is larger in magnitude than the K_Q data and is

less than the J_{Ic} and the δ_Q - COD static data; however, $K_{Id\ 11T}$ is comparable to K_Q static data.

From the above observations, it is apparent that in the upper shelf region there is a close correlation between the static (δ_m, δ_Q) and the dynamic $K_{COD\ 11T}$ fracture toughness values. However, with the exception of the two cases (refer Fig. 6.18.2 and 6.19.3 at - 40 ^{o} C) one for the AF-1 steel with crack running parallel to the pipe axis and one for the AF-2 steel with crack running transverse to the rolling direction, the dynamic $K_{J\ 11T}$ is less than the J_{Ic} static value and the dynamic $K_{Id\ 11T}$ is comparable to the K_Q data, in the upper shelf temperature region.

The δ_Q, δ_m static and the dynamic COD fracture toughness data give a poor indication of the fracture toughness of both steels at upper-shelf temperatures; this is due to the fact that the calculation of δ_m and $K_{COD\ 11T}$ corresponds to a COD for a maximum load where extensive crack extension has occurred. Therefore, in the upper shelf region, if only the $K_{J\ 11T}$ $K_{Id\ 11T}$ and static J_{Ic} and δ_Q values are considered,

it is obvious that static fracture toughness J_{Ic} is higher than the dynamic fracture toughness ($K_{J\ 11T}$), $K_{Id\ 11T}$).

In the transition temperature region the available static and the dynamic data indicated that $K_{Ic} > K_{Id}$.

Shoemaker and Rolfe[62] have established that for structural steels which are strain rate sensitive, dynamic fracture toughness values are more conservative than the static fracture toughness values. Barsom and Rolfe[63] and Barsom[64] advanced the observation that the effect of a slow loading rate ($\dot{\epsilon} = 10^{-5}$/sec) as compared to an impact loading rate ($\dot{\epsilon} = 10$/sec) in steels of various yield strengths is to shift the equivalent fracture-toughness behaviour to a lower temperature, the magnitude of the change being given by the following relation

$$T \text{ deg Shift} = 119 - 0.12\ \sigma_{ys}$$

$$\text{for } 250 \text{ MPa} < \sigma_{ys} < 965 \text{ MPa}$$

$$T \text{ Shift} = o \text{ for } \sigma_{ys} < 965 \text{ MPa}$$

They have also shown that for steels having $\sigma_{ys} > 965$ MPa, $K_{Ic} = K_{Id}$ throughout the transition range.

Therefore, the present relationship between the static and the dynamic fracture toughness data of the AF-1 and the AF-2 steels (σyield strength ≈ 480MPa) is one in which $K_{Id} < K_{Ic}$ for the entire temperature range down to - 100 °C. This behaviour of the static and the dynamic fracture toughness of the AF-1 and AF-2 steels is in good agreement with the observations of Shoemaker and Rolfe [62], Barsom and Rolfe [63] and Barsom [64]. In contrast, G.R. Irwin [65] reported that for structural steels the variations of loading speed from slow to fast did not change K_{Ic} when the fracture was mainly by cleavage and the testing temperature was sufficiently low. A.H. Priest [55] also made a similar observation, that when fracture occurs by cleavage, K_{Ic} values are relatively independent of the tensile properties and the K_{Ic} values do not vary with strain rate. In the present investigation static data is available in the cleavage range but dynamic data from 11T tests is available only down to the - 100 °C transition range. Therefore, no comparison is possible in the

cleavage range. But the test results of this study did indicate that up to - 100 °C, the fracture toughness of the AF-1 and the AF-2 steels are strain rate sensitive.

7. CONCLUSIONS

7.1 Conclusions:

1. The tensile studies established that with a decrease in the test temperature, the yield strength and flow strength of both the AF-1 and the AF-2 steel increased. The AF-1 steel, containing more sulphur, possesses inferior yield strength and exhibits higher anisotropy than the AF-2 steel. The isotropy of AF-2 steel may be also due to rare earth addition.

2. K_{Ic} as well as J_{Ic} and COD test methods established that with increasing temperature, the fracture toughness of both the AF-1 and AF-2 steels increased.

3. All three test methods showed similar fracture toughness transition behaviour for both steels; -130^{o}, -150^{o}, -196^{o}C toughness data constituted the lower shelf, -40^{o}C and RT toughness data constituted the upper shelf and -80^{o}C, -100^{o}C, -110^{o}C toughness data, the transition region.

4. The K_Q test established that both steels possessed valid K_{IC} up to a temperature of - 130 °C and the fracture toughness transition was from a plane-strain to plane-stress testing condition.

5. All of the test methods established that the AF-1 steel is anisotropic, possessing its highest toughness in specimens having the crack transverse to the rolling direction (L-T) and its minimum toughness for the crack parallel to the rolling (T-L) direction.

6. All three test methods confirmed that the AF-2 steel is more isotropic and tougher than the AF-1 steel in the upper shelf region. The J-Integral test method indicated that the AF-2 steel is also tougher than the AF-1 steel in the transition region. The AF-2 steel possesses twice the toughness of the AF-1 steel at RT and - 40 °C for a crack running parallel to the rolling (T-L) direction.

7. The lowest toughness of the AF-1 steel was realized for samples having a crack parallel to the

rolling (T-L) direction as described in McConnell's 11T study. Therefore, both static and dynamic fracture toughness data reveal that the current pipeline toughness specification for the crack propagating parallel to the pipe axis may be inadequate for ensuring fracture control; minimum toughness properties (dynamic and static) are realized for the T-L orientation i.e. crack running parallel to the rolling direction.

8. A comparison of static and dynamic fracture toughness data revealed that for the complete temperature range of testing, $K_{Ic} > K_{Id}$, which indicates both AF-1 and AF-2 steel are strain rate sensitive.

7.2 Suggestions for Future Work:

i) To further analyse the strain rate sensitive character of both AF-1 and AF-2 steels, the fracture toughness measurements under dynamic strain rate conditions ($\dot{\varepsilon} = 10 - 20/\text{sec}$, $\dot{K} = 10^5$ ksi$\sqrt{\text{in}}$/sec) should be carried out for the same range of temperatures by the ASTM standard E - 399 - 74 method and compared

with K_{Ic} fracture toughness.

To confirm the validity of the 11T data on these steels, direct measurement of the dynamic fracture toughness data (K_{Id}) will be useful.

ii) A fractographic analysis of the specimens tested in the present work would reveal a clear picture of the micromode mechanism of failure in entire transition temperature range.

iii) More correlation between K_{Ic} or K_{Id} with Drop Weight Tear Test will be useful for developing an effective fracture control plan.

iv) 11T, K_{Ic}, K_{Id} and Drop Weight test data for each steel should be stored to make an effective comparison. This may contribute towards toughness design considerations of pipeline steels.

REFERENCES

1. Molybdenum Mosaic - J. of Molybdenum Metallurgy, climax Molybdenum, v-1, No. 3, Spring 1976, P.14.

2. M.P. **Boussel**, K. Miyano, J.A. Straatmann - Tech. Report M-316, " x-70 Mo-Nb. A new family of HSLA steels designated for Arctic and offshore pipelines", climax Molybdenum, 1978.

3. A.O. Coldren and J.L. Mihelich - "In Mo-containing steels for Gas and Oil Industry Applications". TR-M321, climax Molybdenum, 1977, P.14.

4. J.L. Mihelich and R.L. Cryderman - ASME, publication No. 72 - Pet - 36, New York, 1972.

5. Leon Luyckx,John R. Bell, Alex Mclean and Michael Korchynsky - Met. Trans. v-1, Dec. 1970, P.3341.

6. Y.E. Smith, A.P. Coldren and R.L. Cryderman: Toward Improved Ductility and Toughness, Symp. climax Molybdenum Co, Kyoto 1971, P. 119.

7. D.B. Clay and D.B. McCutcheon - Rosenhain Centenary conf; Metals Soc; National Physical Laboratory and Royal Soc. London, 1975, P.305.

8. M.J. Bibby and A.B. Rothwell: Noranda Tech. Memorandum No. 37, Noranda Research Centre, Pointe Claire, P.Q, 1975.

9. R.J. Cooke: Prairie Mat. Sc. Meeting, Aug. 11, 1977, Univ. of Saskatchewan.

10. W.L. Mercer - in ref. 7, P. 41.

11. F.S. Somerville and T.C. Slimon: Proc. Conf. Materials Engg in the Arctic, ASM, St. Jovite, P.Q. 1976, P. 143.

12. J.M.E. Wallbridge - ibid, P. 149.

13. W.A. Maxey: 5th Symposium on Line Pipe Research, American Gas Association, Nov. 1974.

14. W.A. Maxey et al: ASTM STP-514, Philadelphia, 1972, P. 70.

15. Paul McConnell - M.A.Sc. Thesis, The Univ. of British Columbia, Jan, 1978.

16. S.T. Rolfe and J.M. Barsom - Fracture and Fatigue control in Structures, Prentice Hall Inc., Englewood Cliffs, New Jersey, 1977.

17. H. Tada, P.C. Paris and G.R. Irwin ed. Stress Analysis of Cracks Handbook, Del Research Corporation, Hellertown, Pa. 1973.

18. R.W. Hertzberg - Deformation and Fracture Mechanics of Engineering Materials - John Wiley & Sons. Inc., U.S.A. 1976.

19. J.F. Knott - Fundamentals of Fracture Mechanics - Butterworth & Co. Ltd; London, 1973.

20. F.A. McClintock & G.R. Irwin - "Fracture Toughness Testing and its Applications", ASTM STP-381, ASTM, 1965.

21. W.F. Brown, JR and J.E. Strawley, "Plane Strain Crack Toughness Testing" - ASTM STP 410, 1967.

22. L.A. Simpson: Elastic-Plastic Fracture Mechanics - TR AECL - 5991, Pinawa, Manitoba, July 1978.

23. J.R. Rice - J. of Applied Mech. ASME, Ser E, 1968, P. 379.

24. J.W. Hutchinson - J. Mech. Phys. Solids, vol. 16, 1968, P.13.

25. J.R. Rice and G.F. Rosengreen - ibid, P.1.

26. F.A. McClintock, Fracture - Ed. H. Liebowitz, v-3, Academic Press, New York, 1971, P.47.

27. J.R. Rice - Fracture, Ed. H. Liebowitz, v-2 Academic Press, New York, 1968, P. 191.

28. J.A. Begley and J.D. Landes: Fracture Toughness, ASTM, STP-514, 1972, P.1.

29. J.R. Rice, P.C. Paris, J.G. Merkle - "Progress in Flow Growth and Fracture Toughness Testing" - ASTM. STP - 536, ASTM, 1973, P. 231.

30. J.D. Landes and J.A. Begley: "Fracture Analysis", ASTM, STP - 560, 1974, P. 170.

31. W.A. Logsdon: "Mechanics of Crack Growth" ASTM, STP - 590, 1976, P. 43.

32. G.A. Clarke: RR76 - 1E7 - JINTF - R1, Nov. 23, 1976, Westinghouse Research Lab, Pa.15235.

33. G.A. Clarke, W.R. Andrews, P.C. Paris and D.W. Schmidt, - "Mechanics of Crack Growth", ASTM - STP 590, 1976, P.27.

34. J.D. Landes and J.A. Begley: "Fracture Toughness", ASTM - STP - 514, 1972, P. 24.

35. W.A. Logsdon and J.A. Begley: "Flow Growth and Fracture", ASTM STP - 631, 1977, P. 477.

36. G. Frederick: Centre De Recherches Metallurgignes, Metallurgical Reports - 31, June, 1972, PP 27-37.

37. F.M. Burdekin and D.E. Stone: J. of Strain Analysis, Vol. 1, No. 2, 1966, P. 145.

38. A.A. Wells - "Crack Propagation in Metals" - Cleavage and Fast Fracture", Cranfield crack propagation symposium, V.1, Sept. 1961, P.210.

39. G.R. Egan: Engg. Fracture Mechanics, vol. 5, 1973, P. 167.

40. D.S. Dugdale: J. Mech. Phys. Solids, vol. 8, 1960, P. 100.

41. B.A. Bilby, A.H. Cottrell, K.H. Swinden: Proc. Roy. Soc. A272, 1963, P. 304.

42. R.W. Nichols - Proc. Pipe Welding Cont. The Welding Institute, Abington, 1970, P. 107.

43. P.C. Hughes and M.E. de Morton - J. of Australian Institute of Metals, vol. 16, No. 3, Sept. 1971, P. 167.

44. J.N. Robinson and A.S. Tetelman - Fracture Toughness and Slow - Stable Cracking, ASTM STP 559, 1974, P. 139.

45. Methods for crack opening Displacement (COD) Testing, "British Standards Institution Draft for Development 19", London, 1972.

46. T. Ingham, G.R. Egan, D. Elliot, and T.C. Harrison - Practical Application of Fracture Mechanics to Pressure Vessel Tech. Cont. Proc., London, May, 1971, P. 200.

47. R.R. Barr, D. Elliot, R. Terry and E.G. Walker - Metal Construction, Dec. 1975, P. 604.

48. D.E. Diesberg: Tech. Report - L - 176 - 137 climax Molybdenum Co. of Michigan, March 26, 1975.

49. R.F. Smith, J.F. Knott, "Practical Applications of Fracture Mechanics to Pressure Vessel Tech. Conf. Proc." - Inst. Mech. Eng, London, 1971, P. 65.

50. J.M. Lowes - Inst. of Metallurgists Spring Meeting, Younger Met'ls Comm; Newcastle-upon-Tyne, March, 1973.

51. C.F. Tiffany and J.N. Masters - "Fracture Toughness Testing", ASTM STP - 381, P. 249.

52. Metals Handbook - "Failure Analysis and Prevention", vol. 10, P. 54.

53. ASTM Standards E 399 - 74, in anual Standards, 1975, P.955.

54. J.D.G. Sumpter - Metal Science, October, 1976, P. 354.

55. A.H. Priest - Dynamic Fracture Toughness, WI and ASM, Intl. Conf. v-1, London, 1976, P. 95.

56. G.D. Fearnehough - 'Physical basis of Yield and Fracture' - Conf. Proc. Oxford, September, 1966. P. 88.

57. G.R. Irwin - Trans ASME, J. of Engg for Power, Ser A, Oct 1964, P. 444.

58. R.O. Ritchie, J.F. Knott and J.R. Rice - J. Mech. Phys. Solids, vol. 21, 1973, P. 395.

59. E.T. Wessel: LEFM for thick walled welded steel pressure vessels: Material property considerations. 'Practical Fracture Mechanics for Structural Steel' - 1969, UKAEA, Risley.

60. J.M. Barsom and S.T. Rolfe: Engg. Fracture Mechanics. vol. 2, 1971, P. 341.

61. W.G. Wilson, Q.J. Klems - Industrial Heating, vol. 41, Oct. 1974, P. 12.

62. A.K. Shoemaker and S.T. Rolfe - Engg. Fracture Mechanics, vol. 2, 1971, PP 319.

63. J.M. Barsom and S.T. Rolfe - ASTM STP - 466, 1970, P. 281.

64. J.M. Barsom - in ref. 55, P. 113.

65. G.R. Irwin - in ref. 55. P.1.

APPENDIX - I

Calculation of $P_{f(max)}$

We know for CT specimen (16,53)

$$K_Q = \frac{P_Q}{BW^{1/2}} \quad f\ (a/w)$$

considering $K_Q = 100\ ksi\sqrt{in}$, $K_{f(max)} = 15\%\ K_Q$

$a = 0.50$ inch

$w = 1.00$ inch

$a/w = 0.50$

$f(a/w) = 9.60$ from Standard Table

$$K_{f(max)} = \frac{P_{f(max)}}{BW^{1/2}} f(a/w)$$

$$P_{f(max)} = \frac{15{,}000 \times .50 \times 1}{9.60} = 781 \text{ lbs.}$$

TABLE

		Settings for Precracking m/c	
$\frac{K_{f(max)}}{(ksi\sqrt{in})}$	$\frac{P_{f(max)}}{(lbs)}$	$\frac{P_{f(max)}}{2}$ lbs	$\frac{P_{f(max)}}{2x4.05}$ = xx.001"
10% K_Q	520	260.00	64.30
11% K_Q	573	286.50	70.70
12% K_Q	625	312.50	77.10
13% K_Q	677	338.50	83.59
14% K_Q	729	364.50	90.00
15% K_Q	781	390.50	96.45
16% K_Q	833	416.50	102.90
17% K_Q	885	442.50	109.30
18% K_Q	937	468.50	115.76
19% K_Q	989	494.50	122.17
20% K_Q	1041	520.50	128.60

APPENDIX - II

AF-2 Steel crack parallel to Rolling Direction

Sp. No.	$K_{f(max)}$	No. of Stress Cycles	Sp. for	Time taken (Min.)
1	15% K_Q	30,000	K_Q	17
2	15% K_Q	32,000	K_Q	18
3	15% K_Q	41,000	K_Q	25
4	15% K_Q	29.000	K_Q	16
5	15% K_Q	31,000	K_Q	17
35	15% K_Q	58.000	J-1	33
36	15% K_Q	50.000	J-1	29
37	15% K_Q	64,000	J-1	35
38	15% K_Q	50,000	J-1	28
39	15% K_Q	61,000	J-1	36

AF-1 Steel crack parallel to Rolling Direction

10	15% K_Q	31,000	K_Q	17
12	15% K_Q	35,000	K_Q	19
20	15% K_Q	35,000	K_Q	19
26	15% K_Q	38,000	K_Q	21
29	15% K_Q	37,000	K_Q	20
21	15% K_Q	60.000	J-1	34
22	15% K_Q	72,000	J-1	39
23	15% K_Q	55,000	J-1	31
24	15% K_Q	65,000	J-1	38
25	15% K_Q	60,000	J-1	33

PUBLICATIONS

1. R.MAITI,P.DUTTA, & Y.G.ANDREEV, "A study on the mechanical behaviour of low carbon martensite", Metallurgical Engineers,Department of Metallurgical Engineering,I.I.T. Kharagpur,1972.
2. Y.G.ANDREEV,& R.MAITI, "Experimental techniques for studying microplasticity of metals", Sixteenth Congress Of Indian Society of Theoritical and Applied Mechanics, Allahabad,India,1972.
3. R.MAITI & Dr.M.K.MUKHERJEE, "Effect of thermal cycling on the hardening behaviour of wrought AZ- 61 Mg-Alloy," I.R.S. Symposium, Trivandrum, India, September,1973.
4. S.K.DUTTA,Dr.M.K.MUKHERJEE & R.MAITI, "Experimental and theoretical studies on the problem of shielding in welding of Mg-Alloy", I.I.W. Symposium, Durgapur, November, 1974.
5. S.K.DUTTA,R.MAITI & Dr.M.K.MUKHERJEE, "Development of a procedure for surfacing welded Mg-Alloy pressure vessels", I.I.W. Symposium,Tiruchirapally, India,December, 1975.
6. R.MAITI,B.R.GHOSH et all, "Critical heat treatment parameters for AZ-92 Mg-Alloy casting for satellite application", I.I.F. Symposium, I.I.T. Madras,January,1976.
7. P.P.SINHA,R.MAITI,Dr.K.V.NAGRAJAN,Dr.M.K.MUKHERJEE, "Kinetics of elevated temperature reactions in maraging steel",I.I.M. Symposium, Suratkal, March,1976.